

# **General Utility Lattice Program**

**Version 5.2**

**Julian D. Gale**

**Curtin Institute for Computation,  
School of Molecular and Life Sciences,  
Curtin University,  
P.O. Box U1987, Perth, WA 6845,  
Australia  
email: [gulpcode@curtin.edu.au](mailto:gulpcode@curtin.edu.au)**

# Chapter 1

## Introduction & background

The General Utility Lattice Program (GULP) is designed to perform a variety of tasks based on force field methods. The original code was written to facilitate the fitting of interatomic potentials to both energy surfaces and empirical data. However, it has expanded now to be a general purpose code for the modelling of condensed phase problems. While version 1.0 focussed on solids, clusters and embedded defects, the latest version is also capable of handling surfaces, interfaces, and polymers.

As with any large computer program (and GULP currently runs to about 750,000 lines) there is always the possibility of bugs. While every attempt is made to ensure that there aren't any and to trap incorrect input there can be no guarantee that a user won't find some way of breaking the program. So it is important to be vigilant and to think about your answers - remember GIGO! Immature optimising compilers can also be a common source of grief. As with most programs, the author accepts no liability for any errors but will attempt to correct any that are reported.

As from GULP3.4, the program has migrated to Fortran 90 (including subsequently some features from later standards). From version 4.0 the code included several major additions, the most significant of which are the addition of the ReaxFF reactive force field and also the facility to use continuum dielectric solvation in multiple dimensions through the COSMIC algorithm, derived as the name would suggest from COSMO. A further major improvement is the addition of a stochastic thermostat/barostat with a new integrator in molecular dynamics. This is far more robust than the old schemes used and less sensitive to the choice of parameters. Finally, the ability to calculate PDF data has been added courtesy of Beth Cope and Martin Dove (University of Cambridge at the time; now Queen Mary, University of London). In version 4.2 the calculation of thermal conductivity has been added based on the Allen-Feldman approach for diffusors. This was achieved through a collaboration with Jason Larkin (Carnegie Mellon, Pittsburgh).

For GULP5.0 onwards the major change is the parallelisation of second derivatives with distributed memory. This allows much large problems to be tackled

where full second or even third derivatives are needed, such as phonon calculations and free energy minimisation. Because this represents a major change in the code not all features are currently enabled with parallel second derivatives. Currently the main restrictions are that partial occupancies, variable charges and the breathing shell model are not yet available in this mode. However, these restrictions will be removed in future versions.

In GULP5.1 there have been several additions. Split bond charge equilibration has been added, along with multiple charge ranges for electronegativity parameters. This allows the MEAM\_2NN\_QEq method to be used. An interface to the code Alamode has been added that automates the calculation of the thermal conductivity using the Boltzmann Transport Equations based on third order force constants.

## 1.1 References for GULP

The following papers describe various aspects of GULP:

### **Basic algorithms and symmetry adaption:**

- J.D. Gale, J.C.S. Faraday Transactions, 93, 629-637 (1997)

### **Detailed background theory:**

- J.D. Gale and A.L. Rohl, Molecular Simulation, 29, 291-341 (2003)

### **Free energy minimisation:**

- J.D. Gale, J. Phys. Chem. B, 102, 5423 (1998)

### **Review of status and functionality:**

- J.D. Gale, Z. Krist., 220, 552-554 (2005)

### **Solvent models in GULP:**

- J.D. Gale and A.L. Rohl, Molecular Simulation, 33, 1237-1246 (2007)

### **ReaxFF in GULP:**

- J.D. Gale, P. Raiteri and A.C.T. van Duin, PCCP, 13, 16666-16679 (2011)

### **Pair Distribution Functions in GULP:**

- E.R. Cope and M.T. Dove, J. Appl. Cryst., 40, 589-594 (2007)

### **Thermal conductivity in GULP:**

- J.M. Larkin and A.J.H. McGaughey, Phys. Rev. B, 89, 144303 (2014)

## **1.2 Overview of program**

The following is intended to act as a brief summary of the capabilities of GULP to enable you to decide whether your required task can be performed without having to read the whole manual. Alternatively it may suggest some new possibilities for calculations!

### **System types**

- 0-D (clusters and embedded defects)
- 1-D (polymers, screw dislocations)
- 2-D (slabs, surfaces, grain boundaries, interfaces)
- 3-D (bulk materials)

### **Energy minimisation**

- constant pressure / constant volume / unit cell only / isotropic / orthorhombic
- thermal/optical calculations
- application of external isotropic or anisotropic pressure
- user specification of degrees of freedom for relaxation
- relaxation of spherical region about a given ion or point
- symmetry constrained relaxation
- unconstrained relaxation
- constraints for fractional coordinates and cell strains
- Newton/Raphson, conjugate gradients or Rational Function optimisers
- BFGS or DFP updating of hessian
- limited memory variant of BFGS for large systems
- search for minima by genetic algorithms with simulated annealing

- free energy minimisation with analytic first derivatives
- choice of regular or domain decomposition algorithms for first derivatives
- minimisation of gradient/force norm instead of energy
- uniaxial stress
- finite strain derivatives relative to a reference structure

### **Transition states**

- location of  $n$ -th order stationary points
- mode following

### **Crystal properties**

- elastic constants
- bulk modulus (Reuss/Voigt/Hill conventions)
- shear modulus (Reuss/Voigt/Hill conventions)
- Young's modulus
- Poisson ratios
- compressibility
- piezoelectric stress and strain constants
- static dielectric constants
- high frequency dielectric constants
- frequency dependent dielectric constants
- static refractive indices
- high frequency refractive indices
- NMR chemical shifts
- stress tensor
- phonon frequencies
- phonon densities of states (total and projected)

- phonon dispersion curves
- group velocities
- S/P-wave velocities
- Born effective charges
- zero point vibrational energies
- heat capacity (constant volume)
- entropy (constant volume)
- Helmholtz free energy
- pair distribution function (PDF) calculation
- Grueneisen parameters
- group velocities
- thermal conductivity (Allen-Feldman model)
- thermal conductivity (output of files for AlamoDe to use Boltzmann Transport Equations)
- Raman susceptibility tensors
- phonon mean-squared displacements

### **Molecular properties**

- centre of mass
- moment of inertia tensor
- rotational partition function
- translational partition function
- rotational/translational free energy
- Eckart purification of vibrational modes

## **Defect calculations**

- vacancies, interstitials and impurities can be treated
- explicit relaxation of region 1
- implicit relaxation energy for region 2
- energy minimisation and transition state calculations are possible
- defect frequencies can be calculated (assuming no coupling with 2a)

## **Surface calculations**

- calculation of surface and attachment energies
- multiple regions allowed with control over rigid or unconstrained movement
- can be used to simulate grain boundaries and interfaces
- calculation of phonons allowed for region 1
- continuum solvation of surfaces

## **Fitting**

- empirical fitting to structures, energies and most crystal properties
- fit to multiple structures simultaneously
- simultaneous relaxation of shell coordinates during fitting
- fit to structures by either minimising gradients or displacements
- variation of potential parameters, charges and core/shell charge splits
- constraints available for fitted parameters
- simplex or BFGS minimisation algorithms for fitting
- generate initial parameter sets by the genetic algorithm for subsequent refinement
- fit to quantum mechanically derived energy hypersurfaces
- bond lengths, bond angles, volume and reaction energies now available as observables

### **Structure analysis**

- calculate bond lengths/distances
- calculate bond angles
- calculate torsion angles
- calculate improper torsion angles
- calculate out of plane distances
- calculation of the density and cell volume
- electrostatic site potentials
- electric field gradients

### **Structure manipulation**

- convert centred cell to primitive form
- creation of supercells
- rotation of frame based on moment of inertia tensor
- twisting of 1-D periodic structures about repeat direction

### **Electronegativity equalisation method**

- use EEM to calculate charges for systems containing H, C, N, O, F, Al, Si, P
- use QEq to calculate charges for any element
- new modified scheme for hydrogen within QEq that has correct forces
- Gasteiger charge calculation based on bond increments
- calculation of charges from ReaxFF
- use split bond charges for EEM

### **Generation of files for other programs**

- GDIS (.gin/.res)
- THBREL/THBPHON/CASCADE (.thb)
- MARVIN (.mvn)
- Insight (.xtl file)
- Insight (.arc/.car files)
- G-Vis (.xr)
- Cerius2 (.arc/.xtl/.cssr)
- Materials Studio
- COSMO solvent accessible surface for Materials Studio
- SIESTA (.fdf)
- Molden (.xyz)
- QMPOT (.frc)
- General (.cif/.xml)
- DLV (.str)
- Alamode files (for calculation of thermal conductivity using Boltzmann Transport Equations)
- lammmps\_pot (Table of potentials for use in LAMMPS)

### **Output files for post-processing**

- Pressure tensor (.pre)
- Oscillator strengths
- Pair distribution function (.pdf)
- Charges and bond orders (.qbo)
- MD trajectory file (.trg)

## Interatomic potentials available

- Buckingham
- Four-range Buckingham
- Buckingham in MM3 format
- Lennard-Jones (with input as A and B)
- Lennard-Jones (with input in  $\epsilon$  and  $\sigma$  format)
- Lennard-Jones (with ESFF combination rules)
- Morse potential (with or without Coulomb subtract)
- Harmonic (with or without Coulomb subtract)
- MM3 bond stretching potential (with or without Coulomb subtract)
- General potential (Del Re) with energy and gradient shifts
- Spline
- Spring (core-shell)
- Spring with cosh functional form
- Coulomb subtract
- Coulomb with erfc
- Coulomb with short range taper
- Inverse Gaussian
- Damped dispersion (Tang-Toennies)
- Rydberg potential
- Covalent exponential form
- Breathing shell harmonic
- Breathing shell exponential
- Coulomb with complementary error function
- Coulomb with short range taper

- Covalent-exponential
- Fermi-Dirac form
- Three body potentials - harmonic with or without exponential decay
- Exponential three-body potential
- Urey-Bradley three-body potential
- Stillinger-Weber two- and three-body potentials
- Stillinger-Weber with charge softening
- Axilrod-Teller potential
- Four-body torsional potential
- Ryckaert-Bellemans cosine expansion for torsional potential
- Out of plane distance potential
- Tsuneyuki Coulomb correction potential
- Squared harmonic
- Mei-Davenport twobody
- Glue potential
- Short range potentials based on (complementary) error functions
- Embedded atom method for metals (Sutton-Chen potentials and others)
- Modified Embedded Atom Method of Baskes and co-workers
- Two-body potentials can be intra- or inter-molecular, or both
- Two-body potentials can be tapered to zero using cosine, polynomial or Voter forms
- Universal force field functional forms for three-, four-body cases and out of plane
- Universal force field combination rules available
- Angle-angle cross out of plane potential
- Lennard-Jones potential between atoms and a plane

- Radial force between all atoms and a point in space
- Sixbody out of plane - out of plane cross potentials
- Grimme C6 damped dispersion
- Environmentally Dependent Interatomic Potential (EDIP)
- ReaxFF
- Central Force Model (CFM) potentials
- Baskes twobody potential
- Ziegler-Biersack-Littmark (ZBL) potential
- Torsion potentials can be specified as improper
- Externally defined potentials via OpenKIM version 2
- Constant potentials for 2 and 3 body interactions for use in Ising models

### **Coulomb summations**

- Ewald sum for 3-D
- Parry sum for 2-D
- Saunders et al sum for 1-D
- Cell multipole method for 0-D
- Wolf et al sum for 0-,1-,2-, & 3-D
- Smooth Particle Mesh Ewald for 3-D (energy and first derivatives only)

### **Molecular dynamics**

- Shell model (dipolar and breathing) molecular dynamics
- Finite mass or adiabatic algorithms
- Forward extrapolation of shells added for adiabatic algorithms
- NVE or NVT (Fixed cell) or NPT (Variable cell shape)
- Stochastic integrator with thermostat/barostat
- isotropic or orthorhombic cell constraints
- Atom-based potential energy decomposition and forces added to trajectory file

## Monte Carlo

- Rigid molecules allowed for
- Displacement or rotation of species
- NVT or Grand Canonical ensembles allowed
- Particle swaps (single or multiple) allowed

## 1.3 Introduction

The simulation of ionic materials has a long history going back over most of the last century. It began with lattice energy calculations based on experimental crystal structures through the use of Madelung's constant [1]. This was then expanded through the inclusion of short-range repulsive interactions, as found in the work of Born-Landé and Born-Mayer [2], in order that the crystal structure be a minimum with respect to isotropic expansion or compression. For many simple ionic materials a reasonable estimate of the lattice energy may even be obtained without knowledge of the structure, as demonstrated by the work of Kapustinskii [3]. Over the last few decades atomistic simulation, in which we are only concerned with atoms, rather than electrons and sub-atomic particles, has developed significantly with the widespread use of computers. Correspondingly the field has evolved from one that was initially concerned with reproducing experimental numbers, to one where predictions are being made, and insight is being offered.

The widespread use of atomistic simulation for solid state materials clearly resulted from the availability of computer programs for the task, just as much as the advent of the hardware to run the calculations. In the early days of solid state forcefield simulation for ionic materials much of the work in the UK was centred around the Atomic Energy Authority at Harwell. Consequently a number of computer codes arose from this work, such as HADES [4], MIDAS [5], PLUTO [6], METAPOCS and CASCADE [7]. Eventually these migrated into the academic domain, leading to the THB suite of codes, including THBREL, THBFIT and THBPHON from Leslie. Further development of these programs led to the PARAPOCS code from Parker and co-workers [8], for free energy minimisation of solids using numerical derivatives, and the DMAREL code from the group of Price for the simulation of molecular crystals through the use of distributed multipoles [9]. There were also several other prominent codes developed contemporaneously to the above family, in particular the WMIN code of Busing [10], the PCK series of programs from Williams [11], and the UNISOFT program of Eckold *et al* [12]. While the codes mentioned above focus specifically on static lattice and quasiharmonic approaches to simulation, it should not be forgotten that there was a much larger, parallel, development of forcefield software for performing molecular dynamics

simulation leading to programs such as GROMOS [13], AMBER [14], CHARMM [15], and DL\_POLY [16, 17], to name but a few.

This article focuses on the General Utility Lattice Program which began development in the early 90's, and is therefore subsequent to much of the aforementioned software, but implements many of the same ideas. However, there are increasingly many new, and unique, developments as well. The key philosophy was to try to bring together many of the facilities required for solid state simulation, with particular emphasis on static lattice/lattice dynamical methods, in a single package, and to try to make it as easy to use as possible. Of course, this is an aim and the degree of success depends on the perspective of the end user! It is important to also mention here the programs METADISE from Parker and co-workers[18], and SHELL from the group of Allan [19], which are also contemporary simulation codes sharing some of the same ideas.

In this work, the specific aim is to document the very latest version of GULP, 4.0 onwards, which includes many new features over previous versions. Firstly, we detail the background theory to the underlying methods, some of which is not readily available in the literature. Secondly, we present a brief review of the utilisation of the code to date, in order to highlight the scope of its previous application. Finally, we present some results illustrating the new capabilities of the latest version.

## 1.4 Methods

The starting point for the majority simulation techniques is the calculation of the energy, and so will it be for this article. Most methods are based around the initial determination of the internal energy, with subsequent treatment of the nuclear degrees of freedom in order to determine the appropriate free energy to the ensemble of interest. In principle, the internal energy of a solid is a manybody quantity that explicitly depends upon the positions and momenta of all electrons and nuclei. However, this is an intractable problem to solve at any level of theory, and thus approximations must be made to simplify the situation. To tackle this we assume that the effect of the electrons will largely be subsumed into an effective atom, and that the energy can be decomposed into an expansion in terms of interactions between different subsets of the total number of atoms,  $N$ :

$$U = \sum_{i=1}^N U_i + \frac{1}{2} \sum_{i=1}^N \sum_{j=1}^N U_{ij} + \frac{1}{6} \sum_{i=1}^N \sum_{j=1}^N \sum_{k=1}^N U_{ijk} + \dots$$

where the first term represents the self energies of the atoms, the second the pairwise interaction, etc. This decomposition is exact if performed to a high enough order. However, we know that the contribution from higher order terms becomes progressively smaller for most systems, and so we choose to neglect the terms beyond a certain point and introduce a degree of parameterisation of the remaining terms

to compensate. Justification for this is forthcoming from quantum mechanics. It is well known that the Hartree-Fock method is a reasonable first approximation for the description of many systems, albeit with a systematic quantitative error for most observables. Here the highest term included is a four-centre integral, which indicates that including up to four-body terms should be reasonable approach, which is indeed found to be the case for most organic systems, for example. Furthermore, it is intuitively obvious that the further apart two atoms are, the weaker their interaction will be. Thus the introduction of distance cut-offs is a natural way to simplify the computational task.

The form of the explicit interaction between atoms is usually chosen based on physical insights as to the nature of the forces between the particles. For instance, if considering a covalent diatomic molecule the natural representation of the potential energy surface would be a Morse potential since this is harmonic at the minimum and leads to dissociation at large bond lengths, in accord with spectroscopic observation. In the following sections we will review some of the common types of potential that are widely used, as well as some novel approaches which point towards the future of forcefield methods.

### 1.4.1 Coulomb interaction

When considering ionic materials, the Coulomb interaction is by far the dominant term and can represent, typically, up to 90% of the total energy. Despite having the simplest form, just being given by Coulomb's law;

$$U_{ij}^{Coulomb} = \frac{q_i q_j e^2}{4\pi\epsilon_0 r_{ij}}$$

it is in fact the most complicated to evaluate for periodic systems (subsequently atomic units will be employed and the factors of  $4\pi\epsilon_0$  and  $e^2$  will be omitted). This is because the Coulomb energy is given by a conditionally convergent series, i.e. the Coulomb energy is ill-defined for an infinite 3-D material unless certain additional conditions are specified. The reason for this can be readily understood - the interaction between ions decays as the inverse power of  $r$ , but the number of interacting ions increases with the surface area of a sphere, which is given by  $4\pi r^2$ . Hence, the energy density of interaction increases with distance, rather than decaying. One solution to the problem, proposed by Evjen [20], is to sum over charge-neutral groups of atoms. However, by far the most widely employed approach is the method of Ewald [21] for three-dimensional materials. Here the conditions of charge neutrality and zero dipole moment are imposed to yield a convergent series with a well-defined limit. To accelerate the evaluation, the Coulomb term is subjected to a Laplace transformation and then separated into two components, one of which is rapidly convergent in real space, and a second which decays quickly in reciprocal space. Conceptually, this approach can be viewed as adding and subtracting a

Gaussian charge distribution centred about each ion [22]. The resulting expressions for real and reciprocal space, as well as the self-energy of the ion, are given below:

$$\begin{aligned}
U^{real} &= \frac{1}{2} \sum_{i=1}^N \sum_{j=1}^N \frac{q_i q_j}{r_{ij}} \operatorname{erfc} \left( \eta^{\frac{1}{2}} r_{ij} \right) \\
U^{recip} &= \frac{1}{2} \sum_{i=1}^N \sum_{j=1}^N \sum_G \frac{4\pi}{V} q_i q_j \exp(iG \cdot r_{ij}) \frac{\exp\left(-\frac{G^2}{4\eta}\right)}{G^2} \\
U^{self} &= - \sum_{i=1}^N q_i^2 \left( \frac{\eta}{\pi} \right)^{\frac{1}{2}} \\
U^{electrostatic} &= U^{real} + U^{recip} + U^{self}
\end{aligned}$$

Here  $q$  is the charge on an ion,  $G$  is a reciprocal lattice vector (where the special case  $G = 0$  is excluded),  $V$  is the volume of the unit cell, and  $\eta$  is a parameter that controls the division of work between real and reciprocal space. It should also be noted that although the reciprocal space term is written as a two-body interaction over pairs of atoms, it can be rewritten as a single sum over ions for more efficient evaluation. The above still leaves open the choice of cut-off radii for real and reciprocal space. One approach to defining these in a consistent fashion is to minimise the total number of terms to be evaluated in both series for a given specified accuracy,  $A$  [23]. This leads to the following expressions:

$$\begin{aligned}
\eta_{opt} &= \left( \frac{Nw\pi^3}{V^2} \right)^{\frac{1}{3}} \\
r_{max} &= \left( \frac{-\ln(A)}{\eta} \right)^{\frac{1}{2}} \\
G_{max} &= 2\eta^{\frac{1}{2}} (-\ln(A))^{\frac{1}{2}}
\end{aligned}$$

Note that the above expressions contain one difference from the original derivation, in that a weight parameter,  $w$ , has been included that represents the relative computational expense of calculating a term in real and reciprocal space. Tuning of this parameter can lead to significant benefits for large systems. There have been several modifications proposed for the basic Ewald summation that accelerate its evaluation for large systems, most notably the particle-mesh [24], and fast multipole methods [25, 26]. Furthermore, there are competitive approaches that operate purely in real space for large unit cells and that scale linearly with increasing size, such as the hierarchical fast multipole methods, though care must be taken to obtain the same limiting result by imposing the zero dipole requirement. This latter approach can also be applied to accelerating the calculation of the Coulomb energy of finite clusters.

In principle, it is possible to calculate the Coulomb energy of a system with a net dipole,  $\mu$ , as well. The nature of the correction to the Ewald energy can be determined as a function of the shape of the crystal, and the formula below can also be employed [27]:

$$U^{dipole} = \frac{2\pi}{3V}\mu^2$$

However, the complication of using the above correction is that it depends on the macroscopic dipole of the crystal, and even on any compensating electric field due to the environment surrounding the particle. Hence the dipole moment is usually ill-defined, since it depends on the surfaces, as well as the bulk material. Even if we neglect surface effects, the definition of the dipole moment is ambiguous since the operator is not invariant under translation of atomic images by a lattice vector. Consequently, we will take the Ewald result as being definitive.

Similarly, it is possible to relax the charge neutrality constraint, and to perform calculations on charged supercells [28], provided care is taken when constructing thermodynamic cycles. This is often used when probing defect energetics as an alternative to the Mott-Littleton method. Here the net charge,  $Q$  ( $Q = \sum q_i$ ) is neutralised by a uniform background charge, leading to an energy correction of:

$$U^{background} = -\frac{\pi}{2V\eta}Q^2$$

It should be noted that this correction ensures that a consistent Ewald sum energy is computed regardless of the value of eta. However, to correct the energy to the limit of no net interaction between the charged cells (and therefore no cell stress) requires the addition of a positive Madelung correction. For the special case of a simple cubic lattice, the correction is given by:

$$U^{madelung} = \frac{2.837297}{2a\epsilon}Q^2$$

Here the value 2.837297 is the Madelung constant,  $a$  is the cell length and  $\epsilon$  is the dielectric constant. The general situation is more complex and therefore only the simple cubic case correction can be automatically added at present.

As the size of a system increases then the cost of evaluating the reciprocal space part of the Ewald sum can become potentially a bottleneck. One alternative to the standard Ewald sum is to use the Smooth Particle Mesh Ewald (SPME) approach. Here the reciprocal space contribution is handled by mapping the charge density onto a grid of points in real space and then using Fourier transforms to convert to reciprocal space in order to evaluate the energy. A second Fourier transform is required in order to evaluate the forces in real space. Interpolation between the grid points and the atomic positions is performed using B-splines. The mathematical detail can be found in the original article [29]. The precision of the SPME calculation is control by both the order of the B-splines and the grid size used, where higher

values are better in both cases. Typically 8th order B-splines are used in GULP and the order has to be high enough to allow differentiation to first order. The grid size is specific to the unit cell being employed by the user and so it is important to test the convergence of the forces with respect to this choice. In order to obtain the best performance it is important to experiment with the use of either the rspeed or ewaldrealradius options that change the balance between real and reciprocal space, as well as the grid size, to find the best compromise between speed and precision. Often a good approach is to set the real space cut-off radius to be less than or equal to the twobody potential cutoff (especially if this allows the use of the spatial keyword to make things more efficient) and then tune the reciprocal space settings.

So far we have only considered how to handle infinite 3-D solids, but the same issues exist for lower dimensionalities. Again for a 2-D slab, the Coulomb sum is only conditionally convergent and so an analogous approach to the Ewald sum is usually taken, originally devised by Parry [30, 31]. Here the slab, or surface, is taken so as to be oriented with the surface vectors in the  $xy$  plane and with the surface normal lying parallel to  $z$ . The energy contributions in real and reciprocal space are given by:

$$\begin{aligned}
U^{real} &= \frac{1}{2} \sum_{i=1}^N \sum_{j=1}^N \frac{q_i q_j}{r_{ij}} \operatorname{erfc} \left( \eta^{\frac{1}{2}} r_{ij} \right) \\
U_1^{recip} &= \frac{1}{2} \sum_{i=1}^N \sum_{j=1}^N \sum_G \frac{\pi q_i q_j \exp(iG \cdot r_{ij})}{A |G|} \left[ \exp(|G| z_{ij}) \operatorname{erfc} \left( \frac{|G|}{2\eta^{\frac{1}{2}}} + \eta^{\frac{1}{2}} z_{ij} \right) + \right. \\
&\quad \left. \exp(-|G| z_{ij}) \operatorname{erfc} \left( \frac{|G|}{2\eta^{\frac{1}{2}}} - \eta^{\frac{1}{2}} z_{ij} \right) \right] \\
U_2^{recip} &= -\frac{1}{2} \sum_{i=1}^N \sum_{j=1}^N \frac{2\pi q_i q_j}{A} \left[ z_{ij} \cdot \operatorname{erf} \left( \eta^{\frac{1}{2}} z_{ij} \right) + \frac{\exp(-\eta z_{ij}^2)}{(\pi\eta)^{\frac{1}{2}}} \right] \\
U^{self} &= -\sum_{i=1}^N q_i^2 \left( \frac{\eta}{\pi} \right)^{\frac{1}{2}}
\end{aligned}$$

Note, there are now two terms in reciprocal space involving the 2-D reciprocal lattice vector,  $G$ , and here  $A$  is the surface area of the repeat unit, while  $z_{ij}$  is the component of the distance between two ions parallel to the surface normal. Again it is possible to relax the dipolar and charge neutrality constraints within the repeat directions. However, the approach to correcting the energy is far more uncertain, and it is necessary to make approximations [32]. As per the 3-D case, the optimum value of the convergence parameter can also be determined [33]:

$$\eta_{opt} = \frac{\pi w}{A}$$

Recently, another approach has been proposed for the calculation of the 2-D Coulomb sum, which is reported to be faster than the Parry method for all cases, and especially beneficial as the number of atoms increases [34].

Lowering the dimensionality further, we arrive at 1-D periodic systems which represents a single polymer strand, for example. At this dimensionality the Coulomb sum becomes absolutely convergent, though at a very slow rate when performed directly in real space. Summing over charge neutral units accelerates the process, though convergence is still somewhat tardy. While there have been several proposed approaches to accelerating the Coulomb sum, we find that the method proposed by Saunders *et al* [35], in which a neutralising background charge is applied, is effective. Here there are three contributions to the energy given by:

$$\begin{aligned}
U_1^{real} &= \frac{1}{2} \sum_{m=-M}^{+M} \sum_{i=1}^N \sum_{j=1}^N \frac{q_i q_j}{r_{ij} + ma} \\
U_2^{real} &= -\frac{1}{2} \sum_{i=1}^N \sum_{j=1}^N \frac{q_i q_j}{a} \left[ \ln \left( \sqrt{(u+x)^2 + y^2 + z^2} + u+x \right) + \right. \\
&\quad \left. \ln \left( \sqrt{(u-x)^2 + y^2 + z^2} + u-x \right) - 2 \ln a \right] \\
U_3^{real} &= \frac{1}{2} \sum_{i=1}^N \sum_{j=1}^N q_i q_j [\xi(M, r_{ij}) + \xi(M, -r_{ij})]
\end{aligned}$$

where the first term is summed over all images of  $i$  and  $j$  in the unit cells from  $-M$  to  $M$ ,  $a$  is the 1-D repeat parameter in the  $x$  direction, and the remaining variables and functions are defined as below:

$$\begin{aligned}
u &= a \left( M + \frac{1}{2} \right) \\
\xi(M, r_{ij}) &= - \sum_{i=1}^M E_i a^{2i-1} W_{2i-1}(u+x, y^2 + z^2) \\
W_n(u+x, \alpha) &= \left( \frac{\partial}{\partial u} \right)^n \left( (u+x)^2 + \alpha \right)^{-\frac{1}{2}}
\end{aligned}$$

Although the required extent of the summations, given by  $M$ , to achieve a given precision is not known *a priori*, the method can be implemented in an iterative fashion so that the degree of convergence is tested as the number of lattice repeats is increased.

One alternative approach to the above methods for performing the Coulomb sum in any dimensionality is that due to Wolf *et al* [36]. Their approach involves a purely real space summation that is asymptotic to the Ewald limit given a suitable choice

of convergence parameters. It is based around the concept of ensuring that the sum of the charges of all ions within a spherical cut-off region is equal to zero and that the potential goes smoothly to zero at that cut-off. This is achieved by placing an image of every ion that a given atom interacts with at the cut-off boundary, but in the diametrically opposite direction. While this approach can be applied directly to the Coulomb potential, convergence is slow. Better results are obtained by using a damped form of the potential, which is chosen to be equivalent to the real space component of the Ewald sum, with subtraction of the associated self-energy of the corresponding Gaussian. In this form the expression for the energy is:

$$U^{Wolf} = \frac{1}{2} \sum_i \sum_j q_i q_j \left( \frac{\text{erfc}(\alpha r_{ij})}{r_{ij}} - \lim_{r_{ij} \rightarrow r_{cut}} \left\{ \frac{\text{erfc}(\alpha r_{ij})}{r_{ij}} \right\} \right) - \sum_i q_i^2 \left\{ \frac{\text{erfc}(\alpha r_{cut})}{2r_{cut}} + \frac{\alpha}{\pi^{\frac{1}{2}}} \right\}$$

where  $\alpha$  is the convergence parameter, closely related to the factor  $\eta$  in the Ewald sum, and  $r_{cut}$  is the cut-off radius. There is a trade-off to be made in the choice of parameters within this sum. The smaller the value of  $\alpha$ , the closer the converged value will be to the Ewald limit. However, the cut-off radius required to achieve convergence is also increased. This summation method has been implemented within GULP for 1-D, 2-D and 3-D calculations, though by default the term due to the limit of the distance approaching the cut-off is omitted from the derivatives in order to keep them analytically correct at the expense of the loss of smoothing.

Before leaving the topic of how Coulomb interactions are evaluated, it is important to note the special case of molecular mechanics forcefields. Here the Coulomb interaction, and usually the dispersion one too, is subtracted for interactions which are between neighbours (i.e. bonded or 1-2) and next nearest neighbours (i.e. which have a common bonded atom, 1-3) according to the connectivity. This is done so that the parameters in the two- and three-body potentials can be directly equated with experimentally observable quantities, such as force constants from spectroscopy. Furthermore, long-range interactions for atoms that are 1-4 connected are often scaled, usually by  $\frac{1}{2}$ .

So far we have discussed the methods for evaluating Coulomb sums. However, we have yet to comment on how the atomic charges are determined. In most simulations, the charges on ions are fixed (i.e. independent of geometry) for simplicity and their magnitude is determined parametrically along with other forcefield parameters, or extracted from quantum mechanical information. In the later situation there is the question as to what is the appropriate charge to take since it depends on how the density matrix is partitioned. Although Mulliken analysis [37] is commonly used as a standard, this is not necessarily the optimum charge definition for use in a forcefield. Arguably a better choice would be to employ the Born effective

charges [38] that describe the response of the ions to an electric field, about which more will be said later. If the charges are purely regarded as parameters then the use of formal charges is convenient as it removes a degree of freedom and maximises the transferability of the forcefield, especially to charged defects.

An alternative to using fixed charges is to allow the charges to be determined as a function of the geometry. It is well documented that this environment dependence of the charge is very important in some cases. For example, the binding energy of water in ice is much greater than that in the water dimer. This arises due to the increased ionicity of the O-H bond in the solid state and cannot be described correctly by a simple two-body model. In order to implement a variable charge scheme, a simple Hamiltonian is needed that is practical for forcefield simulations. Consequently most approaches to geometry-dependent charges have been based around the concept of electronegativity equalisation [39]. Here the energy of an atom is expanded with respect to the charge,  $q$ , where the first derivative of the energy with respect to charge is the electronegativity,  $\chi$ , and the second is the hardness,  $\mu$ :

$$U_i = U_i^0 + \chi_i^0 (q_i - q_0) + \frac{1}{2} \mu_i^0 (q_i - q_0)^2 + \frac{1}{2} q_i V_i$$

The final term in the above expression is the interaction with the Coulomb potential due to other atoms within the system. In this equation the term  $q_0$  is the charge about which electronegativity parameters are assumed to be quadratic. Usually this value is 0 (i.e. the parameters are determined from the ionisation potential and first electron affinity of the neutral atom). However, an exception will be noted below. In some charge equilibration schemes, multiple sets of parameters are used for different ranges of charge values. This is possible within the implementation within GULP. If using multiple charge ranges it is important to ensure that the equations are continuous (i.e. the energy and electronegativity are the same for both parameter sets at the boundary between ranges).

By solving the coupled set of equations for all atoms simultaneously, this leads to a set of charges that balance the chemical potential of the system. There are two variants of this method in general use. In the first, typified by the work of Mortier and co-workers [40], the Coulomb interaction,  $J$ , is described by a simple  $\frac{1}{r}$  form. The alternative, as used by Rappe and Goddard in their QEq method [41], is to use a damped Coulomb potential that allows for the fact that at short distances the interaction arises from the overlap of electron density, rather than from just simple point ions. Hence, in QEq the potential is calculated based on the interaction of  $s$  orbitals with appropriate exponents. A further variant tries to encapsulate the short range damping of the Coulomb interaction in a mathematically more efficient form [42];

$$J_{ij} = \frac{1}{\left(r_{ij}^3 + \gamma_{ij}^{-3}\right)^{\frac{1}{3}}}$$

where the pairwise terms  $\gamma_{ij}$  are typically determined according to combination rules in order to minimise the number of free parameters:

$$\gamma_{ij} = \sqrt{\gamma_i \gamma_j}$$

In the case of hydrogen, the variation of charge is so extreme between the hydride and proton limits that it was necessary to make the electronegativity a function of the charge itself in the original QEq scheme. As a result, the solution for the charges now requires an iterative self-consistent process. Here we propose a modified formulation from that of Rappe and Goddard that drastically simplifies the calculation of analytic derivatives:

$$U_H = U_H^0 + \chi_H^0 q_H + \frac{1}{2} J_{HH}^0 \left( 1 + \frac{2q_H}{3\xi_H^0} \right) q_H^2 + \frac{1}{2} q_H V_H$$

The reason for the simplification is based on the Hellmann-Feynman theorem and can be understood as follows. If we consider the Cartesian first derivatives of the variable charge energy we arrive at:

$$\left( \frac{dU}{d\alpha} \right) = \left( \frac{\partial U}{\partial \alpha} \right)_q + \left( \frac{\partial U}{\partial q} \right)_\alpha \left( \frac{\partial q}{\partial \alpha} \right)$$

where the first term represents the conventional fixed charge derivative, and the second term is the contribution from the variation in charge as a function of structure. However, if the charges at each geometry are chosen so as to minimise the total energy of the system, then the first derivative of the internal energy with respect to charge is zero and so the correction disappears. Consequently it only becomes necessary to evaluate the first derivatives of the charges with respect to position when calculating the second derivative matrix.

A variant of the QEq method has been proposed, known as EQeq [43]. This method is essentially the same as the QEq method, except that the charge about which the quadratic expansion of the energy as a function of charge is made (i.e.  $q_0$ ) is no longer zero for all elements.

An alternative parameterisation of electronegativity equalisation has been developed by Marc Henry known as PACHA [44]. The parameters for this method are also included in GULP. Through the PACHA formalism it is now possible to estimate NMR chemical shifts for groups of species based on the PACHA variable charges [45].

One of the known problems of electronegativity equalisation as formulated above is that charge transfer can occur regardless of distance and there is no requirement that the total charge on fragments at dissociation are integers. A consequence of this is that when breaking bonds it is common for the final fragments to have a partial charge even at infinite separation. A solution to this is to use so-called split bond charges [46]. Here the charge on an atom is expressed as the sum of the charge

transferred for each bond to this atom. If a bond is broken then charge is no longer transferred. To use this method it is therefore important to ensure that the connectivity is correctly defined for the system. Since the number of bonds is often larger than the number of atoms within the system, then the charge equilibration problem written in terms of bonds can be overdetermined. If a matrix inversion route is used to determine the charges then GULP tries to find the minimal set of bonds to connect all atoms, but this algorithm is still under development and may not be robust. Instead, charges can be found through iterative minimisation and this approach will work regardless of whether there are redundant bond charge variables.

## 1.4.2 Dispersion interactions

After the Coulomb energy, the most long-ranged of the energy contributions is usually the dispersion term. From quantum theory we know that the form of the interaction is a series of terms in increasing inverse powers of the interatomic distance, where even powers are usually the most significant:

$$U_{ij}^{dispersion} = -\frac{C_6}{r_{ij}^6} - \frac{C_8}{r_{ij}^8} - \frac{C_{10}}{r_{ij}^{10}} - \dots$$

The first term represents the instantaneous dipole - instantaneous dipole interaction energy, and the subsequent terms correspond to interactions between higher order fluctuating moments. Often in simulations only the first term,  $\frac{C_6}{r^6}$ , is considered as the dominant contribution. Again, the dispersion term can cause difficulties due to the slow convergence with respect to a radial cut-off. Although the series is absolutely convergent, unlike the Coulomb sum, the fact that all contributions are attractive implies that there is no cancellation between shells of atoms. The problem can be remedied by using an Ewald-style summation [47] to accelerate convergence for materials where the dispersion term is large:

$$U_{C6}^{recip} = -\frac{1}{2} \sum_{i=1}^N \sum_{j=1}^N C_{ij} \left( \frac{\pi^{\frac{3}{2}}}{12V} \right) \sum_G \exp(iG \cdot r_{ij}) G^3 \left[ \pi^{\frac{1}{2}} \text{erfc} \left( \frac{G}{2\eta^{\frac{1}{2}}} \right) + \left( \frac{4\eta^{\frac{3}{2}}}{G^3} - \frac{2\eta^{\frac{1}{2}}}{G} \right) \exp \left( -\frac{G^2}{4\eta} \right) \right]$$

$$U_{C6}^{real} = -\frac{1}{2} \sum_{i=1}^N \sum_{j=1}^N \frac{C_{ij}}{r^6} \left( 1 + \eta r_{ij}^2 + \frac{\eta^2 r_{ij}^4}{2} \right) \exp(-\eta r_{ij}^2)$$

$$U_{C6}^{self} = \frac{1}{2} \sum_{i=1}^N \sum_{j=1}^N -\frac{C_{ij}}{3V} (\pi\eta)^{\frac{3}{2}} + \sum_{i=1}^N \frac{C_{ii}\eta^3}{6}$$

There can also be problems with the dispersion energy at short-range since it tends to negative infinity faster than some expressions for the repulsion between

atoms, thus leading to collapse of the system. This can be resolved by recognising that the above expansion for the dispersion energy is only valid for non-overlapping systems, and that at short-range the contribution decays to zero as it becomes part of the intrinsic correlation energy of the atom. To allow for this, Tang and Toennies [48] proposed that the dispersion energy is exponentially damped as the distance tends to zero according to the function:

$$f_{2n}(r_{ij}) = 1 - \left\{ \sum_{k=0}^{2n} \frac{(br_{ij})^k}{k!} \right\} \exp(-br_{ij})$$

### 1.4.3 Two-body short-range interactions

Contributions to the energy must be included that represent the interaction between atoms when they are bonded, or ions when they are in the immediate coordination shells. For the ionic case, a repulsive potential is usually adequate, with the most common choices being either a positive term which varies inversely with distance, or an exponential form. These lead to the Lennard-Jones and Buckingham potentials, respectively, when combined with the attractive  $C_6$  term:

$$U_{ij}^{Buckingham} = A \exp\left(-\frac{r_{ij}}{\rho}\right) - \frac{C_6}{r_{ij}^6}$$

$$U_{ij}^{Lennard-Jones} = \frac{C_m}{r_{ij}^m} - \frac{C_6}{r_{ij}^6}$$

The Buckingham potential is easier to justify from a theoretical perspective since the repulsion between overlapping electron densities, due to the Pauli principle, which take an exponential form at reasonable distances. However, the Lennard-Jones potential, where the exponent is typically 9-12, is more robust since the repulsion increases faster with decreasing distance than the attractive dispersion term.

For covalently bonded atoms, it is often preferable to Coulomb subtract the interaction and to describe it with either a harmonic or Morse potential. In doing so, the result is a potential where the parameters have physical significance. For instance, in the case of the Morse potential the parameters become the dissociation energy of the diatomic species, the equilibrium bond length and a third term, which coupled with the dissociation energy, is related to the vibrational frequency for the stretching mode.

This does not represent an exhaustive list of the forms used to describe short-range interactions, but most other forms are closely related to the above functional forms, with the exception of the use of a spline function, which consists of a tabulation of function values versus distance. A full list of the two-body potential functional forms presently available is given in Tables 1.1, 1.2 and 1.3.

Table 1.1: Common two-body interatomic potentials currently available within GULP. Here  $r$  represents the interatomic distance of which the potential is a function. All other values are parameters of the potentials.

Potential name	Functional form
Buckingham	$A \exp\left(-\frac{r}{\rho}\right) - \frac{C}{r^6}$
MM3 Buckingham	$\varepsilon \left( A \exp\left(-\frac{Br}{r_v}\right) - C \left(\frac{r_v}{r}\right)^6 \right)$
Lennard-Jones	$\frac{A}{r^m} - \frac{B}{r^n}$
Lennard-Jones ( $\varepsilon, \sigma$ )	$\varepsilon \left[ \left(\frac{n}{m-n}\right) \left(\frac{\sigma}{r}\right)^m - \left(\frac{m}{m-n}\right) \left(\frac{\sigma}{r}\right)^n \right]$
Lennard-Jones ( $\varepsilon, \sigma$ ) zero	$\varepsilon \left[ \left(\frac{n}{m-n}\right) \left(\frac{m}{n}\right)^{\frac{m}{m-n}} \left(\frac{\sigma}{r}\right)^m - \left(\frac{m}{m-n}\right) \left(\frac{m}{n}\right)^{\frac{n}{m-n}} \left(\frac{\sigma}{r}\right)^n \right]$
Lennard-Jones buffered	$\frac{A}{(r+r_0)^m} - \frac{B}{(r+r_0)^n}$
Morse	$D_e \left[ \left(1 - \exp(-a(r-r_0))\right)^2 - 1 \right]$
Harmonic	$\frac{1}{2}k_2(r-r_0)^2 + \frac{1}{6}k_3(r-r_0)^3 + \frac{1}{24}k_4(r-r_0)^4$
MM3 Bond stretch	$Ak_2(r-r_0)^2(1-B(r-r_0)(1-C*B(r-r_0)))$
Coulomb-subtract	$\frac{-q_i q_j}{r}$
Stillinger-Weber 2-body	$A \exp\left(\frac{\rho}{r-r_{cutoff}}\right) \left(\frac{B}{r^4} - 1\right)$
Polynomial	$c_0 + c_1 r + c_2 r^2 + c_3 r^3 + c_4 r^4 + c_5 r^5$
Spring	$\frac{1}{2}k_2 r^2 + \frac{1}{24}k_4 r^4$
Breathing shell harmonic	$\frac{1}{2}k(r-r_0)^2$
Squared harmonic	$\frac{1}{4}k(r^2 - r_0^2)^2$

Table 1.2: Less common two-body interatomic potentials currently available within GULP. Here  $r$  represents the interatomic distance of which the potential is a function, and  $q$  denotes the atomic charge of the species. All other values are parameters of the potentials.

Potential name	Functional form
General/Del Re	$\frac{A \exp\left(-\frac{r}{\rho}\right)}{r^m} - \frac{C}{r^n}$
Four-range Buckingham	$A \exp\left(-\frac{r}{\rho}\right), a_0 + a_1 r + a_2 r^2 + a_3 r^3 + a_4 r^4 + a_5 r^5$ $b_0 + b_1 r + b_2 r^2 + b_3 r^3, -\frac{C}{r^6}$
Inverse Gaussian	$-A \exp\left(-b(r-r_0)^2\right)$
Tang-Toennes	$-\left(\frac{C_6}{r^6}\right) f_6(r) - \left(\frac{C_8}{r^8}\right) f_8(r) - \left(\frac{C_{10}}{r^{10}}\right) f_{10}(r)$
Qtaper	$\left(\frac{q_i q_j}{r}\right) f(r) + C(1-f(r))$ where $f(r)$ is a taper function
Polynomial-harmonic	$(c_0 + c_1 r + c_2 r^2 + c_3 r^3 + c_4 r^4 + c_5 r^5)(r-r_0)^2$
Qerfc	$\left(\frac{q_i q_j}{r}\right) \operatorname{erfc}\left(\frac{r}{\rho}\right)$
Covalent exponential	$-D \exp\left(-\frac{a(r-r_0)^2}{2r}\right)$
Rydberg	$-A \left(1 + B \left(\frac{r}{r_0} - 1\right)\right) \exp\left(-B \left(\frac{r}{r_0} - 1\right)\right)$
Fermi-Dirac	$\frac{A}{(1 + \exp(B(r-r_0)))}$
Cosh-spring	$k_2 d^2 \left(\cosh\left(\frac{r}{d}\right) - 1\right)$
Tsuneyuki - form 1	$\frac{(Q_1 Q_2 - q_1 q_2) g(r)}{r}$ where $g(r) = (1 + \zeta r) \exp(-2\zeta r)$
Tsuneyuki - form 2	$\frac{(Q_1 Q_2 - q_1 q_2) g(r)}{r}$ where $g(r) = \left(1 + \frac{11\zeta r}{8} + \frac{3(\zeta r)^2}{4} + \frac{(\zeta r)^3}{6}\right) \exp(-2\zeta r)$
Q over r2	$\frac{Q_i Q_j}{r^2}$
Force constant	$\frac{d^2 E}{da db} = (K_L - K_T) \frac{a b}{r^2} + \delta_{ab} K_T$ where $a, b$ are Cartesian coordinates
Erf-Erfc	$\frac{A \operatorname{erf}\left(\frac{r}{\alpha}\right) \operatorname{erfc}\left(\frac{r}{\beta}\right)}{r}$
Repulsive Erfc	$\frac{A \operatorname{erfc}\left(\frac{r}{\beta}\right)}{r}$
Erf	$\frac{A \operatorname{erf}\left(\frac{r}{\beta}\right)}{r}$

Table 1.3: More of the less common two-body interatomic potentials currently available within GULP. Here  $r$  represents the interatomic distance of which the potential is a function. All other values are parameters of the potentials.

Potential name	Functional form
Short-range glue	$a_{14}(r-d)^4 + a_{13}(r-d)^3 + a_{12}(r-d)^2 + a_{11}(r-d) + a_{10}$ if $r < d$ $a_{26}(r-d)^6 + a_{25}(r-d)^5 + a_{24}(r-d)^4 + a_{23}(r-d)^3 +$ $a_{22}(r-d)^2 + a_{21}(r-d) + a_{20}$ if $d < r < r_{max}$
Mei-Davenport	$-\phi_0(1 + \delta(\frac{r}{r_0} - 1)) \exp(-\gamma(\frac{r}{r_0} - 1))$
Baskes 2-body	$-\frac{2}{Z}(1 + a + d * a^3) \exp(-a) - Ax \ln x$ where $x = \frac{\rho_{ref}(r)}{\rho_0}$ and $a = \left(\frac{\alpha}{r_0}\right) (r - r_0)$
VBO 2-body	$N \exp\left(-\frac{\gamma}{1 - \sqrt{\left(\frac{r}{\delta}\right)}}\right)$ where $N = 2 \exp\left(\frac{\gamma}{1 - \sqrt{\left(\frac{r_0}{\delta}\right)}}\right)$
Exp powers	$A \exp(B_0 + B_1 r + B_2 r^2 + B_3 r^3)$
Grimme C6	$-\frac{C_6 f_{damp}(r)}{r^6}$ where $f_{damp}(r) = \frac{1}{1 + \exp(-d(\frac{r}{r_0} - 1))}$
CFM_harmonic	$\frac{1}{2}k(r - r_0)^2 (1 - t(r))$ where $t(r) = \frac{1}{2} \left(1 + \tanh\left(\frac{r-R}{w}\right)\right)$
CFM_Gaussian	$k \exp\left(-\zeta(r - r_0)^2\right) t(r)$ where $t(r) = \frac{1}{2} \left(1 + \tanh\left(\frac{r-R}{w}\right)\right)$
CFM_power	$\left(\frac{A}{r^n}\right) t(r)$ where $t(r) = \frac{1}{2} \left(1 + \tanh\left(\frac{r-R}{w}\right)\right)$
CFM_Fermi	$\frac{k}{1 + \exp(\zeta(r - r_0))} t(r)$ where $t(r) = \frac{1}{2} \left(1 + \tanh\left(\frac{r-R}{w}\right)\right)$
GCoulomb	$-\frac{A}{(r^3 + \gamma)^{\frac{1}{3}}}$

#### 1.4.4 Polarisability

The Coulomb interaction introduced previously is just the first term of an expansion involving moments of the charge density of an atom which includes the monopole, dipole, quadrupole, etc. Unlike the monopole term, it is generally unreasonable to assume that the dipole moment of an atom is fixed, since both the magnitude and direction readily alter within the crystalline environment according to the polarisability of the species. There are two approaches to modelling the polarisability that have been widely used, which we will now introduce.

The first, and most intuitive model is to use a point ion dipolar polarisability,  $\alpha$ , which, in the presence of an electric field,  $V_f$ , will give rise to a dipole moment,  $\mu$ , and energy of interaction as given below:

$$\mu = \alpha V_f$$
$$U^{polarisation} = -\frac{1}{2}\alpha V_f^2$$

This approach has the advantage that it is readily extended to higher order polarisabilities, such as quadrupolar, etc [49]. It has been applied both in the area of molecular crystals, though often fixed moments are sufficient here [50], and, more recently, to ionic materials by Wilson, Madden and co-workers [51]. The only disadvantage of this approach is that the polarisability is independent of the environment, which implies that it is undamped at extreme electric fields and can lead to a polarisation catastrophe. It is well documented that the polarisability of the oxide ion is very sensitive to its location, since in the gas phase the second electron is unbound and only associates in the solid state due to the Madelung potential [52]. A further complication is that the scheme naturally involves a self-consistency cycle if the induced multipoles on one atomic centre are allowed to interact with those on another. Within GULP a simplified point-ion polarisation model is currently implemented in which the induced dipoles do not interact with each other, thereby removing the need for self-consistency and making the calculations significantly faster. The polarisation catastrophe can also be avoided by using short-range damping such that the Coulomb potential is screened at small distances. In GULP the Tang-Toennies functional form is used for the optional short-range damping where the range of the damping is controlled by a single Universal parameter.

The second approach to the inclusion of dipolar polarisability is via the shell model first introduced by Dick and Overhauser [53]. Here a simple mechanical model is used, whereby an ion is divided into a core, which represents the nucleus and inner electrons of the ion and therefore has all of the mass associated with it, and a shell, which mimics the valence electrons. Although it is convenient to think in terms of this physical picture, it should not be taken too literally as in some situations the shell can carry a positive charge, particularly for metal cations. The core and shell are Coulombically screened from each other, but coupled by a

harmonic spring of force constant  $k_{cs}$ . If the shell charge is  $q_s$ , then the polarisability of the ion *in vacu* is given by;

$$\alpha = \frac{q_s^2}{k_{cs}}$$

By convention, the short-range forces are specified to act on the shell, while the Coulomb potential acts on both. Hence, the short-range forces act to damp the polarisability by effectively increasing the spring constant, and thus the polarisability is now environment dependent. The shell model has been widely adopted within the ionic materials community, particularly within the UK. Although the same issue exists as for point ion polarisabilities, namely that self-consistency has to be achieved for the interaction of the dipoles due to the positions of the shells, the problem is transformed into a coordinate optimisation one. This can be solved concurrently with the optimisation of the atomic core positions. The main disadvantage of this approach is that is not naturally extensible to higher order moments, though some attempts have been made, such as the spherical and elliptical breathing shell models. Furthermore, when performing molecular dynamics special treatment of the shells must be made by either using an adiabatic approach, in which the shells are optimised at every timestep, or by using a technique analogous to the Car-Parrinello method [54], in which a fictitious mass is assigned to the shell [55].

As a final note on the topic of polarisability, it is impossible to distinguish from a phenomenological point of view between on site ion polarisation and charge transfer between ions. This may explain why the combination of formal charges with the shell model has been so successful for modelling materials that are quite covalent, such as silica polymorphs. Provided the crystal symmetry is low enough, the shell model could be viewed as representing charge transfer/covalency.

### 1.4.5 Radial interactions

There is a refinement to the conventional point particle shell model, which is the so-called breathing shell model, that introduces non-central ion forces [56]. Here the ion is assigned a finite radius,  $R_0$ , and then all the short-range repulsion potentials act upon the radius of the ion, rather than the nuclear position. A radial constraining potential is then added which represents the self-energy of the ion. Two functional forms are most commonly used:

$$U_i^{BSM-Harmonic} = \frac{1}{2} K_{BSM} (R_i - R_0)^2$$

$$U_i^{BSM-Exponential} = K'_{BSM} (\exp(\rho (R_i - R_0)) + \exp(-\rho (R_i - R_0)))$$

This model has two important consequences. Firstly, it allows the change of radius between two different coordination environments to be modelled - for example, octahedral versus tetrahedral. This represents an alternative to using different repulsive parameters in the Buckingham potential by scaling the  $A$  term according to

$\exp(-\rho_{tet}/\rho_{oct})$  to correct for this effect. Secondly, the coupling of the repulsive interactions via a common shell radius creates a many-body effect that is able to describe the Cauchy violation ( $C_{12} \neq C_{44}$ ) for rock salt structured materials.

### 1.4.6 Three-body interactions

There are two physical interpretations for the introduction of three-body terms, depending on whether you take a covalent or ionic perspective. Within the former view, as adopted by molecular mechanics, the three-body potential represents the repulsion between bond pairs, or even occasionally lone pairs. Hence, the form chosen is usually a harmonic one that penalises deviation from the expected angle for the coordination environment, such  $120^\circ$  for a trigonal planar carbon atom:

$$U_{ijk} = \frac{1}{2}k_2(\theta - \theta_0)^2$$

At the other end of the spectrum, ionic materials possess three-body forces due to the three-centre dispersion contribution, particularly between the more polarisable anions. This is typically modelled by the Axilrod-Teller potential [57]:

$$U_{ijk} = k \frac{(1 + 3 \cos(\theta_{ijk}) \cos(\theta_{jki}) \cos(\theta_{kij}))}{r_{ij}^3 r_{jk}^3 r_{ik}^3}$$

As with two-body potentials, there are many variations on the above themes, such as coupling the three-body potential to the interatomic distances, but the physical reasoning is often the same. A full tabulation of the three-body potentials is given in Table 1.4.

### 1.4.7 Four-body interactions

Specific four-body interactions are usually only included in molecular mechanics forcefields where they act to describe torsional angles. Hence the functional form usually involves the cosine of the torsional angle with factors that reflect the equilibrium torsional angle,  $\phi_0$ , and the periodicity with respect to rotation about the central bond. The most widely used form is therefore:

$$U_{ijkl} = k_4(1 + m \cos(n\phi - \phi_0))$$

The other form of torsional potential more occasionally found is one that employs a harmonic potential to describe the out of plane bending mode of a central atom that has a planar coordination geometry. This is of utility when describing aromatic systems, and has also been used in the modelling of the carbonate anion. An alternative to this potential is to use so-called improper torsions, where the planar geometry is maintained by specifying a torsional potential between atoms that are

Table 1.4: Three-body interatomic potentials currently available in GULP. For potentials with a unique pivot atom, this atom is taken to be atom 1 and  $\theta$  is the angle between the vectors  $r_{12}$  and  $r_{13}$ . All terms other than  $\theta$ ,  $\theta_{123}$ ,  $\theta_{231}$ ,  $\theta_{312}$ ,  $r_{12}$ ,  $r_{13}$ ,  $r_{23}$  are parameters of the potential.

Potential name	Functional form
Three (harmonic)	$\frac{1}{2}k_2(\theta - \theta_0)^2 + \frac{1}{6}k_3(\theta - \theta_0)^3 + \frac{1}{24}k_4(\theta - \theta_0)^4$
Three (exponential-harmonic)	$\frac{1}{2}k_2(\theta - \theta_0)^2 \exp\left(-\frac{r_{12}}{\rho_{12}}\right) \exp\left(-\frac{r_{13}}{\rho_{13}}\right)$
Three (exponential)	$k \exp\left(-\frac{r_{12}}{\rho_{12}}\right) \exp\left(-\frac{r_{13}}{\rho_{13}}\right) \exp\left(-\frac{r_{23}}{\rho_{23}}\right)$
Axilrod-Teller	$k \frac{(1+3\cos(\theta_{123})\cos(\theta_{231})\cos(\theta_{312}))}{r_{12}^3 r_{13}^3 r_{23}^3}$
Stillinger-Weber 3-body	$k \exp\left(\frac{\rho_{12}}{r_{12}-r_{12}^{cutoff}} + \frac{\rho_{13}}{r_{13}-r_{13}^{cutoff}}\right) (\cos(\theta) - \cos(\theta_0))^2$
Bcross	$k(r_{12} - r_{12}^0)(r_{13} - r_{13}^0)$
Urey-Bradley	$\frac{1}{2}k_2(r_{23} - r_{23}^0)^2$
Vessal	$\frac{k_2((\theta_0 - \pi)^2 - (\theta - \pi)^2)^2}{8(\theta_0 - \pi)^2} \exp\left(-\frac{r_{12}}{\rho_{12}}\right) \exp\left(-\frac{r_{13}}{\rho_{13}}\right)$
Cosine-harmonic	$\frac{1}{2}k_2(\cos(\theta) - \cos(\theta_0))^2$
Murrell-Mottram	$k \exp(-\rho Q_1) f_{MM}(Q_1, Q_2, Q_3)$ $f_{MM} = c_0 + c_1 Q_1 + c_2 Q_1^2 + c_3(Q_2^2 + Q_3^2) + c_4 Q_1^3 + c_5 Q_1(Q_2^2 + Q_3^2) +$ $(c_6 + c_{10} Q_1)(Q_3^3 - 3Q_3 Q_2^2) + c_7 Q_1^4 + c_8 Q_1^2(Q_2^2 + Q_3^2) + c_9(Q_2^2 + Q_3^2)^2$ $Q_1 = \frac{R_1 + R_2 + R_3}{\sqrt{3}}, Q_2 = \frac{R_2 - R_3}{\sqrt{2}}, Q_3 = \frac{2R_1 - R_2 - R_3}{\sqrt{6}}$ $R_1 = \frac{r_{12} - r_{12}^0}{r_{12}^0}, R_2 = \frac{r_{13} - r_{13}^0}{r_{13}^0}, R_3 = \frac{r_{23} - r_{23}^0}{r_{23}^0}$
BAcross	$(k_{12}(r_{12} - r_{12}^0) + k_{13}(r_{13} - r_{13}^0))(\theta - \theta_0)$
Linear-three-body	$k(1 \pm \cos(n\theta))$
Bcoscross	$k(1 + b \cos^m(n\theta))(r_{12} - r_{12}^0)(r_{13} - r_{13}^0)$
Hydrogen-bond	$\left(\frac{A}{r^m} - \frac{B}{r^n}\right)(\cos \theta)^p$ if $\theta > 90^\circ$ , else 0
Equatorial	$\frac{2K}{n^2}(1 - \cos(n\theta)) + 2K \exp(-\beta(r_{13} - r_0))$
UFF3	$K(C_0 + C_1 \cos \theta + C_2 \cos 2\theta)$
BAcoscross	$(k_{12}(r_{12} - r_{12}^0) + k_{13}(r_{13} - r_{13}^0))(\cos(\theta) - \cos(\theta_0))$
3Coulomb	$-\frac{s Q_2 Q_3}{r_{23}}$
exp2	$K \exp(-\rho_1(r_{12} - r_0)) \exp(-\rho_{13}(r_{13} - r_0))$
g3coulomb	$-\frac{A}{(r^3 + \gamma)^3}$

Table 1.5: Four-body interatomic potentials currently available in GULP. Here the potential acts on the sequence of atoms 1-2-3-4 (except for the out of plane potential), where the torsion angle  $\phi$  lies between the plane containing atoms 1-2-3 and atoms 2-3-4,  $\theta_{ijk}$  is the angle between the vectors  $r_{ji}$  and  $r_{jk}$ , and  $d$  represents the distance of atom 1 out of the plane of atoms 2-3-4. Note, the standard torsional and ESFF forms can also be multiplied by exponential decays or taper functions to create smooth potentials.

Potential name	Functional form
Torsional	$k_4 (1 \pm \cos(n\phi - \phi_0))$
Ryckaert-Bellemans	$\sum_{n=0}^5 c_n \cos^n \phi$
Out of plane	$k_2 d^2 + k_4 d^4$
ESFF torsion	$k_1 \sin^2 \theta_{123} \sin^2 \theta_{234} + k_2 \sin^n \theta_{123} \sin^n \theta_{234} \cos(n\phi)$
Torsional harmonic	$\frac{1}{2} k_2 (\phi - \phi_0)^2$
Inversion	$k(1 - \cos \phi)$
Inversion squared	$\frac{1}{2} \left( \frac{k}{\sin^2(k_0)} \right) (\cos \phi - \cos k_0)^2$
UFF4	$\frac{1}{2} k (1 - \cos n\phi \cos n\phi_0)$
Angle-angle cross	$k_{213/4} (\theta_{213} - \theta_{0,213}) (\theta_{214} - \theta_{0,214}) + k_{312/4} (\theta_{312} - \theta_{0,312}) (\theta_{314} - \theta_{0,314}) + k_{412/3} (\theta_{412} - \theta_{0,412}) (\theta_{314} - \theta_{0,314})$
UFF out of plane	$k(c_0 + c_1 \cos \phi + c_2 \cos 2\phi)$
Torsion-angle cross	$k \cos \phi (\theta - \theta_o) (\theta' - \theta'_o)$

not bonded. The option of specifying a sub-option of improper has been added to some torsional potentials to allow them to be handled using the bonding topology. A full list of the available functional forms of four-body potential is given in Table 1.5.

### 1.4.8 Six-body interactions

Although for many molecular systems four-body interactions are the highest order needed to describe the properties, there are some cases where six-body interactions are important. The many case is for two  $sp^2$  or resonant atoms that are bonded together, where the six-body interaction aims to keep the both groups of atoms in the same plane and to prevent rotation about the resonant or double bond.

At present there is only one potential type for this kind of interaction, which is the cross out of plane potential that couples two out of plane interactions for groups of atoms that share a common bond and the energy takes the form of the product of the out of plane distances times a constant.

## 1.4.9 Many-body interactions

Some important interactions for particular systems cannot be described within the above forcefield framework. Below we describe a few selected higher order interaction potentials that are of significance and that are becoming more widely used, despite the greater computational cost.

### 1.4.9.1 The Embedded Atom Method

The Embedded Atom Model (EAM) is an approach that has been successful in the description of metallic systems. Its foundations lie within density functional theory, and is based on the tenet that the energy is a function of the electron density. To simplify things, the EAM considers that the electron density is a superposition of the atomic densities, and that instead of integrating the density across all space it is sufficient just to express the energy as a function of the density at the nucleus of an atom, summed over all particles:

$$U^{EAM} = - \sum_{i=1}^N f(\rho_i)$$

The above equations encapsulate the idea that the interaction between any given pair of atoms is dependent on the number of other atoms within the coordination sphere. Within this generic scheme there are a number of variations, based around different functionals of the density (Table 1.6) and different representations of how the density varies with distance (Table 1.7).

In the original work of Sutton and Chen [59], which developed and extended the ideas of Finnis and Sinclair [60], a square root was used as the density functional, while the density itself was represented as an inverse power of the interatomic distance. The densities from the paper of Finnis and Sinclair, both the quadratic and combined quadratic-cubic form, can both also be used. One of the beauties of the EAM is that, in principle, once the metal is parameterised it can be studied in other environments, such as alloys, without further modification. On the downside, the prediction of the relative stability of phases can be sensitive to the cut-off radius chosen, though if care is taken this problem can be surmounted [61].

### 1.4.9.2 The Modified Embedded Atom Method

In the Embedded Atom Method it is assumed that the density of an atom is spherically symmetric. However, for some atoms, such as transition metals, this may not be such a good approximation. In the Modified Embedded Atom Method (MEAM) of Baskes [62] the density becomes a sum of terms including higher order contributions:

$$\rho^0 = \sum_i \rho_i^0$$

Table 1.6: Density functionals available within the Embedded Atom Method.

Functional	Functional form
Power law	$f(\rho) = A\rho^{\frac{1}{n}}$
Banerjea and Smith [58]	$f(\rho) = c_0 \left(1 - \frac{1}{n} \ln\left(\frac{\rho}{\rho_0}\right)\right) \left(\frac{\rho}{\rho_0}\right)^{\frac{1}{n}} + c_1 \left(\frac{\rho}{\rho_0}\right)$
Numerical	splined data from data file
Johnson	$f(\rho) = F_0(1 - \ln(x))x + F_1y$ where $x = \left(\frac{\rho}{\rho_0}\right)^{\frac{\alpha}{\beta}}$ and $y = \left(\frac{\rho}{\rho_0}\right)^{\frac{\gamma}{\beta}}$
Glue	$f(\rho) = c_{14}(\rho - \rho_1)^4 + c_{13}(\rho - \rho_1)^3 + c_{12}(\rho - \rho_1)^2 + c_{11}(\rho - \rho_1) + c_{10}$ if $\rho < \rho_1$ $f(\rho) = c_{24}(\rho - \rho_2)^4 + c_{23}(\rho - \rho_2)^3 + c_{22}(\rho - \rho_2)^2 + c_{21}(\rho - \rho_2) + c_{20}$ if $\rho_1 < \rho < \rho_2$ $f(\rho) = c_{33}(\rho - \rho_2)^3 + c_{32}(\rho - \rho_2)^2 + c_{31}(\rho - \rho_2) + c_{30}$ if $\rho > \rho_2$
Foiles	$f(\rho) = F_0\rho^2 + F_1\rho + F_2\frac{\rho^{\frac{3}{2}}}{F_3 + \rho}$
Mei-Davenport	$-E_c \left[1 - \frac{\alpha}{\beta} \ln(\rho)\right] \rho^{\frac{\alpha}{\beta}} +$ $\sum_{m=1}^3 \frac{\phi_0 s_m}{2} \exp(-\gamma(\sqrt{m}-1)) \left[1 + \delta(\sqrt{m}-1) - \frac{\delta\sqrt{m}\ln\rho}{\beta}\right] \rho^{\frac{\gamma\sqrt{m}}{\beta}}$
Baskes	$AE_0x \ln(x)$ where $x = \frac{\rho}{\rho_0}$
VBO	$f(\rho) = A\rho^{rn}$
Spline	$f(\rho) = A(\rho - \rho_0)^3 + B(\rho - \rho_0)^2 + C(\rho - \rho_0) + D$

$$(\rho^1)^2 = \sum_{\alpha} \left( \sum_i \rho_i^1 \frac{r_{\alpha}^i}{r^i} \right)^2$$

$$(\rho^2)^2 = \sum_{\alpha, \beta} \left( \sum_i \rho_i^2 \frac{r_{\alpha}^i}{r^i} \frac{r_{\beta}^i}{r^i} \right)^2 - \frac{1}{3} \left( \sum_i \rho_i^2 \right)^2$$

$$(\rho^3)^2 = \sum_{\alpha, \beta, \gamma} \left( \sum_i \rho_i^3 \frac{r_{\alpha}^i}{r^i} \frac{r_{\beta}^i}{r^i} \frac{r_{\gamma}^i}{r^i} \right)^2$$

The total density is then the combination of these terms weighted by a separate coefficient,  $t^m$  for each order,  $m$ :

$$\rho = \sum_{m=0}^3 t^m \left( \frac{\rho^m}{\rho_0} \right)^2$$

The radial forms of the density and the embedding expressions closely resemble those found for the EAM scheme and so they are not repeated here.

In the MEAM approach the interaction between a pair of atoms is weighted by a screening function that naturally truncates the terms at long-range in the solid. Unlike the more common use of a taper function, the screening function for MEAM is a many-body term that depends on the neighbours of the pair of atoms. The idea is that any neighbouring atom that comes between a pair of atoms will shield the

Table 1.7: Functional forms for the distance dependence of the atomic density available within the Embedded Atom Method.

Density	Functional form
Power law	$\rho_{ij} = cr_{ij}^{-n}$
Fractional power	$\rho_{ij} = cr_{ij}^{-rn}$
Exponential	$\rho_{ij} = cr_{ij}^n \exp(-d(r_{ij} - r_0))$
Gaussian	$\rho_{ij} = cr_{ij}^n \exp(-d(r_{ij} - r_0)^2)$
Cubic	$\rho_{ij} = c(r_{ij} - r_0)^3$ for $r_{ij} < r_0$
Quadratic	$\rho_{ij} = c(r_{ij} - r_0)^2$ for $r_{ij} < r_0$
Quartic	$\rho_{ij} = c(r_{ij} - r_0)^4$ for $r_{ij} < r_0$
Voter-Chen	$cr_{ij}^6 (\exp(-\beta r_{ij}) + 2^9 \exp(-2\beta r_{ij}))$
EVoter	$cr_{ij}^6 (\exp(-\beta r_{ij}) + 2^9 \exp(-2\beta r_{ij})) \exp(-\frac{1}{r_{max}-r_{ij}})$
Glue	$\rho_{ij} = b_{13}(r - r_1)^3 + b_{12}(r - r_1)^2 + b_{11}(r - r_1) + b_{10}$ if $r < r_1$
	$\rho_{ij} = b_{23}(r - r_2)^3 + b_{22}(r - r_2)^2 + b_{21}(r - r_2) + b_{20}$ if $r_1 < r < r_2$
	$\rho_{ij} = b_{33}(r - r_m)^3 + b_{32}(r - r_m)^2 + b_{31}(r - r_m) + b_{30}$ if $r_2 < r < r_m$ ; else 0
Mei-Davenport	$\sum_{l=0}^5 \frac{c_l}{12} (\frac{r}{r_0})^l$
Baskes	$\rho_{ij} = A \exp\left(-\beta \left(\frac{r_{ij}-r_0}{r_0}\right)\right)$
VBO	$\rho_{ij} = cN\sigma \exp\left(-\frac{\gamma}{1-\sqrt{\frac{r_{ij}}{\delta}}}\right)$ where $N = \exp\left(\frac{\gamma}{1-\sqrt{\frac{r_0}{\delta}}}\right)$

interaction. Because of the somewhat complex nature of this many-body screening function, which is then coupled with the many-body embedding potential, at present only analytic first derivatives are available for MEAM when the screening function is employed. In the absence of this term, analytic second derivatives are also available. Both the MEAM-1NN (first nearest neighbour) and MEAM-2NN (second nearest neighbour) schemes can be used in GULP.

### 1.4.9.3 Bond Order Potentials

Related in many ways to the embedded atom method, but with a more sophisticated formalism, are so-called bond order potentials. It was recognised by Abell [63] that the local binding energy could be expressed as follows:

$$U^{BO} = \sum_{i=2}^N \sum_{j=1}^{i-1} \left[ U^{repulsive}(r_{ij}) - B_{ij} U^{attractive}(r_{ij}) \right]$$

where  $B_{ij}$  is the bond order between the atoms  $i$  and  $j$ . The bond order is dependent on the local environment of both atoms and thereby converts an apparent two-body interaction into a many-body one. Several different formulations have been proposed, most notably by Tersoff [64, 65], and also more recently by Pettifor and co-workers [66], where the latter use a more extensive analysis of the contributions to the bond order and appeal to first principles methods to extract the parameters. One particular model has had an enormous impact in recent years due to its applicability to carbon polymorphs and hydrocarbon systems, that due to Brenner and co-workers [67]. Unsurprisingly, it has been extensively applied to fullerenes, nanotubes and diamond, as systems of topical interest. One of the other reasons for the popularity of the model is the fact that Brenner makes his code freely available. An independent implementation of the Brenner model has been made within GULP, since the capabilities of the program require that analytic derivatives to at least second order, and preferably third, are present, which is not the case for the existing code. To date, there exist three published variants of the Brenner potentials, but we have implemented just the latest of these models since it supercedes the previous two [68].

The terms in the expression for the energy in the Brenner model are expressed as follows:

$$U^{repulsive}(r) = A f^c(r) \left( 1 + \frac{Q}{r} \right) \exp(-\alpha r)$$

$$U^{attractive}(r) = f^c(r) \sum_{n=1}^3 B_n \exp(-\beta_n r)$$

where  $A$ ,  $Q$ ,  $\alpha$ ,  $B_{1-3}$ , and  $\beta_{1-3}$  are parameterised constants that depend on the atomic species, C or H, involved and  $f^c(r)$  is a cosine tapering function to ensure that the potential goes smoothly to zero of the form:

$$f^c(r) = \begin{cases} 1 & r < r^{min} \\ \frac{1}{2} \left[ 1 + \cos \left( \frac{(r-r^{min})}{(r^{max}-r^{min})} \pi \right) \right] & r^{min} < r < r^{max} \\ 0 & r > r^{max} \end{cases}$$

The bond order term itself is composed of several terms;

$$B_{ij} = \frac{1}{2} \left( b_{ij}^{\sigma-\pi} + b_{ji}^{\sigma-\pi} \right) + \frac{1}{2} \left( \Pi_{ij}^{RC} + b_{ij}^{DH} \right)$$

Note that the above expression for  $B_{ij}$  differs from the one given in the defining manuscript due to the factor of a half for the second term, but is required to obtain results that agree with those quoted. The first two terms in the above equation represent the influence of local bond lengths and angles about the atoms  $i$  and  $j$ , respectively, while the third term is a correction for radical character, and the fourth one for the influence of dihedral angles. Both of the last two terms are related to the degree of conjugation present. Full defining equations for these terms, along with the parameters, can be found in the original reference and the subsequent errata.

In the above many-body contributions to the bond order, bicubic and tricubic splines are used to interpolate parameter values. For the distributed Brenner potential code, the spline coefficients are precomputed and supplied as data files. In the present implementation the splines are performed internally on the fly. This has two advantages in that it both avoids possible transcription errors, as well as loss of precision through I/O, and allows for the possibility of parameter fitting to be readily implemented.

Because of the short-ranged nature of the Brenner potential we have implemented two different algorithms for the evaluation of the interactions. The first involves a conventional search over all atoms to find neighbours with a non-zero interaction. The second uses a spatial decomposition of the system into cubes of side length equal to the maximum range of the potential. Consequently only atoms within neighbouring cubes can possibly interact. This leads to a linear scaling algorithm that is far more efficient for large systems. A comparison is presented in the results section.

While the Brenner model does have many strengths, such as its ability to describe bond dissociation, there are also a few limitations. Perhaps the most significant is the difficulty in describing long-range forces. For instance, there is no bonding between the sheets for graphite. There have been a number of remedies proposed, including adding on two-body potentials to describe these effects, either only between different molecules, or with a tapering that removes the interaction at short-range so as not to invalidate the parameterisation. However, there are limitations to these approaches, though a more sophisticated expression for removing the contribution of long-range forces where the existing interactions due to the Brenner potential are significant shows promise [69]. As yet, this is still to be implemented.

#### 1.4.9.4 ReaxFF

The ReaxFF force field is a reactive bond order potential model that explicitly includes long-range interactions and electrostatic effects. Developed by Adri van Duin and co-workers, this model is far more sophisticated (and therefore complex) than the other bond order potentials currently available in GULP. The bond order can contain separate contributions for  $\sigma$ ,  $\pi$  and  $\pi - \pi$  bonding. From this bond order, several energy contributions are calculated:

- Bond energy
- Bond penalty energy
- Lone pair energy
- Overcoordination energy
- Undercoordination energy
- Three-body valence energy
- Three-body penalty energy
- Torsional energy
- Conjugation energy
- Hydrogen bonding

On top of these terms, there are energy contributions from van der Waals interactions that are damped at short-range where the bonding terms are important. In addition, a charge equilibration calculation is performed to determine geometry dependent charges, and thereby electrostatic and self energy contributions. It should be noted that the electrostatics in ReaxFF use a screened Coulomb expression:

$$U^{Coulomb} = \frac{1}{2} \sum_{i=1}^N \sum_{j=1}^N \frac{q_i q_j}{\left( r_{ij}^3 + \left( \frac{1}{\gamma_{ij}} \right)^3 \right)^{\frac{1}{3}}} f(r_{ij})$$

In the interests of speed, the Coulomb and van der Waals interactions are truncated at 10 Å by use of taper function,  $f$ , and so no Ewald or Parry summation is necessary. This is an implicit part of ReaxFF and so any errors associated with this truncation are subsumed into the parameterisation. When computing the charges there are two approaches available in GULP. The default method is to solve the matrix equations directly. Alternatively an iterative approach can be used which employs sparse matrix storage of the Coulomb interactions. For medium to large

systems the iterative method will be far more efficient and is recommended. When running in parallel then the iterative approach must be used. It is worth noting that the domain decomposition in GULP is particularly effective for ReaxFF because of the relatively short cut-off. Using the `spatial` keyword in combination with setting a domain size of 2-2.5 Å can often lead to maximum efficiency.

For full details of the ReaxFF formalism we refer the reader to the original paper by van Duin et al [70]. There are a few important points to note though relating to the implementation in GULP. Firstly, the formalism for ReaxFF has evolved since the original paper and some of the expressions for the bond order terms have changed. Therefore older parameter sets from the literature (approximately pre-2006) may not give exactly the right results. Secondly, at present there are only analytic first derivatives implemented for this force field. However, second derivative properties can be computed using finite difference methods with the caveat that there will be some numerical error.

Because there are a large number of parameters for a ReaxFF force field then the easiest way to run calculations is by using a library file. A number are provided already with GULP and more can be generated from the format of Adri van Duin's program (`ffield/fort.4`) using a utility that is provided. When testing converted parameter files it is important to note that the cut-offs for bond order terms (which are in the control file of Adri's program) can make a significant difference and so it is important to set these values to be the same. Furthermore, there is some additional tapering of terms added in GULP for smoothness that might lead to small changes in the values. The `verbose` keyword can be useful for checking as this causes GULP to print the energy decomposition and all the bond orders that arise from ReaxFF.

#### 1.4.9.5 EDIP

Another form of bond-order potential that is supported is the Environment-Dependent Interatomic Potential (EDIP). This was originally proposed by Bazant et al [71] and parameterised for silicon, including defective structures [72]. It consists of two- and three-body energy terms that depend on interatomic distances and the coordination number, which in turn is determined by a sum over neighbouring atoms. The original form of the potential was extended to carbon by Marks [73], which involved the addition of  $\pi$  contributions to the coordination number and a modification of the three-body term. Both forms of EDIP are supported by GULP and library files are provided containing the parameters.

#### 1.4.10 One-body interactions

Going to the other extreme of complexity from many-body interactions, we have the simplest possible atomistic model, namely the Einstein model [74]. This approach deviates from those that have gone before in that there is no interaction between

particles and all atoms are simply tethered to their lattice site by harmonic springs:

$$U^{Einstein} = \frac{1}{2} \sum_{i=1}^N k_i \left( (x_i - x_i^0)^2 + (y_i - y_i^0)^2 + (z_i - z_i^0)^2 \right)$$

This model acts as a reference state since all interactions are purely harmonic and consequently the phonon density of states, and also the structure, are independent of temperature. This implies that all the quantities that can be derived from the vibrational partition function can be analytically determined for any temperature without approximation, unlike other potential models. Even a structure that consists of atoms coupled together by a series of harmonic potentials has implied anharmonicity that arises from the derivatives of the transformation matrix from the bond-oriented pairwise frame of reference to the Cartesian one.

Given that the results of the Einstein model can be derived without recourse to a structural description, there is no need to employ an atomistic simulation program in order to calculate the required quantities. However, it can be useful to combine the Einstein model with a conventional, more accurate, representation of the interactions for use in thermodynamic integration [75]. Since the free energy of the Einstein crystal is known under any conditions, it is possible to extract free energies from molecular dynamics via a series of perturbative runs in which the Einstein model is introduced to an anharmonic potential in a series of steps, as a function of a switching parameter,  $\lambda$ , in order to obtain the difference relative to the known value.

It is worth highlighting the differences between the Einstein model and all others within the program. Because of the lack of interatomic interactions, there can be no optimisation of the structure and no strain related properties calculated. For the same reason, there is no phonon dispersion across the Brillouin zone. Finally, because the particles are tethered to lattice sites there is no translational invariance, and consequently all vibrational frequencies are positive and non-zero (assuming all force constants are specified to be likewise).

### 1.4.11 External forces

All of the above interactions are the result of interatomic forces. However, it is sometimes useful to include external forces on a system. One of the most common scenarios is to applied an external electric field. While the application of an electric field is allowed in any arbitrary direction, it is usually only sensible to apply this in a non-periodic direction. Only attempt to apply an electric field in a periodic direction if you are an expert and really know what you are doing. You have been warned! For example, in a slab calculation then a field can be applied normal to the surface leading to a polarisation of the atoms based on their charges. There are several important points to note when using an electric field. Firstly, when optimising the system it is important to fix at least one atom other the force will cause the system

to translate indefinitely since translational invariance is broken. Secondly, because a field will generally not conform to the space group of a material, the turning off of symmetry is enforced when a field is applied. Finally, there is no absolute energy of interaction with an electric field and so the energy is computed relative to the initial configuration,  $\alpha_0$ :

$$U^{field} = \sum_{i=1}^N \sum_{\alpha} q_i V_{\alpha} (\alpha^i - \alpha_0^i)$$

A consequence of this relative definition of the energy is that there will be a discontinuity in the absolute energy, but not the forces, on restarting.

In the same way that an external force can be applied by an electric field, it is also possible to specify an external force on specific atoms without reference to their charge. This can be static or time-dependent if performing molecular dynamics. For the time-dependent case, the force is of the oscillatory form;

$$F = A \cos(2\pi(Bt + C))$$

where  $t$  represents the time.

## 1.4.12 Potential truncation

As previously mentioned, all potentials must have a finite range in order to be calculable. However, there are a range of conditions for a potential to act between two species, as well as various methods for handling the truncation of potentials. Hence, it is appropriate to describe a few of these issues here.

### 1.4.12.1 Radial truncation

The natural way to truncate a potential is through the use of a spherical cut-off radius. It is also possible to specify a minimum radius from which the potential should act too. Hence, it is possible to create multiple distance ranges within a potential with different forcefield parameters, as well as to overlay different potentials. Of course, where there is a cut-off boundary, there will be a discontinuity in the energy for most interaction terms, unless the potential smoothly tends to zero at that distance by design. This can lead to problems during energy minimisation, since the point of lowest energy may not be a point of zero force anymore, and in other simulation techniques, such as molecular dynamics, where energy conservation will be affected by discontinuities. Other than increasing the cut-off radius, there are several approaches to minimising these difficulties as described briefly in the subsequent subsections.

### 1.4.12.2 Cut and shift

To avoid a discontinuity in the energy at the potential cut-off, a constant shift can be added to the potential so that the energy at the cut-off boundary becomes zero:

$$U_{ij}^{shifted}(r_{ij}) = U_{ij}(r_{ij}) - U_{ij}(r_{cut})$$

where  $r_{cut}$  is the cut-off radius. However, the gradient is still discontinuous at the cut-off distance, so the procedure can be extended by adding a linear term in the distance such that the gradient is also zero at this point. While in principle this method can be applied to make any order of derivative go exactly to zero at the boundary by construction, the increasing powers of distance lead to the correction terms modifying the variation of the potential with distance more strongly as the order rises. This characteristic, that the potential is modified away from the point of cut-off, makes this method of smoothing less desirable than some.

### 1.4.12.3 Tapering

In this approach, the potential is multiplied by a smooth taper function that goes to zero, both for its value and its derivatives typically up to second order. This is usually applied over a short range from an inner radius,  $r_{taper}$ , to the cut-off distance:

$$U_{ij}(r_{ij}) \begin{cases} U_{ij}(r_{ij}) & r_{ij} < r_{taper} \\ U_{ij}(r_{ij}) f^{taper}(r_{ij}) & r_{taper} < r_{ij} < r_{cut} \\ 0 & r_{ij} > r_{cut} \end{cases}$$

Hence, within  $r_{taper}$  the potential is unchanged. There are numerous possible functional forms that satisfy the required criteria for a taper function. Perhaps the two most commonly used are a fifth order polynomial or a cosine function with a half a wavelength equal to  $r_{cut} - r_{taper}$ . Both of these are available within GULP as part of the overall two-body potential cut-off.

### 1.4.12.4 Molecular mechanics

In the simulation of molecular systems, it is often preferable to use a molecular mechanics forcefield. This implies that certain cut-offs are determined by connectivity, rather than by distance alone. For example, particular potentials may only act between those atoms that are bonded, such as a harmonic force constant, whereas others may specifically only act between those that aren't covalently linked. Fundamental to this is the notion of a bond between atoms. Within GULP these can either be determined automatically by comparing distances between pairs of atoms with the sum of the covalent radii, multiplied by a suitable tolerance factor, or alternatively the connectivity can be user specified. From this information, it is possible

for the program to determine the number of molecules and, in the case of periodic systems, their dimensionality.

A number of options are possible that control how both the potentials and the Coulomb terms act, as described below:

- *Bonded*: A potential may act only between atoms that are bonded (1-2).
- *Exclude 1-2*: The case of bonded atoms is specifically omitted from the allowed interactions.
- *Exclude 1-3*: Interactions between bonded atoms and those with a common bonded atom are excluded.
- *Only 1-4*: Potentials only act between atoms that are three bonds apart. This can be useful in the description of torsional interactions.
- *1-4 and greater*: Potentials only act between atoms that are three bonds apart or further. This can be useful in the description of torsional interactions.
- *Intramolecular*: Only interactions within a given molecule are permitted for the potential.
- *Intermolecular*: Only interactions between atoms of different molecules are allowed.
- *Bond order*: An interaction may be limited to bonds of a specific order. Valid bond orders are; single, double, triple, quadruple, resonant, amide, custom, half, quarter and third. Note, that the automatic bond calculation assigns all bonds to be single bonds. Hence, to use this facility it is necessary to use the `connect` option to set the bond order between particular atoms.
- *Molecular Coulomb subtraction*: All electrostatic interactions between atoms within the same molecule are excluded. This implies that the charges on the atoms within a molecule purely serve to describe its interaction with other molecules.
- *Molecular mechanics Coulomb treatment*: This implies that Coulomb terms are excluded for all 1-2 and 1-3 interactions. In addition, it is sometimes desirable to remove, or scale down, 1-4 electrostatic interactions too. The benefit of this is that the parameters of the intramolecular potentials then have a direct correspondance with the equilibrium bond lengths, bond angles and localised vibrational frequencies. It should be noted that two-body potentials can also be scaled for the 1-4 interaction, if so desired.

### 1.4.13 Partial occupancy

Many materials have complex structures which include disorder of one form or another. This can typically consist of partial occupancy where there are more symmetry degenerate sites than there are ions to occupy them, or where there are mixtures of ions that share the same structural position. In principle, the only way to accurately model such systems is to construct a supercell of the material containing a composition consistent with the required stoichiometry and then to search through configuration space for the most stable local minima, assuming the system is in thermodynamic equilibrium (which may not always be the case). This includes allowing for the contribution from the configurational entropy to the relative stability. While this approach has been taken for several situations, most notably some of the disordered polymorphs of alumina [76, 77], it is demanding because of the sheer number of possibilities which increases with a factorial dependence.

There is an approximate approach to the handling of disorder, which is to introduce a mean-field approach. Here all atoms are assigned an occupancy factor,  $o_i$ , where  $0 \leq o_i \leq 1$ , and all interactions are then scaled by the product of the relevant occupancies:

$$U_{ij}^{m-f} = o_i o_j U_{ij}$$

$$U_{ijk}^{m-f} = o_i o_j o_k U_{ijk}$$

and so on for high order terms. This approach can be utilised in any atomistic simulation program by scaling all the relevant potential parameters according to the above rules. However, for complex forcefields this can be tedious, and it also precludes fitting to multiple structures where the occupancies of ions of the same species are different. Hence, the inclusion of partial occupancies has been automated in GULP so that only the site occupancies have to be specified and everything else is handled by the program. This includes the adding of constraints so that atoms that share the same site move together as a single particle, as well as checking that the sum of the occupancies at any given site do not exceed one. It should be noted that the handling of partial occupancies requires particular care in determining phonons where the matrix elements for all coupled species must be condensed in order to obtain the correct number of modes.

The use of a mean field model is clearly an approximation. For structures, it can often work quite well, since crystallography returns an average anyway. However, for other quantities, such as thermodynamic data it has limitations. For example, the excess enthalpy of mixing of two phases is typically overestimated since the stabilisation that arises from local structural distortions to accommodate particular species is omitted [78].

### 1.4.14 Structural optimisation

Having defined the internal energy of a system, the first task to be performed is to find the minimum energy structure for the present material. To be more precise, this will typically be a local minimum on the global potential energy surface that the starting coordinates lie closest to. Trying to locate the global energy minimum is a far more challenging task and one that has no guarantee of success, except for the simplest possible cases. There are several approaches to searching for global minima, including simulated annealing [79], via either the Monte Carlo or molecular dynamics methods, and genetic algorithms [80, 81]. Here we will focus the quest for a local minimum.

At any given point in configuration space, the internal energy may be expanded as a Taylor series:

$$U(x + \delta x) = U(x) + \frac{\partial U}{\partial x} \delta x + \frac{1}{2!} \frac{\partial^2 U}{\partial x^2} (\delta x)^2 + \dots$$

where the first derivatives can be collectively written as the gradient vector,  $g$ , and the second derivative matrix is referred to as the Hessian matrix,  $H$ . This expansion is usually truncated at either first or second order, since close to the minimum energy configuration we know that the system will behave harmonically.

If the expansion is truncated at first order then the minimisation just involves calculating the energy and first derivatives, where the latter are used to determine the direction of movement and a line search is used to determine the magnitude of the step length. In the method of steepest descents this process is then repeated until convergence. However, this is known to be an inefficient strategy since all the previous information gained about the energy hypersurface is ignored. Hence it is far more efficient to use the so-called conjugate gradients algorithm [82] where subsequent steps are made orthogonal to the previous search vectors. For a quadratic energy surface, this will converge to the minimum in a number of steps equal to the number of variables,  $N$ .

If we expand the energy to second order, and thereby use a Newton-Raphson procedure, then the displacement vector,  $\Delta x$ , from the current position to the minimum is given by the expression;

$$\Delta x = -H^{-1}g$$

which is exact for a harmonic energy surface (i.e. if we know the inverse Hessian matrix and gradient vector at any given point then we can go to the minimum in one step). For a realistic energy surface, and starting away from the region close to the minimum, then the above expression becomes increasingly approximate. Furthermore, there is the danger that if the energy surface is close to some other stationary point, such as a transition state, then simply applying this formula iteratively may

lead to a maximum, rather than the minimum. Consequently, the expression is modified to be

$$\Delta x = -\alpha H^{-1} g$$

where  $\alpha$  is a scalar quantity which is determined by performing a line search along the search direction to find the one-dimensional minimum and the procedure becomes iterative again, as per conjugate gradients.

By far, the most expensive step of the Newton-Raphson method, particularly once the size of the system increases, is the inversion of the Hessian. Furthermore, the Hessian may only vary slowly from one step to the next. It is therefore wasteful and undesirable to invert this matrix at every step of the optimisation. This can be avoided through the use of updating formulae that use the change in the gradient and variables between cycles to modify the inverse Hessian such that it approaches the exact matrix. Two of the most widely employed updating schemes are those due to Davidon-Fletcher-Powell (DFP) [83] and Broyden-Fletcher-Goldfarb-Shanno [84], which are given below:

$$H_{i+1}^{DFP} = H_i^{DFP} + \frac{\Delta x \otimes \Delta x}{\Delta x \cdot \Delta g} - \frac{(H_i^{DFP} \cdot \Delta g) \otimes (H_i^{DFP} \cdot \Delta g)}{\Delta g \cdot H_i^{DFP} \cdot \Delta g}$$

$$H_{i+1}^{BFGS} = H_i^{BFGS} + \frac{\Delta x \otimes \Delta x}{\Delta x \cdot \Delta g} - \frac{(H_i^{BFGS} \cdot \Delta g) \otimes (H_i^{BFGS} \cdot \Delta g)}{\Delta g \cdot H_i^{BFGS} \cdot \Delta g} +$$

$$\left[ \Delta g \cdot H_i^{BFGS} \cdot \Delta g \right] v \otimes v$$

$$v = \frac{\Delta x}{\Delta x \cdot \Delta g} - \frac{H_i^{BFGS} \cdot \Delta g}{\Delta g \cdot H_i^{BFGS} \cdot \Delta g}$$

The BFGS algorithm is generally recognised as the more efficient one and so is the default optimiser. However, if performing a transition state search then DFP is preferred due to the different tendencies of the updates with regard to targetting a positive definite character for the Hessian. The practical approach taken in a BFGS optimisation is to initialise the Hessian by performing an exact inversion of the second derivatives and then subsequently updating for a number of cycles. Occasionally it is necessary to calculate the exact inverse Hessian again. This is triggered by one of a number of possible situations:

- The maximum number of cycles for updating is exceeded
- The angle between the gradient vector and the search vector exceeds a given threshold
- The energy has dropped by more than a certain threshold in one cycle, so the curvature is likely to have altered

- The energy cannot be lowered by line minimisation along the current search vector

There is one variation upon the BFGS strategy above, in which, rather than calculating the exact second derivative matrix and inverting it, the Hessian is initialised approximately and then updated such that it tends to the true Hessian. Two possible starting approximations to the Hessian are either to use a unit matrix or to perform a finite difference estimate of the on-diagonal elements only in order to achieve better preconditioning. By taking this approach the cost is similar to conjugate gradients, though with a higher memory requirement, but the convergence is typically twice as fast since more information from previous energy/gradient evaluations is retained.

The choice of appropriate algorithm for minimisation depends on the size of the system and number of variables. For small systems, the Newton-Raphson methods that use second derivatives will be far more efficient. As the size of system increases, the computational cost of building and inverting the Hessian matrix will ultimately grow as  $N^3$  while the memory requirements also increase as  $N(N+1)/2$  for lower-half triangular storage. Hence, ultimately it will become necessary to use first the unit Hessian approach and then ultimately the conjugate gradients method as  $N$  continues to increase. This balance may also be influenced by the use of symmetry, where possible, as will be discussed later. A further issue is that for minimisation where the initial structure lies outside the harmonic region, Newton-Raphson methods may not be particularly advantageous, whereas they will be as convergence is approached. Hence GULP includes the facility to change the minimiser from, for example, conjugate gradients, to BFGS when a criterion is met, such as the gradient norm falling below a specified threshold.

Aside from the minimisation algorithm itself, something should be said about the criteria for convergence of an optimisation. Typically some or all of the following can be checked for convergence:

- the gradient norm (root mean square gradient per variable)
- the maximum individual gradient component
- the norm of the estimated displacement vector
- the change in the function (energy, enthalpy or free energy) between successive cycles
- the change in the variables between successive cycles

Normally all of these quantities are well converged (and often excessively so - i.e. well beyond chemical accuracy) with Newton-Raphson optimisation for a force-field. Occasionally convergence is not achieved, which is nearly always indicative

of a significant discontinuity in the energy surface, such as that caused by inter-atomic potential cut-offs. Ideally all potentials should be tapered so that their value, first and second derivatives go smoothly to zero at the cut-off radius. In practice, most repulsive potentials are negligibly small by a typical cut-off distance of 10 Angstroms and so it is usually the attractive potentials that mimic dispersion that are responsible. The other common cause are discontinuities in bonding - i.e. an atom is displaced beyond a bond cut-off during minimisation and so the whole nature of the interaction potential changes. While this can be overcome by maintaining a fixed connectivity list, the real issue is that the forcefield is inadequate for the system being modelled.

All of the above discussion has related to the search for a local minimum where the first derivatives are zero and the second derivative matrix is positive definite. However, there are many instances in which it is necessary to locate other stationary points on the potential energy surface, and in particular transition states, such as for ion diffusion. There are a number of algorithms available for locating transition states, of which the most widely used class in solid state optimisations tend to be constrained minimisations. Here the reaction path is discretised in some way and the system minimised so that the variable changes are orthogonal to the direction of the pathway. Arguably the most successful and widely used approach is the Nudged Elastic Band method [85]. However, the disadvantage of these constrained techniques is that some assumption usually has to be made about the nature of the mechanism before the calculations are performed. In contrast, there are algorithms which use Newton-Raphson techniques in order to locate stationary points with an arbitrary number of negative eigenvalues for the Hessian (where a transition state is the special case of a single negative eigenvalue). In the case of GULP, the method implemented is so-called Rational Functional Optimisation (RFO) [86].

In the RFO method, the inverse Hessian matrix is diagonalised to obtain the eigenvalues and eigenvectors. From the eigenvalues it is possible to examine whether the matrix has the required characteristics for the stationary point being sought. If the number of negative eigenvalues is incorrect, then the spectrum is level-shifted to correct this and the search direction constructed appropriately. By default, the Hessian modes with the smallest eigenvalues are followed towards the corresponding stationary point. However, eigenvector following can also be performed in which different modes from the spectrum are selected. Hence the RFO optimiser will, in principle, locate various possible transition states starting from a given position. There are a few provisos though, most notably that there must be a non-zero projection of the gradient vector in the search direction leading to the stationary point. Furthermore, the step size must be quite small in order to ensure convergence to a transition state. Since the line search can no longer be used, the optimisation relies on a fixed proportion of the search vector to achieve convergence. In the implementation in GULP, this step magnitude is correlated to the gradient norm, so that as the calculation approaches convergence, and therefore enters the harmonic region, the

proportion of the search vector used approaches 100%. Hessian updating can also be applied while optimising towards a transition state. However, because the rate of convergence depends more critically on the inverse Hessian being accurate, more frequent exact calculations are usually required. RFO can also be used to accelerate optimisations to minima once the harmonic region is approached, since it is able to better handle soft modes. In extreme cases, the number of cycles is reduced by an order of magnitude by use of RFO towards the end of an optimisation, as well confirming that the Hessian has the required structure. A final note of caution is that this method does not guarantee that a local minimum has been achieved, even if the Hessian is confirmed as having all positive eigenvalues. This is because the Hessian only spans the space of the allowed optimisation variables and there may be directions of negative curvature with respect to constrained degrees of freedom. Hence, a  $\Gamma$ -point phonon calculation should always be used as a final validation.

Often it is desirable to apply external forces to a system when performing a minimisation. The most common example is the application of an isotropic external pressure, such as used in the determination of the equation of state for a material. This situation can be straightforwardly handled by making the objective function for minimisation the enthalpy instead of the internal energy:

$$H = U + pV$$

More complex is the case when an external force is to be applied to individual atoms. This arises when the program is being coupled to a separate quantum mechanical calculation as part of a QM/MM method (i.e. a quantum mechanics/molecular mechanics coupled calculation). Here the forces on the forcefield atoms arise from the quantum mechanical region, which is not explicitly considered in the present calculation. Adding the negative of the external forces to the internal derivatives is simple to implement. However, for minimisation the internal energy is no longer a well-behaved objective function (i.e. the minimum of the internal energy does not correspond to a configuration of zero gradients). One solution to this would be to minimise the gradient norm instead, but this requires either one order higher of energy derivatives or that conjugate gradients are used to minimise, which is less efficient.

The approach implemented within GULP to handle the application of external forces is to define a new additional term in the internal energy, which is the work due to the external force:

$$U^{external} = - \int_{initial}^{final} F^{external} \cdot \alpha$$

where  $\alpha$  represents the vector of atomic coordinates and  $F^{external}$  is the vector of external forces. With this correction to the internal energy, the minimum coincides with force balance and so the full range of standard minimisers are applicable. However, the final energy is an arbitrary quantity unless taken with respect to a standard reference set of atomic positions.

The framework of structural optimisation in GULP is designed to be flexible and to allow the user as much freedom as possible to control the degrees of freedom. Intrinsically, there are four main classes of variables possible within the forcefield models available, namely, atomic coordinates, the unit cell periodicity (for polymers, surfaces, and bulk materials), shell coordinates, and breathing shell radii. Each variable can be controlled by optionally specifying a binary flag that indicates whether it is to be varied or held fixed. Alternatively there are keywords that select default settings of the flags, such that those quantities not constrained by symmetry are allowed to vary. In particular, the defaults automatically handle the fact that one atom must be fixed in order to remove the three translational degrees of freedom. For bulk systems, the first atom is usually the one chosen to be fixed, since the choice is arbitrary. In the case of slab calculations, the atom nearest the centre of the slab is fixed since this is the one least likely to move by a substantial amount. When there is a centre of symmetry in the space group, then there is no need to fix any atoms since the origin is already immovable. The default optimisation options also automatically construct the constraints necessary to preserve the space group symmetry as the atoms are displaced.

When minimising periodic systems there are a couple of choices that have to be made. The first concerns the representation of the unit cell. This can be achieved through either the unit cell parameters,  $a$ ,  $b$ ,  $c$ ,  $\alpha$ ,  $\beta$ ,  $\gamma$ , or via the Cartesian cell vectors as a (3x3) matrix. Correspondingly, when optimising the unit cell this can be done with respect to the cell parameters directly, the Cartesian cell vectors or by using a strain tensor. Here we chose to use the Voigt strain tensor to scale the Cartesian lattice vectors:

$$\begin{pmatrix} 1 + \epsilon_1 & \frac{1}{2}\epsilon_6 & \frac{1}{2}\epsilon_5 \\ \frac{1}{2}\epsilon_6 & 1 + \epsilon_2 & \frac{1}{2}\epsilon_4 \\ \frac{1}{2}\epsilon_5 & \frac{1}{2}\epsilon_4 & 1 + \epsilon_3 \end{pmatrix}$$

Through using the six Voigt strains as the variables, we have the same advantage as working with the unit cell parameters in that cell rotation is eliminated by construction. However, as will be demonstrated later, the derivatives with respect to strain are closely related to the Cartesian internal derivatives and therefore readily calculated at almost no extra cost. We should note that when strain derivatives are taken, they are done so with respect to infinitesimal strain about the current configuration, rather than with respect to a single constant reference cell. For 2-D systems, the strain tensor is correspondingly reduced to a (2x2) matrix and for polymers there is a single scalar strain value. At this point we should also comment on the absolute spatial orientation of systems, since this a matter of convention, rather than an absolute choice. For 3-D systems, GULP orients the  $a$  cell vector along the  $x$ -axis, the  $b$  cell vector in the  $xy$ -plane, and then the orientation of the  $c$  cell vector is fixed, except for an issue of chirality, which is resolved by selecting the orientation that has a positive dot product with the  $z$ -axis. For 2-D systems, the same two conventions are followed for the surface vectors, which leaves the surface normal

parallel to the  $z$ -axis. Finally, for 1-D systems, the repeat direction is taken to lie along the  $x$ -axis.

By default, when the derivatives of the energy with respect to strain are computed then the values are those in the limit of zero strain. In other words, the strains are determined with respect to straining the current structure at that point of the optimisation. From version 5.2 onwards, there is now also the option to define a reference structure and then to use the finite strain values with respect to this as the optimisation variables. This means that the strain derivatives are evaluated at finite strain. The value of this alternative is that it is possible to drive the shear of a structure, for example, by altering the strain with respect to the reference while keeping one or more values fixed.

### 1.4.15 Genetic algorithms

The approach to minimisation of a structure has already been discussed when considering the case of a local stationary point. Now we turn to consider the quest for a global minimum. In order to do this, a technique is required that allows barriers to be overcome in some way. While hyperdynamic [87] and basin-filling approaches are becoming increasingly useful, the more traditional approach has been to employ methods that incorporate random changes in the structure with a tendency to minimise a so-called cost function. Here the cost function is a quantity that represents a measure of the quality of the structure. In the most obvious case, this might be just the total energy of the system. However, because stochastic processes require many moves, it is often convenient to use a more computationally efficient cost function. For example, one form that has previously been successfully used for oxides is a combination of bond-valence sum rules with a short-ranged Coulomb penalty that prevents ions of like charge approaching each other [88].

There are two main approaches to the global optimisation of structures via a random walk - the Monte Carlo method [89] and Genetic Algorithms (GAs) [80, 88]. Although both are in principle equally capable of performing the task, it could be argued that genetic algorithms are more naturally suited to coarse grained global optimisation, while the Monte Carlo technique is also able to yield an integration within the phase space of a statistical ensemble. Here we will concentrate on the use of GAs.

In the genetic algorithm, each optimisation variable is discretised within a specified range. This is particularly well suited to fractional coordinates where there are natural bounds of 0 and 1. Then all that need be specified is the number of allowed intervals within the range. If a coarse grid of points is specified then configuration space will be rapidly searched, but the solution will be very approximate and the global minimum may not be resolvable with the level of resolution available. Conversely, if a fine grid is utilised then the search is capable of locating a more accurate estimate of the global minimum. However, because of the large number of

possible configurations, the optimal state may never be visited. Clearly a hierarchical approach may be ideal, where a coarse discretisation is initially used and then refined as the process progresses. The state of each configuration is represented by a binary number which is a concatenation of the binary representations of the grid point numbers for each individual variable.

The fundamental idea behind genetic algorithms is to perform a process that mimics natural selection through survival of the fittest. Here the concept of fitness equates to the value of the chosen cost function. Each cycle of the GA begins with an even number of so-called parents. In the first step these are typically randomly chosen initial configurations. These parents then are randomly paired up in order to breed to produce two children in order to maintain the size of the population. This is the tournament phase, in which a probability is set for the parent with the lower cost function to go through to the next generation and to form the children. A random number is chosen and compared to this probability in order to make the decision. Choosing this probability threshold is a balance between wanting to ensure that the better configurations survive against trying to maintain diversity in the population during the initial stages. More sophisticated tournament procedures have also been proposed where an exponential weighting is used in favour of the fitter candidates. Usually the number of children is set equal to the number of parents in order to maintain a stable population size.

Apart from the tournament phase, there are two other processes that can occur, which are mutation and crossover. In the mutation phase, a number of binary digits are changed from 0 to 1 or *vice versa*. Again the chance of this occurring is determined by comparison of a random number to the mutation probability. During crossover, two configurations are selected, the binary strings split at a random point, and the two parts switched between configurations. Both mutation and crossover represent genetic defects that are designed to introduce randomness with the aim of exploring configuration space.

The above three genetic algorithm steps are applied repeatedly with the aim of gradually reducing the cost functions of the population down and focussing in on the global minimum. When the procedure is stopped after the specified number of steps, then hopefully the configuration with the lowest cost function will be the global minimum, though this can never be known for certain for complex systems. If the cost function used was an approximation to the total energy that is ultimately desired to be the criterion for selection, then a selection of the best configurations can be subsequently minimised according to the total energy and hopefully the global minimum will lie amongst this set, even though it is not the structure with the absolutely lowest cost function.

There are several possible refinements to the genetic algorithm procedure, which, somewhat appropriately, is itself still evolving. However, the above basic formulation is capable of correctly predicting the atomic coordinates of binary, and even some ternary oxides, given the unit cell. Indeed, the method had an early success

through assisting in the solution of the previously unknown structure of  $Li_3RuO_4$  [81]. More details of the background to, and application of, the genetic algorithm for solid state structural optimisation can be found elsewhere [88].

## 1.4.16 Calculation of bulk properties

Having determined the optimised structure for a material it is then possible to calculate a wide range of physical properties based on the curvature of the energy surface about the minimum. These include both mechanical properties, such as the bulk modulus and elastic constants, as well as dielectric properties. The expressions used for the calculation of the individual properties that may be determined routinely from the second derivative matrix are detailed below.

### 1.4.16.1 Elastic constants

The elastic constants represent the second derivatives of the energy density with respect to strain:

$$C_{ij} = \frac{1}{V} \left( \frac{\partial^2 U}{\partial \epsilon_i \partial \epsilon_j} \right)$$

thereby describing the mechanical hardness of the material with respect to deformation. Since there are 6 possible strains within the notation scheme we employ, the elastic constant tensor is a 6 x 6 symmetric matrix. The 21 potentially independent matrix elements are usually reduced considerably by symmetry [90]. For example, for a cubic material the only unique elements are  $C_{11}$ ,  $C_{12}$ , and  $C_{44}$ . The calculation of elastic constants is potentially very useful, since the full tensor has only been measured experimentally for a very small percentage of all known solids. This is primarily because the practical determination typically requires single crystals with a size of a few micrometres at least.

In calculating the second derivatives of the energy with respect to strain it is important to allow for the response of all internal degrees of freedom of the crystal to the perturbation. If we introduce the following notation for the second derivative matrices:

$$D_{\epsilon\epsilon} = \left( \frac{\partial^2 U}{\partial \epsilon \partial \epsilon} \right)_{internal}$$

$$D_{\epsilon i} = \left( \frac{\partial^2 U}{\partial \epsilon \partial \alpha_i} \right)_{\epsilon}$$

$$D_{ij} = \left( \frac{\partial^2 U}{\partial \alpha_i \partial \beta_j} \right)_{\epsilon}$$

then the full expression for the elastic constant tensor can be written as:

$$C = \frac{1}{V} \left( D_{\epsilon\epsilon} - D_{\epsilon i} D_{ij}^{-1} D_{j\epsilon} \right)$$

The elastic compliances,  $S$ , can be readily calculated from the above expression by inverting the matrix (i.e.  $S = C^{-1}$ ). The above expressions are valid for adiabatic conditions and at zero pressure. The adiabatic elastic constants can be extended to the case of finite external pressure according to the corrections:

$$C_{\alpha\beta\gamma\zeta} = \frac{1}{V} \left( \frac{\partial^2 U}{\partial \varepsilon_{\alpha\beta} \partial \varepsilon_{\gamma\zeta}} \right) + \frac{p}{2} (2\delta_{\alpha\beta}\delta_{\gamma\zeta} - \delta_{\alpha\zeta}\delta_{\beta\gamma} - \delta_{\alpha\gamma}\delta_{\beta\zeta})$$

Here the strains are expressed directly in terms of the Cartesian components, as opposed to in the Voigt notation, so as to make the corrections more transparent.

Under isothermal conditions the expressions for the elastic constant tensor are analogous, except for the fact that the differentials are with respect to the Helmholtz free energy, rather than the internal energy. Because the evaluation of the isothermal elastic constants requires the fourth derivative of the internal energy with respect to internal coordinates and strains, this is not presently implemented within GULP analytically. However, finite differences may be used in combination with free energy minimisation in order to determine this tensor.

#### 1.4.16.2 Bulk and shear moduli

Like the elastic constant tensor, the bulk ( $K$ ) and shear ( $G$ ) moduli contain information regarding the hardness of a material with respect to various types of deformation. Experimentally a bulk modulus is much more facile to determine than the elastic constant tensor. If the structure of a material is studied as a function of applied isotropic pressure, then a plot of pressure versus volume can be fitted to an equation of state where the bulk modulus is one of the curve parameters. Typically a third or fourth order Birch-Murnaghan equation of state is utilised. Alternatively, the bulk and shear moduli are also clearly related to the elements of the elastic constant. However, there is no unique definition of this transformation. Here we give three different definitions due to Reuss, Voigt and Hill [90]. Below are the equations for the Reuss and Voigt definitions, while the Hill values are defined as the average of the other two:

$$K_{Voigt} = \frac{1}{9} (C_{11} + C_{22} + C_{33} + 2(C_{12} + C_{13} + C_{23}))$$

$$K_{Reuss} = (S_{11} + S_{22} + S_{33} + 2(S_{12} + S_{13} + S_{23}))^{-1}$$

$$G_{Voigt} = \frac{1}{15} (C_{11} + C_{22} + C_{33} + 3(C_{44} + C_{55} + C_{66}) - C_{12} - C_{13} - C_{23})$$

$$G_{Reuss} = \frac{15}{4(S_{11} + S_{22} + S_{33} - S_{12} - S_{13} - S_{23}) + 3(S_{44} + S_{55} + S_{66})}$$

### 1.4.16.3 Young's moduli

When a uniaxial tension is applied to a material then the lengthening of the material is measured according to the strain. The ratio of stress to strain defines the value of the Young's modulus for that axis:

$$Y_{\alpha} = \frac{\sigma_{\alpha\alpha}}{\epsilon_{\alpha\alpha}}$$

Since a material will always increase in length under tension, the value of this quantity should always be positive. The Young's moduli in each of the Cartesian directions can be calculated from the elastic compliances:

$$Y_x = S_{11}^{-1}$$

$$Y_y = S_{22}^{-1}$$

$$Y_z = S_{33}^{-1}$$

### 1.4.16.4 Poisson's ratio

Complementary to Young's modulus is the Poisson ratio, which measures the change in a material at right angles to the uniaxial stress. Formally it is defined as the ratio of lateral to longitudinal strain under a uniform, uniaxial stress. The expression used to calculate this property, assuming an isotropic medium, is given below [90]:

$$\sigma_{\alpha}(\beta) = -S_{\alpha\alpha\beta\beta}Y_{\beta}$$

Because most materials naturally shrink orthogonal to an applied tension this leads to positive values for Poisson's ratio, with a theoretical maximum of 0.5. Typical values for many materials lie in the range 0.2-0.3, though negative values are also known. For an isotropic material this quantity can also be related to the bulk modulus:

$$K = \frac{1}{3} \frac{Y}{(1 - 2\sigma)}$$

### 1.4.16.5 Acoustic velocities

The acoustic velocities are key quantities in the interpretation of seismic data. The polycrystalline averages of these acoustic velocities in a solid can be derived from the bulk and shear moduli of the material, as well as the density,  $\rho$ . There are two values, that for a transverse wave,  $V_s$ , and that for a longitudinal wave,  $V_p$ , which are given by:

$$V_s = \sqrt{\frac{G}{\rho}}$$

$$V_p = \sqrt{\frac{4G + 3K}{3\rho}}$$

As to be expected, there is some degree of variability in the calculated values according to the definition of the bulk and shear moduli employed.

#### 1.4.16.6 Static and high frequency dielectric constants

The dielectric properties of a material are of crucial importance in many contexts, including those beyond the strictly bulk properties. For example, the response of a solid to a charged defect depends on the inverse of the dielectric constant. The actual value of the dielectric constant varies according to the frequency of the electromagnetic field applied. Commonly two extreme values are quoted, namely the static and high frequency dielectric constants. In the static limit all degrees of freedom of the crystal, both nuclear and electronic, are able to respond to the electric field and therefore to provide screening. At the high frequency limit the oscillation is greater than the maximum vibrational frequency of the material and therefore only the electrons are able to respond to the perturbation fast enough. Here we describe how to calculate these extremal values, while the case of intermediate frequencies will be presented later.

The static dielectric constant (3 x 3) tensor can be determined from the Cartesian second derivative matrix of all particles,  $D_{\alpha\beta}$ , and the vector,  $q$ , containing the charges of all particles:

$$\epsilon_{\alpha\beta}^0 = \delta_{\alpha\beta} + \frac{4\pi}{V} (qD_{\alpha\beta}^{-1}q)$$

The expression for the high frequency dielectric constant is identical to that for the static equivalent, except that the second derivative matrix,  $D_{\alpha\beta}$ , now only includes the Cartesian components for any shells present within the model. If a core only model is being used then the high frequency dielectric tensor is just a unit matrix. Hence information regarding the high frequency dielectric constants is particularly useful in determining the parameters of a shell model due to the relatively direct correlation.

Because the dielectric constant tensor depends on the inverse second derivative matrix, it has many of the characteristics of the Hessian matrix and is therefore quite a sensitive indicator of whether a potential model is sensible. Extreme values, particularly negative ones, instantly point to the fact that the potential model is inadequate or that the system wishes to undergo a symmetry change.

#### 1.4.16.7 Refractive indices

The refractive indices of a material,  $n$ , are simply related to the dielectric constant by:

$$n = \sqrt{\epsilon}$$

For orthorhombic, tetragonal or cubic unit cells, in the standard orientation, this represents a trivial mapping since the dielectric constant tensor is a diagonal matrix and so the square roots can be taken directly. For other crystal systems it is necessary to diagonalise the tensor first and then find the refractive indices in this new axis eigensystem.

#### 1.4.16.8 Raman susceptibility tensors

The calculation of Raman intensities uses the Raman susceptibilities. Here the key quantities are related to the derivatives of the high frequency dielectric constant tensor with respect to the atomic displacements through the quantity  $\chi$ :

$$\chi = \frac{\epsilon^\infty - \delta}{4\pi}$$

If the keyword is specified to compute the Raman properties then the derivatives of  $\chi$  with respect to the Cartesian coordinates of each atom in the system are output in units of inverse Angstroms. Because this requires the use of analytical third derivatives this functionality will only work for a subset of force field models where the third derivatives are available, which includes two-, three- and four-body potentials. Note that because this is the derivative of the high frequency dielectric constant then this is only useful if you are working with a shell model, otherwise the answer will be zero. Strictly speaking the derivatives output are components of the Raman susceptibility tensor and they must be projected onto the eigenvectors of the phonons and scaled by a volume factor to get the true susceptibility tensor. If the Raman susceptibilities are computed then these will be used to determine the intensities of the vibrations, if this keyword is specified. The Raman intensity depends on the direction of the incoming and outgoing wave, which can be set using an option.

#### 1.4.16.9 Piezoelectric constants

The piezoelectric constants are key quantities in many technological applications, since they govern the correlation between strain in a material and applied electric field for non-centrosymmetric materials (centrosymmetric materials necessarily have zero for all piezoelectric constants). There are several different types of piezoelectric constant too, depending on whether it is the polarisation being induced by a given strain that it is being considered or the stress/strain induced by an applied electric field. In GULP, both the piezoelectric stress constants,  $d$ , and the piezoelectric strain constants,  $e$ , are calculated:

$$d_{\alpha i} = \frac{\partial P_\alpha}{\partial \sigma_i}$$

$$e_{\alpha i} = \frac{\partial P_\alpha}{\partial \epsilon_i}$$

The two sets are related by a transformation involving either the elastic constant, or the elastic compliance tensor, depending on the direction. The piezoelectric strain constants are calculated from the Cartesian second derivative matrices according to:

$$e_{\alpha i} = - \sum_{k=1}^{N-1} \left[ \frac{4\pi}{V} q_k \left( \frac{\partial^2 U}{\partial \alpha \partial \beta} \right)^{-1} \left( \frac{\partial^2 U}{\partial \beta \partial \epsilon_i} \right) \right]$$

The above piezoelectric strain constants can be readily transformed into piezoelectric stress constants by multiplication by the elastic compliance tensor.

#### 1.4.16.10 Electrostatic potential, electric field and electric field gradients

The electrostatic site potential is a measure of the Coulomb interaction per unit charge experienced by an ion at a given position in space. This can be formally defined by;

$$V_i = \sum_{j=1}^N \frac{q_j}{r_{ij}}$$

where the summation explicitly excludes the case where  $i = j$ . Clearly this is closely defined to the definition of the electrostatic energy, the two simply being related by;

$$U^{electrostatic} = \frac{1}{2} \sum_{i=1}^N q_i V_i$$

Similar considerations also apply with regard to periodic systems (i.e. an appropriate charge summation technique must be utilised with a net charge and dipole of zero).

The electrostatic potential is a useful quantity for qualitative predictions as to certain properties of a material. For instance, if a structure contains several distinct oxygen sites one might expect that there would be a correlation between site potential and basicity. However, the limitations of the point ion, or dipolar shell, model must be kept in mind. Certainly the absolute site potential will be totally dependent on the choice of charges in the potential model, and therefore will be arbitrary, so at best only trends should be considered.

Based on the calculation of the site potential, the electric field, and the electric field gradient may also be determined as the first and second derivatives, respectively, of this quantity, while again excluding the case where  $i = j$ ;

$$\frac{\partial V_i}{\partial \alpha} = \sum_{j=1}^N -\frac{q_j}{r_{ij}^3} \alpha_{ij}$$

$$\frac{\partial^2 V_i}{\partial \alpha \partial \beta} = \sum_{j=1}^N \frac{(3\alpha_{ij}\beta_{ij} - r_{ij}^2 \delta_{\alpha\beta})}{r_{ij}^5}$$

The electric field gradient tensor is perhaps the most useful quantity since it may be transformed into the so-called asymmetry parameter,  $\eta$ , which can be important in the interpretation of solid state NMR data [91]. If we represent the tensorial components of the electric field gradient as  $V_{\alpha\beta}$ , then first the (3x3) matrix can be diagonalised to yield the three principal axis components,  $V_{xx}$ ,  $V_{yy}$ , and  $V_{zz}$ . If the components are labelled  $V_1$ ,  $V_2$ , and  $V_3$ , such that  $|V_3| > |V_2| > |V_1|$ , then the asymmetry parameter is defined as;

$$\eta = \frac{|V_2| - |V_1|}{|V_3|}$$

which ensures that the values lie in the range 0-1. A high symmetry site, such as one of  $O_h$  point group where all components are equal, would therefore have an asymmetry of zero.

#### 1.4.16.11 Born effective charges

The quantification of the charges associated with atoms/ions is one of the most problematic tasks in theoretical chemistry. Given that the atomic charge is not a direct quantum mechanical observable, it is therefore an artificial quantity, but one that is nonetheless useful in the development of understanding from quantitative results. Not surprisingly there are many different definitions of charge, the most famous of which is that due to Mulliken [37], where overlap density is apportioned equally to both nuclear centres. More recently, there has been considerable interest in Bader analysis [92] as a means of partitioning electron density. Both of these aforementioned schemes are based on the analysis of the density matrix, or the density itself. However, there is another family of charge definitions which define the atomic charges in terms of the response of the dipole moment of the system with respect to perturbations. Since the dipole is a genuine observable, such charge definitions are particularly attractive for forcefields as they describe the charges that are consistent with the response of the material to atomic displacements.

The most widely used definition in this second category is the Born effective charge:

$$q_i^{Born} = \frac{\partial \mu^\alpha}{\partial \beta_i}$$

Here the charge of an atom is now a symmetric (3x3) tensorial quantity since it describes the derivative of the three Cartesian components of the dipole moment with respect to the three Cartesian atomic displacements. While the definition of the dipole moment is complicated by the choice of the particular images of each ion, this complication doesn't affect the derivatives of the dipole moment within the present model. Differentiation of the dipole moment leads to the following expression for the Born effective charge;

$$q_i^{Born} = q_i^{core} \delta_{\alpha\beta} - \left( D_{core-shell} D_{shell-shell}^{-1} q^{shell} \right)_i$$

where the first term on the right-hand side is the core charge of the ion, and the second term is the corresponding component of the product of the core-shell second derivative matrix with the inverse of the shell-shell second derivative matrix, scaled by the vector of shell charges,  $q^{shell}$ . Physically, the second term corresponds to the response of all the shells present to the atomic displacement of atom  $i$ , or in other words, the electronic contribution. Hence for a rigid ion model, the Born effective charge tensor is equal to a diagonal matrix with all the diagonal elements equal to the core charge. Increasingly the Born effective charges are being determined from *ab initio* calculations, thus creating a new avenue for determining shell model parameters beyond the fitting of dielectric constants. Beyond this, the Born effective charges are also especially important in the determination of  $\Gamma$ -point phonon frequencies, as will be discussed in the next section.

#### 1.4.16.12 Phonons

Atoms must constantly be in motion as a consequence of the Heisenberg uncertainty principle and this is achieved through vibrations. At low temperatures the vibrations correspond to simple harmonic motion about the position of minimum energy, while as the temperature increases they become increasingly anharmonic.

For a molecule, there will be  $3N - 6$  vibrational modes (or  $3N - 5$  for a linear system). The remaining modes consist of three translations and either 2 or 3 rotations depending on whether the molecule is linear or not. It should be noted that for molecules the rotations can sometimes contaminate the vibrations of the system. In GULP there is the option to explicitly remove rotation and translation by using an Eckart transformation [93].

In the case of an infinitely perfect 3D solid, there will be a corresponding infinite number of phonons. These phonons are described by calculating their values at points in reciprocal space, usually within the first Brillouin zone. Hence we will obtain  $3N$  phonons per  $k$ -point. The lowest three modes represent the so-called acoustic branch which tend to values of zero at the centre of the Brillouin zone ( $k = 0, 0, 0$ ), known as the  $\Gamma$ -point. At this point, the acoustic modes correspond to the pure translation of the crystal lattice, and thus they are modes of zero frequency. A plot of the vibrational frequencies versus  $k$  gives rise to phonon dispersion curves.

To calculate the vibrations or phonons of a system, the starting point is the force constant matrix, given by the second derivatives with respect to the atoms in Cartesian space. In the case of a solid, the terms must be multiplied by the corresponding phase factor,  $\exp(ik \cdot r)$ . Thus the force constant matrix,  $F$ , between two atoms  $i$  and  $j$  is given by;

$$F_{i\alpha j\beta}(k) = \sum_R \left( \frac{\partial^2 U}{\partial \alpha \partial \beta} \right) \exp(ik \cdot (r_{ij} + R))$$

The summation over  $R$  represents the sum over lattice vectors within the cut-off radius. This matrix of force constants is then converted to the dynamical matrix,  $D$ ,

by multiplying by the inverse square root masses of the ions:

$$D_{i\alpha j\beta}(k) = \frac{1}{(m_i m_j)^{\frac{1}{2}}} F_{i\alpha j\beta}(k)$$

The origin of the three acoustic phonons at the  $\Gamma$ -point for a solid, or in the regular vibrational spectrum for a molecule, arises from the sum rules that govern the energy derivatives. Firstly, the sum of all first derivatives, or alternatively forces, must be equal to zero in the absence of an external force:

$$\sum_{i=1}^N \left( \frac{\partial U}{\partial \alpha_i} \right) = 0$$

Secondly, by further differentiating the above expression, it can be shown that the on-diagonal elements of the force constant matrix are equal to the negative sum of the off-diagonal elements:

$$\left( \frac{\partial^2 U}{\partial \alpha_i \partial \beta_i} \right) = - \sum_{j=1}^N \left( \frac{\partial^2 U}{\partial \alpha_i \partial \beta_j} \right)$$

where the summation now excludes the case when  $i = j$ . It should be noted that if a phonon calculation is performed for a surface using a two-region strategy, as will be discussed later, then there will no longer be three modes of zero frequency at the zone-centre. This is because the influence of region 2 acts as an external force, which breaks the translational invariance.

In forming the dynamical matrix from the force constant matrix there are a number of issues relating to particular forcefields and system types. The most common issue relates to the use of the shell model, in which the shells have zero mass. Since the number of vibrational modes is strictly given by three times the number of atoms, which in this case also corresponds the number of cores, then the shell co-ordinates cannot appear directly in the dynamical matrix. Instead the shell contributions are factored into the force constants of the cores according to the expression:

$$F_{cc}^{total} = F_{cc} - F_{cs} F_{ss}^{-1} F_{sc}$$

where  $F_{cc}$ ,  $F_{ss}$ , and  $F_{sc}$  are the core-core, shell-shell and shell-core force constant matrices, respectively, and  $F_{cs}$  is just the transpose of  $F_{sc}$ . In the case of the breathing shell model, the shell index is extended to run over the shell radius, as well as its Cartesian co-ordinates.

At the  $\Gamma$ -point there is an extra complication in the calculation of the phonons. In materials where the atoms possess a charge, the degeneracy of the Transverse Optical (TO) and Longitudinal (LO) Optical modes is broken due to the electric field that is generated during vibration. This effect is not allowed for in the usual analytic evaluation of the dynamical matrix. Furthermore, the precise splitting that

occurs also depends on the direction of approach to the  $\Gamma$ -point in reciprocal space,  $k^\Gamma$  (i.e. the LO and TO modes are likely to be discontinuous at this point in phonon dispersion plots). If the Born effective charges are known then this non-analytic term [94] can be corrected for by adding a correction to the dynamical matrix [38]:

$$D_{i\alpha j\beta}^{na} = \frac{4\pi}{V (m_i m_j)^{\frac{1}{2}}} \frac{(k^\Gamma \cdot q_i^{born})_\alpha (k^\Gamma \cdot q_j^{born})_\beta}{(k^\Gamma \epsilon^\infty k^\Gamma)_{\alpha\beta}}$$

where terms have the meanings as previously defined. As to be expected, the influence of the charges on the splitting is mediated in inverse proportion to the high frequency dielectric constant tensor.

Two scenarios arise with regard to the calculation of the  $\Gamma$ -point phonons. If the value for a specific direction of approach is required, such as in the case of a phonon dispersion curve, then the value of  $k^\Gamma$  may be explicitly specified. The direction of approach is automatically set equal to the direction of the phonon dispersion curve when the  $\Gamma$ -point is part of one in GULP. Alternatively, if the intention is to compute the infra-red spectrum as a polycrystalline average, then the phonons at this point should be a spherical average over all possible orientations. To allow for this last possibility, there is the possibility within GULP to perform a numerical integration by sampling the phonon modes as a function of  $\theta$  and  $\phi$  in spherical polar coordinates and then averaging the resulting frequencies.

#### 1.4.16.13 Molecular vibrational frequencies

The calculation of vibrational frequencies for molecular systems essentially follows the above formalism as described for phonons except that there is no Brillouin zone and therefore no phase factor to consider. However, there is one further consideration in that for a molecule a vibrational frequency calculation will yield 3 translational modes and either 2 or 3 rotational modes depending on whether the molecule is linear or non-linear, respectively. Often there is some mixing between the rotational modes and low frequency vibrations, and so it is advisable to use a method called Eckart purification to explicitly remove translation and rotation from the dynamical matrix in order to obtain the correct frequencies.

#### 1.4.16.14 Vibrational partition function

Statistical mechanics allows the connection to be made between microscopic quantum energy levels and macroscopic thermodynamic observables [95]. Pivotal to this process is the partition function,  $Z^{tot}$ , for the system. In order to determine this quantity we make the assumption that all forms of energy are independent and therefore that the total energy is just the sum of contributions from translation, rotation, vibration and the electronic state. In the case of a solid, we can neglect

the translational and rotational components, and furthermore since we are considering forcefield methods the electronic energy is not directly calculated. Hence, the problem reduces down to one of determining the vibration energy levels, and subsequently the corresponding partition function.

The vibrational energy levels for a harmonic oscillator for the  $m$ th mode are simply given by;

$$U_m^{vib}(n, k) = \left(n + \frac{1}{2}\right) h\omega(m, k)$$

if the frequency is specified in Hz. By summing over all energy levels it is possible to show that the vibrational partition function is equal to;

$$Z^{vib} = \sum_m \sum_k \frac{\exp\left(-\frac{h\omega}{2k_B T}\right)}{\left(1 - \exp\left(-\frac{h\omega}{k_B T}\right)\right)}$$

Here, and subsequently, the explicit dependance of the frequency on mode and  $k$ -point has been dropped for brevity. Substituting this expression into the various statistical mechanical expressions for thermodynamic quantities, we obtain the following relationships:

$$U^{vib} = \sum_m \sum_k w_k \left( \frac{1}{2} h\omega + \frac{h\omega}{\left(\exp\left(\frac{h\omega}{k_B T}\right) - 1\right)} \right)$$

$$A^{vib} = \sum_m \sum_k w_k \left( \frac{1}{2} h\omega + k_B T \ln \left( 1 - \exp\left(-\frac{h\omega}{k_B T}\right) \right) \right)$$

$$C_v^{vib} = \sum_m \sum_k w_k k_B \left( \frac{h\omega}{k_B T} \right)^2 \frac{\exp\left(-\frac{h\omega}{k_B T}\right)}{\left(\exp\left(-\frac{h\omega}{k_B T}\right) - 1\right)^2}$$

Note that the first term in the internal energy is just the zero point vibrational energy. In the above equations a sum over points in the Brillouin zone is included and the term  $w_k$  represents the weight of that particular point, such that the sum of all weights is equal to one. Formally speaking, this sum should be an integration over the phonon density of states. In practice, a discrete sum of points is typically used to numerically integrate the quantities.

There are a number of different choices possible for the set of points in the Brillouin zone for integration of the thermodynamic properties, just as there are for integration of the band structure in an electronic calculation. For high symmetry materials there are occasionally special point(s), such as those due to Baldereschi [96], and Chadi and Cohen [97]. However, the most appropriate in general is usually the Monkhorst-Pack scheme [98]. This involves an evenly spaced mesh of  $k$ -points,

given by three so-called shrinking factors, one along each axis of the Brillouin zone. This still leaves the issue of the translational position of the mesh relative to the origin. The optimal choice is to maximise the distance of all points from the origin along each axis by using an offset of half a mesh spacing from there to the first mesh point. The benefits of this choice are that it increases the rate of convergence as a function of increasing shrinking factor, as well as avoiding the issue of the non-analytic correction to the LO/TO splitting at the  $\Gamma$ -point.

If the space group symmetry has been specified for the material, then it is possible to determine the Patterson group, which is the equivalent of the space group in reciprocal space. Note that all systems have at least inversion symmetry (also known as time-reversal symmetry) in the Brillouin zone - a fact that is always used to accelerate the Ewald sum. By using the Patterson group, it is only necessary to sum over  $k$ -points that lie within the asymmetric wedge of the Brillouin zone, with appropriate weighting of points situated on the boundary [99]. This can lead to substantial computational savings for systems with small unit cells (and therefore high shrinking factors) and high symmetry.

When calculating thermodynamic quantities it is important to ensure convergence to the desired precision with respect to the shrinking factors. Because the mesh is in reciprocal space, the shrinking factor required for a given precision is inversely proportional to the unit cell length along that axis.

#### 1.4.16.15 Group velocities

The group velocities are the derivatives of the frequencies with respect to  $k$  vector at a given point in reciprocal space:

$$v_{ik} = \frac{\partial \omega_i}{\partial k}$$

They are useful in describing phonon propagation through a solid and can now be computed.

#### 1.4.16.16 Mean-squared displacements

Phonon mean-squared displacements within the harmonic approximation can be computed and output for each Cartesian direction. These are usual since they are related to the thermal ellipsoids for the atoms determined from diffraction studies.

#### 1.4.16.17 Frequency-dependent dielectric constants and reflectivity

We have already seen that the limiting dielectric properties in the static and high-frequency limits can be readily calculated for a system. However, the dielectric constant may also be calculated as an explicit function of the frequency of applied field,  $\omega_f$ . In order to determine this, first it is necessary to calculate the oscillator

strength,  $\Omega$ , for each vibrational mode based on the Born effective charges and the eigenvector,  $e$ , for that mode:

$$\Omega_{\alpha\beta} = \left( \sum_{i=1}^N \frac{q_{i\alpha\gamma}^{Born} e_{i\gamma}}{m_i^{\frac{1}{2}}} \right) \left( \sum_{i=1}^N \frac{q_{i\beta\gamma}^{Born} e_{i\gamma}}{m_i^{\frac{1}{2}}} \right)$$

The dielectric constant at the applied field is then given by:

$$\varepsilon_{\alpha\beta}(\omega_f) = \varepsilon_{\alpha\beta}(\infty) + \frac{4\pi}{V} \left( \sum_{m=1}^{modes} \frac{\Omega_{\alpha\beta}^m}{(\omega_m^2 - \omega_f^2)} \right)$$

From the form of the above relationship, it can be readily seen that there is a singularity in the dielectric constant when the applied frequency exactly matches that of one of the vibrational modes of the system. The limiting behaviour of the above expression is such that the results are equivalent to the previously calculated values for the dielectric constant as the frequency of the applied field tends to both zero and infinity.

One further property can be readily extracted from the above data, which is the bulk reflectivity. This measures the ratio of the reflected to absorbed power at a given frequency. While the frequency-dependent dielectric constant is a tensor, the reflectivity,  $R$ , has a value for each specific direction of incidence,  $k^{in}$ , and reflection,  $k^{out}$ , typically specified as vectors in reciprocal space:

$$R(\omega_f) = \left( \frac{\sqrt{\varepsilon(\omega_f)} - 1}{\sqrt{\varepsilon(\omega_f)} + 1} \right)^2$$

$$\varepsilon(\omega_f) = k^{in} \varepsilon(\omega_f) k^{out}$$

#### 1.4.16.18 Thermal Conductivity

Heat transport in materials is an important property that is quantified through the thermal conductivity. Because this depends on phonon-phonon scattering processes, the usual methods to calculate this property typically involve molecular dynamics simulations. However, a number of approximate schemes have been proposed that work within the framework of lattice dynamics. The method implemented in GULP is that of Allen and Feldman [100] and describes the contribution to thermal conductivity of so-called diffusons. Here the phonons are calculated for a supercell and by broadening the phonon density of states using a Lorentzian the thermal conductivity,  $\kappa$ , can be computed according to the following expression:

$$\kappa = \frac{1}{V} \sum_{i=1}^{modes} C_i(T) D_i$$

Here  $V$  is the cell volume,  $C_i(T)$  is the heat capacity of mode  $i$  at temperature  $T$ , and  $D_i$  is the mode diffusivity. The full equations for the method are given in the original reference [100]. The key points to note is that the method, as implemented in GULP, uses the phonons at the  $\Gamma$  point only and therefore the size of the supercell needs to be checked for convergence. Furthermore, the final value will depend on the broadening factor used for the density of states, and to a lesser extent the drop tolerance for the Lorentzian broadening. Since the Allen-Feldman approach in finite super cells only captures the higher frequency contributions to the thermal conductivity, the correct approach is to only compute the contribution above a cut-off frequency that is given by the `omega_af` option. The propagating contribution due to the acoustic branch below this cut-off frequency can then be computed more accurately by a number of approximate formulae that describe the quadratic nature of the density of states as it tends to zero frequency.

If a more accurate calculation of the thermal conductivity is required then it is necessary to solve the Boltzmann Transport Equation (BTE) for the phonons. This now requires the use of the third derivatives of the energy with respect to Cartesian displacements. At present the solution of the BTE is not built into GULP, but it is possible to compute thermal conductivity via an interface to the program Alamode [101]. Provided Alamode is installed on your computer, and the location of the main directory has been specified via the `ALAMODE_DIR` environment variable, then GULP is able to call the appropriate parts of Alamode to generate the symmetry-reduced third order force constants and thereby obtain the thermal conductivity, phonon lifetimes, etc. When using this approach it's important to test the influence of the supercell size being used since force constants are truncated based on the size of the cell being used and so will influence the quality of the results. It should also be noted that the results of the calculation give the result for the infinite bulk crystal. At low temperatures, in particular, these results need correcting for finite size effects of the crystal that limit the thermal conductivity. This can be performed using Alamode to post-process the results of the GULP calculation. NB: Calculation of third order force constants can be expensive and the run time will increase rapidly with the size of system and loss of symmetry.

#### **1.4.16.19 Pair Distribution Functions**

Another use of the phonon information is in the calculation of the Pair Distribution Function (PDF). This has been used (under various names) for many years to provide an understanding of both structure and dynamics on the atomic scale. It was initially developed for liquids [102], and has continued to be useful with amorphous materials [103]. As early as the 1960's, workers were making use of the dynamic contributions to the PDF [104]. More recently it has become an important tool for use with crystalline materials [105].

The PDF, and related correlations functions (see Pair Distribution Functions in

Further Background section), are found experimentally through a Fourier transform of the observed total scattering on neutron or X-ray diffraction experiments, such as those performed on the GEM diffractometer [106] at the ISIS pulsed neutron source. Total scattering experiments involve collecting the complete diffraction pattern; diffuse scattering as well as Bragg peaks. A Fourier transform of the experimental data gives the relative probability of finding a pair of atoms of type  $m$  and  $n$  separated by a distance between  $r$  and  $r + \delta r$ . The atomic positions that contribute to the Bragg peaks in the elastic scattering give the peak positions in the PDF, the crystal arrangement (number of neighbours) gives the area under each peak, while the dynamic properties of the material are responsible for the width of the peak. Working within harmonic lattice dynamics, the PDF can be modelled using Gaussians. Recently, Chung and Thorpe [107] proposed a method for calculating these Gaussian peak widths from phonon calculations, thus providing the phonon-based model of PDFs implemented here.

Taking advantage of crystal symmetry, every atom within the primitive unit cell is used to generate atomic pairs up to a given maximum radius. Phonon information for every  $\mathbf{k}$ -point within a sufficiently dense Monkhorst-Pack grid is used to calculate the contribution to the width of the PDF peak from that pair. These are summed and suitably averaged to give the total  $\rho^{\text{PDF}}(r)$  function, which is converted into each of the total correlation functions described in Further Background section. The contributions from all pairs of each type are also used to output the partial PDFs. Other useful data and statistics are included in the standard output. Standard neutron scattering lengths are supplied with the program, available in the `eledata` Library file, but can be overwritten using `bbar` and `siginc` with the `element` input option.

There are two main applications for this new modelling approach. First, to assist in the design of experiments, giving a theoretical model of experimental outcome. Second, to ‘experiment’ on the model, for example changing cation distribution, or investigating different phonon contributions.

Citation: Please cite the primary reference [108] in any publications produced using the PDF module, together with the citation for the main GULP program [109].

### 1.4.17 Calculation of surface properties

The properties of the surfaces of materials are every bit as important as the bulk properties, since they control the interaction between the substance and the external environment. At the most obvious level, the very shape of the particles or crystallites formed is determined by the properties of the surface relative to the bulk, while catalysis and reactions of the material also predominantly occur at the surface. From the earlier discussion of electrostatics, it is apparent that the surface structure is a key factor in determining the bulk polarisation and net dipole of the material, which has consequences even for the bulk region.

Due to the interest in surface phenomena, the history of modelling surfaces using atomistic simulation is also a long one spanning a number of different computer codes. Of the recent era, the dominant computer code for surface simulation of ionic materials has been MARVIN [110], which has been developed alongside GULP for many years. However, to ensure the maximum integration of functionality between bulk and surface simulations, both in terms of forcefield models, as well as accessible properties, it was decided to incorporate much of the functionality of MARVIN into GULP to produce a single code capable of simulating systems with any type of boundary condition from 0-D, through to 3-D. Here we describe the methodology employed for surface calculations.

There are two phases to any surface calculation, namely the creation of the surface from the bulk material and the subsequent calculation of its optimised structure and properties. Each surface is specified by at least two pieces of information. Firstly, there are the Miller indices ( $hkl$ ) of the plane that defines the orientation of the bulk cleavage. Secondly, there is the so-called shift - i.e. the displacement of the plane relative to the unit cell origin. For simple cases, such as the (001) surface of a rock salt structure there is only one unique choice of shift. However, for more complex cases there may be several shifts for a given plane that lead to distinct surfaces. When cleaving surfaces there are also other important considerations to take into account, in particular the type of surface. As illustrated in Figure 1.1, there are three basic types of surface. In type 1, the atomic structure consists of charge neutral sheets of ions parallel to the surface plane and thus all shifts are guaranteed to yield a surface with no dipole moment in the direction of the surface normal. For type 2 surfaces, there are combinations of layers of cations and anions that possess zero net dipole in the appropriate direction. Hence for well chosen values of the shift a non-dipolar surface can be obtained. Finally, for type 3, all cleavage planes result in a dipolar surface, which is therefore likely to be less stable. While dipolar surfaces can exist, this normally leads to twinning of crystals or strong solvation in order to null the dipole. Alternatively, the surfaces can reconstruct in order to remove the dipole. This typically involves the creation of cation or anion vacancies at the surface or chemical modification. When an ion is conceptually removed, in practice it is moved to the bottom of the surface slab in a calculation in order to maintain charge neutrality [111]. Real examples of the three types of surface are presented for polymorphs of calcium carbonate in Figure 1.2.

From the above, it can be seen that often the creation of the surface is a significant task in its own right and can be a complex process. In previous programs for surface calculations, the structure manipulation has usually been performed via the input deck of the code. Clearly, when reconstructions are involved this can become rather unwieldy. As a result, a different strategy has been adopted for use with GULP. All construction of the surface and structural manipulation is performed independently from the main forcefield engine by graphical means. This is achieved through an interface to the freely available program GDIS developed by Dr Sean

Figure 1.1: The three types of surface as categorised by Tasker (a) type I, where each layer consists of coplanar anions and cations, and all planar cuts lead to a nonpolar surface; (b) type IIa, where the anions and cations comprising the layers are not coplanar, but which allows for some surface cuts to split the layers in such a way as to produce no dipole; (c) type IIb, which is as per type IIa, except that some ions must be moved from the surface to the bottom of region 2 in order to achieve zero dipole; and (d) type III, where there are alternating layers of cations and anions, and all possible planar cuts result in a surface with a dipole moment.

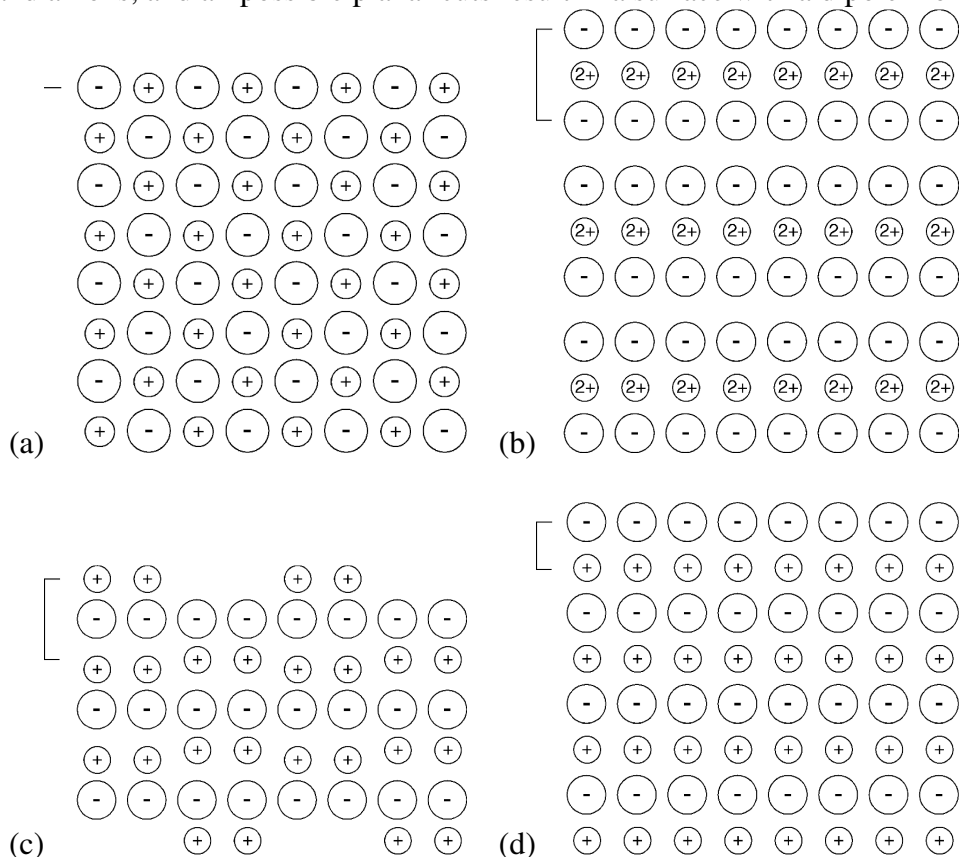
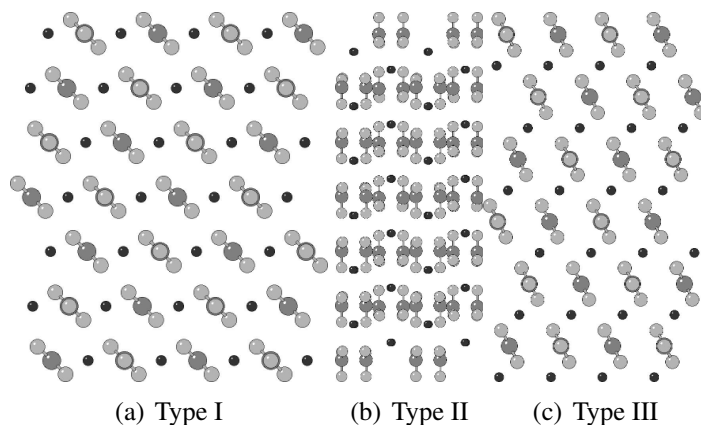


Figure 1.2: The examples of the three types of surface illustrated using polymorphs of calcium carbonate; (a) type I (b) type II and (c) type III. The type I and III surfaces illustrated are from the crystal structure of calcite, which due to its high symmetry has no type II surfaces present. The type II example is from aragonite.



Fleming (<http://gdis.seul.org/>). This interface allows surfaces to be specified by their Miller indices, valid shifts to be searched for, and the geometries then to be manipulated, if necessary. Once the desired surface structure has been generated, then the necessary GULP calculation can be performed.

#### 1.4.17.1 Surface energy

The thermodynamic penalty for cleaving a surface from a bulk material is measured according to the surface energy. Given a bulk energy of  $U_{bulk}$  and an energy for the same system with a surface created of  $U_{surface}$ , then the surface energy,  $\Delta U_{SE}$ , is defined as an intensive quantity according to:

$$\Delta U_{SE} = \frac{(U_{surface} - U_{bulk})}{A}$$

where  $A$  is the resulting surface area. By definition, for any stable material the surface energy will be endothermic. A calculated negative surface energy implies that a material should dissociate, i.e. the crystal should disperse into the surrounding medium.

There are two practical approaches that are widely used to determine the surface energy by computational means. In the first, a two-dimensional slab of material is created from the bulk, thus creating two surfaces overall. This method has the advantage that it can be used within programs that only allow for three-dimensional boundary conditions through the introduction of a sufficiently large vacuum gap between the images, such that the surfaces don't interact across the vacuum. In addition, it becomes necessary to assess whether the slab is also thick enough since

the properties must converge to those of the bulk at the centre of the slab. In the second method, a single surface is created by employing a two region strategy, as shown in Figure 1.3. Here the solid is divided into region 1, which contains the surface and all layers of atoms below it that exhibit a significant atomic relaxation, and region 2, which contains the rest of the bulk material where it is assumed that no displacements from the three-dimensional crystal structure are induced. In practice, only the atoms of region 2 that have an interaction with region 1 need be explicitly considered, and so the depth of region 2 is controlled by the cut-offs of the force-field and the Parry sum used for the electrostatics. This second method is the most efficient and precise for atomistic techniques. However, it is considerably harder to extend to quantum mechanical methods since the electronic perturbations may extend further into the bulk and embedding, typically via Green's functions, is required to determine the influence of the electronic structure of region 2 on region 1. Through the GDIS interface, it is possible to automatically estimate the required region 1 and 2 sizes needed to converge the surface energy (with a default tolerance of  $0.001J/m^2$ ) based on the unrelaxed surface energies. However, if there are strong relaxations of the surface, it may be necessary to further verify that the relaxed surface energy is sufficiently converged.

The total energy for a surface calculation comprising two regions can be written in terms of the interaction energies within, and between, the different regions:

$$U_{tot} = U_{11} + U_{12} + U_{22}$$

The energy of region 2 with itself,  $U_{22}$ , is not particularly meaningful, since the region 2 is just a partial representation of the effectively infinite bulk material below, and any given particle within this region will not experience the full set of interactions that it should. However, this term is just an additive constant that is unaltered on energy minimisation, or any other displacement of region 1. Consequently it can be ignored in calculations. In the two region model, the energy required to determine the surface energy is given by:

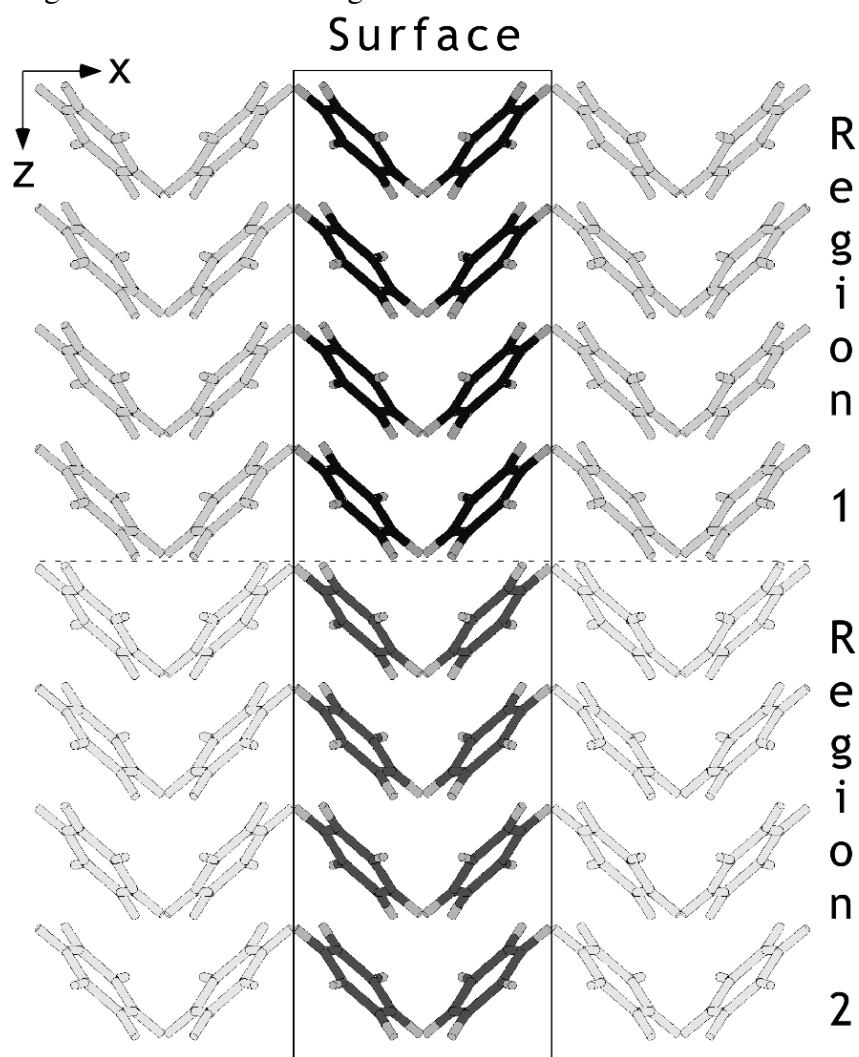
$$U_{surface} = U_{11} + \frac{1}{2}U_{12}$$

Note that while the above energy only includes half of the region 1-region 2 interaction energy, the objective quantity for energy minimisation is the total energy, which includes the full value of  $U_{12}$ . This is because the energy change of region 2 must be allowed for when optimising.

#### 1.4.17.2 Attachment energy

The surface energy, described above, provides a measure of the thermodynamic stability of a cleavage plane. However, there is a widely used alternative criterion

Figure 1.3: The two region surface simulation cell viewed at right angles to the surface normal, where solid vertical lines denote the boundaries between two-dimensional periodic images of the cell and the dash line indicates the boundary between region 1 and the frozen region 2.



which is the attachment energy. This is the energy associated with the addition of a stoichiometric layer of material on to the surface cut:

$$U_{attachment} = U_{tot}^{n+1} - U_{tot}^n - U_{tot}^1$$

where  $U_{tot}^n$  represents the total internal energy of a surface model consisting of  $n$  growth layers, and  $U_{tot}^1$  is the energy of the growth layer alone. For any stable material, this implies that the attachment energy must be an exothermic quantity. In practice, the calculation of the attachment energy is obtained from the energy of interaction of the growth layer at the surface with the rest of the underlying material. This benefits from the fact that the attachment energy can be obtained from a single calculation, just as is the case for the surface energy, rather than by performing the actual addition of a layer as part of a multistage process.

Although the attachment energy is also a strictly thermodynamic quantity, it is often regarded as representing the kinetics of crystal growth because of the conceptual link between the ease of the addition of a growth layer and the rate at which a surface is added to. Consequently, those faces where the attachment energy is most exothermic will tend to grow most rapidly.

### 1.4.17.3 Morphology

The morphology of a crystal is the macroscopic shape that it adopts. Because this can be readily observed for nearly all materials, either under an electron microscope or, in the case of many naturally occurring minerals, by visual inspection with the naked eye, it should provide a ready means to test the validity of a simulation model. Of course, the reality is rather more complex, since the morphology is sensitive to the presence of impurities, the nature of the solvent used as the growth medium, and many other factors relating to the sample preparation. Consequently there are materials where many different morphologies can be observed for the same compound. A classic example, is that of calcite ( $CaCO_3$ ), where there are both several different polymorphs of the bulk material and several hundred different known morphologies. Many of these variations result from biomineralisation by different species. Despite this, for many pure inorganic materials morphological prediction using atomistic techniques is surprisingly successful.

Crystal morphologies can be calculated based on either the surface energy or attachment energy, which are typically taken to represent growth under conditions of thermodynamic and kinetic control, respectively. In order to do this, it is first necessary to determine the objective quantity for all significant faces. Given that dipolar faces are usually unstable, the number of likely cleavage planes for most materials is actually considerably smaller than initially might be conceived of based on permutations of the Miller indices. Furthermore, where there is space group symmetry present for the bulk, many surface planes are equivalent, thus reducing the number of unique faces. Finally, only those faces with the largest interplanar

spacings are likely to appear in the morphology [112]. The actual morphology is generated as a three-dimensional Wulff plot [113]. Here the ratio of the surface normal distances of all planes from the centre of the polyhedron are determined according to the either the surface or attachment energy. The final shape of the polyhedron is then determined by the intersection of the cleavage planes. Unstable surfaces lie outside the polyhedron and never intersect. Morphological plots can also be produced through the GDIS interface to GULP.

In the equilibrium morphology approach, the contribution of a given plane to the total surface area is inversely proportional to its surface energy [114]. For the growth morphology methodology [115], the surface area contribution is again inversely proportional, but now to the negative of the attachment energy. This is because surfaces with a highly exothermic attachment energy will rapidly grow out of the morphology to leave the slow growing bounding faces.

#### **1.4.17.4 Surface phonons**

The calculation of the phonons of a 2-D slab is exactly analogous to that for the three dimensional case, except that the Brillouin zone is also now two dimensional leading to dispersion only in the  $xy$ -plane (taking  $z$  to be the direction of the surface normal).

Turning to consider the standard two region surface model, there are some important issues to consider. Because region 2 is quasi-infinite, it is only possible to determine the phonons for the particles in region 1. Therefore, the dynamical matrix is constructed based on region 1 alone, but with contributions to the on-diagonal matrix blocks from the potential experienced due to a rigid, non-vibrating region 2. Consequently it is assumed that the vibrations of the two regions are completely decoupled. Since this is an approximation, the frequencies near the interface of the regions will be slightly in error, particularly in the low frequency regime where coupling is generally strongest. However, the surface modes, which are usually the ones of primary interest, will be less affected. As always, it is essential to monitor the convergence of all quantities with respect to increasing the region 1 depth. Finally, because region 1 is vibrating under the influence of an external potential, the first three frequencies at the  $\Gamma$ -point will no longer be zero, though they typically will be small.

#### **1.4.18 Continuum solvation of surfaces**

In the above description of surface properties the surface is always assumed to be in contact with vacuum. However, the properties of surfaces in contact with solvent are equally as important. While the interface between a solid and liquid is most accurately studied using molecular dynamics simulations, there are some situations where more approximate methods are valuable. For example, to predict the solvent

dependent morphology of a crystal only requires the ratio of the surface energies to be correct and not the absolute magnitude. To perform molecular dynamics to extract the relative free energies of solvation for a large collection of surface is very challenging and time consuming. Here the use of a more approximate approach is valuable.

In GULP the option to employ a continuum solvation model has been added. Here the solvent accessible surface is described using a grid of points and the response of the solvent due to its dielectric properties calculated at this surface in response to the electrostatic potential of the solid. Full details of the method implemented in GULP can be found in the literature [116]. In brief, the method uses the COnductor-like Screening MOdel (COSMO) of Klamt and Schuurmann [117], but with a few modifications. The solvent accessible surface (SAS) is smoothed by use of tapering functions, and octahedral triangulation is used to generate the points in order to maximise symmetry. Furthermore, the frame of a molecule (if applied in 0-D) is rotated according to the eigenvectors of the moment of inertia tensor in order to ensure rotational invariance. The final change is more significant; because the induced charge on the solvent accessible surface is unconstrained the total charge of a surface and solvent could be non-zero (and non-integer). When working within periodic boundary conditions it is essential to maintain charge-neutrality such that a convergent electrostatic energy can be obtained. To do this GULP uses the COSMO method under the constrain of Integer Charge (COSMIC) to ensure that the electrostatics remain valid.

The current implement of the COSMIC continuum solvation model can be applied to surfaces, polymers, solids and molecules. Both analytic first and second derivatives are available, though phonons can only be evaluated at the gamma point at present.

### **1.4.19 Free energy minimisation**

One of the most important issues in solid state modelling is the variation of materials properties with the applied conditions. While isotropic external pressure is trivial to incorporate, as has already been shown, inclusion of the effect of temperature is more complex. This process is exacerbated by the fact that the majority of potentials have been derived through the use of some empirical (i.e. experimental) data which has been measured under a given set of conditions. Hence the force-field itself can often already contain an implicit temperature, or worse, if multiple pieces of experimental data have been employed that were measured at different conditions, it can be a convolution of several temperatures. One solution to this is to extract forcefields from quantum mechanical methods so that everything is obtained explicitly at absolute zero. For now, we will assume that the forcefield has been derived so as to be free of implicit temperature effects, by whatever means.

There are several distinct approaches to the inclusion of temperature into simu-

lations. Which one is most appropriate depends on the particular temperature and nature of the system. In the low temperature regime, the atoms of the crystal structure just execute vibrations about their lattice sites, which in the limit of absolute zero will be purely harmonic. This situation is best described through the use of lattice dynamics, which is the quasi-static approach to treating a vibrating lattice. As the temperature increases, the motions will become increasingly anharmonic. In principle, this can be handled, to a point, through the use of anharmonic corrections to the harmonic lattice dynamics, in order to allow for weak phonon-phonon coupling. However, when the temperature becomes sufficiently high that diffusion can occur it is necessary to switch to an alternative approach. Typically one of two approaches can then be employed. If detailed information is required concerning the atomic motions and related properties, then the method of choice is molecular dynamics [118]. This propagates Newton's equations of motion through time using a finite difference formalism. Hence it retains time correlation functions and the trajectories of all atoms. Its strength is that anharmonic effects are fully included. However, since it regards nuclei as classical particles, it is invalid at low temperatures due to the neglect of the quantisation of vibration and zero point motion, unless the Path-Integral formalism is employed. It can be seen therefore that lattice dynamics and molecular dynamics are largely complementary in their regions of applicability. Although GULP also includes the capability to perform molecular dynamics, this topic will not be discussed here since this area, in regard to other codes, has been discussed elsewhere [16], and the more unique, static, features will be focussed on here. Likewise, the effect of temperature can also be explored through Monte Carlo simulation [89], if the focus is integration over phase space, with no regard to timescale or kinetic factors, but this topic will not be discussed further because it is not one of the more novel features of GULP.

Concentrating now on the use of lattice dynamics for examining the temperature dependence of crystal properties, the dominant effect is the change in the crystal structure. When heated, most materials undergo thermal expansion which correspondingly leads to softening of many of the mechanical properties. There are a few celebrated examples of materials that actually contract on heating, through the rotation of quasi-rigid polyhedra, which is technologically very important in the quest for zero thermal expansion composites.

It has already been shown that it is possible to calculate the Helmholtz free energy for a given structure as a function of temperature through the determination of the vibrational partition function from the phonon density of states. Hence, a natural approach to determine the dependence of structure on temperature is through free energy minimisation. Here the key foundation is the quasi-harmonic approximation, which assumes that the vibrational frequencies can be determined as if the atoms are vibrating purely harmonically while the cell parameters are adjusted to minimise the free energy. Previous studies have indicated that this is a reasonable approximation until a temperature of approximately half the melting point has been

reached.

The major barrier to free energy minimisation is that we have already seen that efficient optimisation requires at least the first derivatives of the quantity with respect to the structural variables. Hence a number of approaches evolved for tackling this problem. LeSar *et al* [119] developed a method whereby the atoms were represented as Gaussian distributions, whose width represented the vibrational motion. The Gaussian exponent was then regarded as a variational parameter that minimised the free energy. Hence the free energy could be obtained without direct recourse to a phonon density of states, making derivatives straight forward. While this approach is easy to apply to metals, the extension to a more complex ionic systems is more demanding. A method that approximated the phonon density of states was introduced by Sutton [120], which involved taking moments of the dynamical matrix, as pioneered by Montroll [121] several decades earlier, and in the spirit of tight binding theory. This approach has the advantage that the derivatives are taken of the dynamical matrix elements, rather than of phonon frequencies, which are the product of a matrix diagonalisation.

In the field of ionic materials, Parker and Price [8] pioneered the use of free energy minimisation through the use of numerical derivatives. Here central finite differences were taken with respect to the cell strains, with the internal degrees of freedom being formally optimised at every point. This approach had the advantage over the other methods that no approximation was being introduced beyond the quasiharmonic one. However, because this requires  $(2N + 1)$  optimisations and phonon evaluations per energy/gradient evaluation with respect to the free energy, the minimisation was restricted to the strains alone in order to reduce the number of variables,  $N$ , to a maximum of six.

More recently, Kantorovich [122] has derived expressions for the analytical derivatives of the free energy, which were implemented contemporaneously in the program SHELL of Allan and co-workers [123], and in GULP [124]. If we consider the differential with respect to strain, though the expressions would be identical for any degree of freedom, then the first derivative of the free energy is given by:

$$\left(\frac{\partial A}{\partial \epsilon}\right) = \left(\frac{\partial U_{static}}{\partial \epsilon}\right) + \sum_k \sum_m \left\{ \frac{h}{2\omega} \left( \frac{1}{2} + \frac{1}{\exp\left(\frac{h\omega}{k_B T}\right) - 1} \right) \left(\frac{\partial \omega^2}{\partial \epsilon}\right) \right\}$$

where the expression is written in terms of the derivatives of the square of the frequencies, since these values represent the eigenvalues of the dynamical matrix. Their derivatives can be calculated through the application of perturbation theory and expressed as the derivatives of the dynamical matrix projected onto the corresponding eigenvectors:

$$\left(\frac{\partial \omega(k, m)^2}{\partial \epsilon}\right) = e_m^*(k) \left(\frac{\partial D(k)}{\partial \epsilon}\right) e_m(k)$$

In order to determine the derivatives of the phonon frequencies, we therefore require the phased third derivatives of the energy with respect to either three Cartesian coordinates, or two Cartesian coordinates and one strain. for internal and external variables, respectively.

For the most efficient optimisers, based on Newton-Raphson techniques, we strictly need the second derivatives with respect to the free energy, which corresponds to the fourth derivatives of the internal energy. However, this is considerably more expensive and complex, so the Hessian matrix is usually approximated by the conventional internal energy Hessian by assuming that the free energy contribution to the curvature is small. Furthermore, the use of updating formulae will ultimately correct for the discrepancy given sufficient optimisation steps.

With the advent of analytical derivatives, it is now possible to consider two types of free energy minimisation. The first has been christened the Zero Static Internal Stress Approximation (ZSISA) by Allan and co-workers [125], which resembles the approach taken with numerical first derivatives (i.e. the unit cell is minimised with respect to the free energy, while maintaining the internal degrees of freedom at a minimum with respect to the internal energy). When working within this formalism there is an additional contribution to the strain derivatives, which corrects for the fact that internal degrees of freedom are not at a minimum with respect to the free energy:

$$\left(\frac{\partial A}{\partial \varepsilon}\right)_{ZSISA} = \left(\frac{\partial A}{\partial \varepsilon}\right) - \left(\frac{\partial^2 A}{\partial \varepsilon \partial \alpha}\right) \left(\frac{\partial^2 A}{\partial \alpha \partial \beta}\right)^{-1} \left(\frac{\partial A}{\partial \beta}\right)$$

Here the approximation is again made that the second derivative matrices can be approximated by neglecting the free energy contribution; an approximation that should be enhanced by the cancelation that results from taking a ratio. The second type of optimisation can be called full free energy minimisation (FFEM), in which the internal degrees of freedom are also minimised with respect to the free energy. This is potentially appealing since sometimes it is the details of the internal changes that might be of interest, for example, the nature of an adsorption complex within a microporous material.

Results for silicate materials show a number of interesting features regarding the merits of both approaches. Firstly, in the case of  $\alpha$ -quartz where accurate experimental data is available for comparison, it appears that the ZSISA approach underestimates the thermal expansion, while the FFEM method is more accurate, though of course this is subject to the limitations of the specific potential model chosen [124]. However, for all silicates tried so far the full minimisation approach goes catastrophically wrong at about ambient conditions. This is illustrative of a general problem with this approach which tends to drive systems to instability. This can be readily understood, since the free energy is minimised by creating phonons that tend to zero frequency and hence the structure is motivated to create soft modes. This behaviour does not tend to happen in the ZSISA approach where only the cell strains are directly coupled to the free energy and thus the relaxations tend to lead

only to a scaling of modes, rather than more individual changes. Hence the use of ZSISA is far more robust and generally recommended for most purposes.

### 1.4.20 Monte Carlo

An alternative approach to including temperature into results, if one is not interested in the time correlation properties, just the ensemble averages, is Monte Carlo simulation. Here the distribution of positions according to a Boltzmann distribution is determined numerically for a specified temperature and conditions. Under the Metropolis importance sampling scheme, if a randomly chosen move for the system leads to a lowering in the energy then the move is accepted and the system evolves to the new state. If the energy increases, then the move is accepted with a probability given by:

$$P = \exp\left(-\frac{\Delta U}{k_B T}\right)$$

where  $\Delta U$  is the energy change associated with the move. There are several types of move available for a system as listed below:

- Translation - this allows atoms or molecules to move in x, y or z, according to the flags set
- Rotation - for rigid molecules, this allows the molecule to sample the rotational distribution
- Creation/destruction - in the Grand Canonical ensemble, molecules can be inserted or removed to a reservoir of molecules whose chemical potential is specified

Note that the Monte Carlo feature is relatively new and should be considered as a beta release available to those who wish to test.

### 1.4.21 Defect calculations

While the simulation of bulk material properties is important, just as crucial is the study of both intrinsic and extrinsic defects. Many of the key applications of solid state systems, such as catalysis, electronic and ionic conductivity, ion exchange and waste immobilisation, critically depend on the utilisation of the characteristics of defect centres. Consequently, from the early days of the field of atomistic simulation defect studied have been one of the most vigorously pursued topics.

There are two widely used approaches for performing defect calculations on solids; the supercell and the cluster methods, with or without embedding in the latter case. Both approaches have their merits and demerits. Putting computational implementation factors aside, the use of embedded clusters is ideal for the infinitely

dilute limit, while the supercell method is more appropriate for high concentrations of defects where there exists significant defect-defect interaction. In practice, the nature of the computational method often biases the method of choice. However, with atomistic techniques both approaches are feasible. Since the supercell method is simply the extension of a bulk calculation, we will focus here on the embedded cluster approach. In this particular context, the technique is generally referred to as the Mott-Littleton method [126], after the authors of the pioneering work in the field, though the implementational details differ a little from their original work.

The basis of the Mott-Littleton method is the so-called two region strategy. Here a point called the defect centre is defined, which typically lies at a point concentric with the initial defect site, or, where there is more than one defect, at the mid-point of the ensemble of point defects. The crystal around the defect centre is divided into two spherical regions, with the inner sphere being labelled region 1, and the outer spherical shell of ions being region 2a. Atoms outside of these spheres belong to region 2b, which then extends to infinity. The dimensions of these regions are typically specified either by their radii or the number of ions contained within them. The ions in region 1 are assumed to be strongly perturbed by the defect and therefore are relaxed explicitly with respect to their Cartesian coordinates. In contrast, the ions in region 2 are assumed to be weakly perturbed and therefore their displacements, with the associated energy of relaxation, can be approximated in some way. Clearly, as the region 1 radius is increased these approximations will become increasingly valid, and thus an important stage of a defect calculation is to ensure that the defect energy is sufficiently converged with respect to the region radii. In some cases the convergence of the absolute defect energy can be slow, in which case it may be sufficient to monitor the convergence of relative defect energies instead. As a guideline, the radius of region 1 and the difference of the radii of regions 1 and 2 should be both be greater than the short-range potential cut-off to achieve convergence, though for charged defects this may not be adequate.

Within the Mott-Littleton scheme, we can express the total energy of the two region system as the sum of contributions from the energies within the regions and between them:

$$U_{tot}(x, \xi) = U_{11}(x) + U_{12}(x, \xi) + U_{22}(\xi)$$

where  $U_{11}(x)$  represents the energy of region 1 as a function of the Cartesian coordinates,  $x$ ,  $U_{22}(\xi)$  represents the energy of region 2 as a function of the Cartesian displacements,  $\xi$ , and  $U_{12}(x, \xi)$  is the energy of interaction between the two regions. At this stage we do not distinguish between regions 2a and 2b. If the forces acting on region 2 are small, then we can assume that the response of the atoms in this region will be purely harmonic. Hence, the energy of region 2 can be written as:

$$U_{22}(\xi) = \frac{1}{2} \xi^T H_{22} \xi$$

where  $H_{22}$  is the Hessian matrix for region 2. If we now apply the condition that the

displacements in region 2 will be the equilibrium values this yields the following condition:

$$\left( \frac{\partial U_{tot}(x, \xi)}{\partial \xi} \right)_x = \left( \frac{\partial U_{12}(x, \xi)}{\partial \xi} \right)_x + H_{22} \xi = 0$$

Combining this equation, and the previous one, it is possible to eliminate the energy of region 2 from the total energy without direct recourse to the Hessian matrix (which would be of infinite dimension):

$$U_{tot}(x, \xi) = U_{11}(x) + U_{12}(x, \xi) - \frac{1}{2} \left( \frac{\partial U_{12}(x, \xi)}{\partial \xi} \right)_x \xi$$

Thus the problem of calculating the energy of region 1 in the potential of region 2 has been reduced to evaluating the energy of region 1 and its interaction with region 2, without having to evaluate the self energy of region 2. Furthermore, in order to lead to partial cancellation of terms, the quantity calculated is the defect energy - i.e. the difference between the energy of the perfect region 1 and 2,  $U_{tot}^p$ , and the defective case,  $U_{tot}^d$ , rather than the individual contributions:

$$U_{defect}(x, \xi) = U_{tot}^d(x, \xi) - U_{tot}^p(x, \xi)$$

It should be noted that it is assumed that the energy of any species removed or added during the formation of the defect has an energy of zero at infinite separation. If this is not the case, then the defect energy must be corrected *a posteriori* for this. However, such corrections have no influence on the outcome of the defect calculation itself.

There is one important consequence of the above formulation of the total defect energy, in that it becomes necessary to find the optimised energy with respect to the Cartesian coordinates of region 1 by force balance, rather than by energy minimisation. The point at which the forces tend to zero is usually only slightly different from the minimum in the internal energy, depending on the degree of perturbation of region 2. Hence, during an optimisation of the defect energy GULP initially minimises the energy, as per a conventional Newton-Raphson procedure. Once the gradient norm falls below a specified tolerance, and region 1 lies within the harmonic region, then the harmonic displacements according to the Hessian and gradients are applied without the use of a line search until the forces drop below the specified tolerance.

A further important point relates to the state of the bulk crystal when performing defect calculations. Because of the use of displacements in region 2, it is crucial that the bulk structure is at an energy minimum with respect to the internal coordinates before performing a defect calculation. Hence the bulk crystal must be relaxed to equilibrium at least at constant volume, if not at constant pressure. Furthermore, it is also important that there are no imaginary phonon modes within the Brillouin zone otherwise the displacements in region 2 may correspond to unstable harmonic equilibrium. The presence of such modes is the most common cause

of unphysical results, for instance obtaining negative defect energies for intrinsic defects. Because the presence of defects lowers the symmetry, a Mott-Littleton calculation may encounter instabilities not apparent for the bulk material.

Now it is necessary to consider the treatment of region 2 in more detail, and in particular the difference between regions 2a and 2b. In region 2a, the forces on the individual ions due to short-range interatomic potentials and the Coulomb term are explicitly calculated and the local displacement evaluated. While the forces on region 2a are technically due to all ions in region 1, a commonly used approximation is to evaluate the forces due to defect species only. This is the approach taken in the default calculation method for compatibility with earlier results.

In contrast to the above situation for region 2a, for region 2b the energy of relaxation must be determined implicitly since this region extends to infinity. It is assumed that in region 2b the only force acting is that due to the Coulomb potential in order to simplify the problem. By choosing the radius of region 2a to always be greater than that of region 1 by the short-range potential cut-off this can always be arranged to be valid. Even having retained only the Coulomb interaction in the perturbation of region 2b, this still leaves many interactions to consider. To simplify the problem, the electrostatic potential due to defects in region 1 can be represented by the multipole moments of the deformation situated at the defect centre. If region 2a is sufficiently large, then the only significant term will be the monopole moment of the defect (i.e. the net charge). Hence, the energy of region 2b is evaluated as the induced relaxation energy due to the net charge of the defect situated at the specified defect centre. While this is a significant approximation, it usually works well in practice and again becomes valid with increasing region sizes. In the original Mott-Littleton method, the interaction with region 2b was described by a continuum approximation. However, in subsequent implementations a sum of the induced polarisation energy is performed over the atomic sites. For the general case of an anisotropic dielectric constant tensor [127], the energy of region 2b is calculated as:

$$U_{2b} = -\frac{1}{2}Q^2 \left( \sum_{i \in 2b} \sum_{\alpha\beta} \frac{M_i^{\alpha\beta} r_{ci}^\alpha r_{ci}^\beta}{r_{ci}^6} \right)$$

where  $Q$  is the net charge of the defect,  $r_{ci}$  is the distance of the  $i$ th atom from the defect centre, and  $M_i^{\alpha\beta}$  is a 3 x 3 matrix for each atomic site, in the Cartesian frame, that represents the on-site polarisability. The quantitative definition of the matrix elements  $M_i^{\alpha\beta}$  is [4]:

$$M_i^{\alpha\beta} = \sum_{\gamma} \left( (D^{-1})^{\alpha\gamma} q \right)_i (\epsilon^{-1})^{\gamma\beta}$$

where  $D_i^{-1}$  represents the on-diagonal block of a modified inverse second derivative matrix and  $\epsilon$  is the static dielectric constant tensor. Note that the inverse of the second derivative matrix is singular and therefore a further approximation must

be made. Physically, this problem corresponds to the division of the polarisation between the sublattices being arbitrary. The usual solution taken is to assume that the polarisation is divided equally between the cation and anion sublattices, with the second derivative matrix being modified correspondingly. In the special case of a cubic crystal, the expression for the region 2b energy can be simplified to:

$$U_{2b} = -\frac{1}{2}Q^2 \left( \sum_{i \in 2b} \frac{m_i}{r_{ci}^4} \right)$$

where  $m_i$  is the average of the diagonal elements of the matrix  $M$  (for the cubic case these will all be equal, but if the isotropic formula were to be applied in a non-cubic case this would not be so).

Because the expression for the region 2b energy is not particularly short-ranged, it is appropriate to evaluate it using lattice summation techniques analogous to those applied to the monopole-monopole term. Hence the term is summed to convergence based on a perfect infinite lattice and then the contributions from ions in regions 1 and 2a are subtracted off. The distance dependent factor within the expression for the energy can be rewritten as:

$$\frac{r^\alpha r^\beta}{r^6} = \frac{1}{8} \left( \frac{\partial^2 \left( \frac{1}{r^4} \right)}{\partial r^\alpha \partial r^\beta} \right) + \frac{\delta_{\alpha\beta}}{4} \left( \frac{1}{r^4} \right)$$

Hence, by evaluating the equivalent of the Ewald summation for the inverse fourth power of distance, and its second derivatives with respect to Cartesian displacements, it is possible to achieve a rapidly convergent expression for the energy of region 2b.

Having described how defect energies are calculated in theory, we mention a few practical points. There are three types of defect that can be specified within GULP:

- Vacancy
- Interstitial
- Impurity

The last one of these three is clearly the combination of a vacancy and an interstitial at the same atomic position in the structure. The location of a vacancy or an impurity can be specified by reference to either a spatial position or an atom position by referencing the site. An interstitial, by its very nature, must be specified by coordinates. When an atom is designated to be vacant, then both the core and shell will be removed automatically since it would not be sensible to leave one or

the other present in the system. It is also possible to specify that a whole molecule be removed from the system, when the connectivity has been defined.

Most types of calculation, that are logically applicable, can also be applied to defect runs, such as optimisation to a minimum or a transition state. In the case of vibrations, the frequencies are calculated for a dynamical matrix based on region 1. It must be noted that this is a large approximation, since any modes that are coupled between regions 1 and 2 will not be properly described. Only localised modes relating to atoms near the centre of region 1 will be correctly predicted. Consequently such calculations of vibrations must be interpreted cautiously.

Finally, a degree of point group symmetry may be utilised during defect calculations. An automatic search for common symmetry elements is performed about the defect centre, including mirror planes and  $C_2$  axes that are aligned with, or between, the Cartesian axes. Such symmetry is used to reduce the number of region 1 and region 2 atoms stored, thereby reducing the number of degrees of freedom for optimisation, as well as taking advantage of symmetry adapted algorithms to accelerate the calculation of the energy and its derivatives.

### 1.4.22 Derivation of interatomic potentials

One of the major challenges facing anyone wishing to use forcefield methods is to determine the functional form and parameters required to calculate the energy and properties. In the field of organic chemistry and biomolecules, there are a number of well-established forcefields, such as MM3 [128], and those associated with the programs AMBER [14], and CHARMM [15], which are, in principle, capable of handling most elements typically found in these systems (C, H, O, N, S, P, etc) in their common hybridisation states. These are constructed around the molecular mechanics approach where the forcefield is connectivity driven and interactions are described in terms of two-, three-, and four-body bonding terms, plus long-range Coulomb and non-bonded interactions. While there have been several attempts to generate general forcefields that cover the entire periodic table, such as UFF [129], ESFF [130], etc, none have been completely successful. Because of the enormity of the amount of data required when spanning the whole range of elements, it is impractical to determine such a universal forcefield by empirical fitting. Instead general rules must be used to predict parameters based on extrapolations and intrinsic properties of the element that are known - for instance the electronegativity. Not surprisingly, this leads to limitations in the quality of the results. For most inorganic systems it is usually necessary to derive a forcefield for the specific material, or family of materials, of interest.

There are two means by which a forcefield can generally be derived, if we exclude rule based extrapolations. Firstly, it is possible to obtain parameters by fitting to a potential energy surface obtained from a non-empirical theoretical method. This would typically consist of results from *ab initio* calculations, ideally on the

periodic solid [131], or perhaps on a gas phase cluster, or even better, both of the aforementioned sources. The potential energy surface can be fitted either as a sequence of geometries with their corresponding energies, or derivatives of the energy could also be included to maximise the amount of information from each higher level calculation. Many of the early forcefields for ionic materials were determined using electron gas methods [132], in which the energies of interaction between pairs of ions were determined by a density functional calculation using the overlapping ionic electron densities, where the anion is confined in an appropriate potential well. Secondly, parameters can be obtained by empirical fitting in which the normal process of using a forcefield to determine the properties of a material is inverted. This approach depends on the availability of a range of experimental data. Knowledge of the crystal structure is a definite prerequisite for this method, but is insufficient alone since information is required as to the curvature of the energy surface about the minimum. This later data may come from quantities such as elastic constants, bulk moduli, piezoelectric constants, dielectric constants, or phonon frequencies.

In order to perform a fit, first it is necessary to define a quantity that measures the quality of the results, known as the sum of squares;

$$F = \sum_{i=1}^{N_{obs}} w_i \left( f_i^{obs} - f_i^{calc} \right)^2$$

where  $N_{obs}$  is the number of observables,  $f_i^{obs}$  and  $f_i^{calc}$  are the fitted and calculated values of the observable, respectively, and  $w_i$  is the weighting factor for the given observable. Because of the weighting factor, there are an infinite number of possible solutions all of which are equally valid. Hence, one of the most important skills is knowing how to choose appropriate and sensible weighting factors. There are several criteria that can be used for guidance though. Firstly, if fitting experimental data, the weighting factor should be inversely proportional to the uncertainty in the measured value. Obviously trusted, precise values should be given more priority than data where there are large error bars. Secondly, the weight factor should be inversely proportional to the magnitude of the observable squared. This ensures that all values are fitted on an equal footing, regardless of units. For example, fitted vibrational frequencies in wavenumbers are typically two to three orders of magnitude larger than structural variables.

The fitting process itself involves minimising the above function  $F$ . To do this, the default approach is similar to that used in optimisation. For many terms, the evaluation of the derivatives of the sum of squares with respect to the variables is complex, and in some of the fitting algorithms that will be discussed subsequently it is even impossible. As a result, numerical derivatives are employed during fitting since it greatly simplifies the process. Because of this, the default optimiser is to use a BFGS update of an initial on-diagonal only Hessian, obtained by finite differences, in a Newton-Raphson process. However, for particularly difficult cases,

where correlation between variables is strong, there is the option to use a full Hessian matrix, again obtained by finite differences.

Now we turn to specifically consider the fitting methodology for the case of empirical data. Traditionally, the experimental structure is fitted by varying the potential parameters so as to minimise the forces at this configuration, and this is the default strategy. Other observables, such as elastic constants etc, are then calculated at the experimental structure too. When working with the shell model, either dipole or breathing shell, there is an additional complication though in that while the cores are fully specified since they are equated with the nuclei of the ions, the positions/radii of the shells are undefined. One approach is to fit with the shells positioned to be concentric with the cores. However, this is unphysical since it implies that there is no ionic polarisation, which defeats the object of including the model in the first place. A second approach might be to place the shell according to specified ion dipoles, but this information is almost impossible to come by. Only data about the total polarisation of the unit cell is typically available and a unique atomic decomposition is not possible. In order to handle this issue, the simultaneous relaxation of shells approach was introduced into GULP [133]. Here the shells are allowed to move during fitting. Formally, the most correct approach is to allow the shells to be energy minimised at every evaluation of the fitting function. However, a simpler approach has been implemented in which the shell forces are added as observables and the shell positions become fitting variables. In this way, the shells are minimised directly within the fitting procedure. In the absence of any observables other than the structure, this is exactly equivalent to minimising the shells at every step of fitting. When observables are present there will be small differences, but these are usually an acceptable price to pay for the greater ease of implementation.

There is actually a more fundamental flaw with the approach of fitting forces at the experimental geometry as a method of fitting. Often we judge the quality of a fit by the percentage error in the structural variables rather than the forces. Although lowering the forces during a fit generally improves the optimised structure with respect to experiment, this is not guaranteed to be the case (and indeed we have found examples where it is not). This can be understood by making a harmonic estimate of the atomic displacements,  $x$ , based on the forces,  $f$ :

$$x = H^{-1}f$$

It can be readily seen that the magnitude of the displacements also depends on the inverse of the Hessian matrix. Thus if the forces improve, but the description of the curvature about the minimum deteriorates, then the errors can potentially increase. If curvature information is included in the fit, then this can tend to reduce this problem. However, there is a further difficulty here. Formally speaking, the expressions for the elastic constants and other properties are defined about a position of zero stress and zero internal derivative. Therefore, calculating the properties at the experimental structure when the forces are non-zero leads to errors also. The

solution to both of these dilemmas is to use the so-called relax fitting methodology [133] in which the structure is fully optimised at every evaluation of the fitting function and the properties calculated at the optimised configuration. Obviously this is a far more expensive procedure, but does yield the most reliable results. Also there is the requirement that the initial potential set is reasonable enough to actually give a valid minimisation of the structure.

Having obtained an apparently successful fit, it is important to assess the quality of the results, since there are plenty of pitfalls and so convergence shouldn't be taken to represent a good quality solution. Firstly, the potential model should be tested for all reasonable properties, not just those used in the fit. It could easily be the case that a forcefield reproduces a high symmetry structure and, say, a single curvature observable, such as the bulk modulus. However, examination of the full elastic constant tensor, dielectric properties and phonons might reveal that the system is unstable with respect to a lowering of symmetry which wouldn't show up in the fit. Secondly, the forcefield could be transferred to a different material, not used in the original fit, to test whether the results are sensible. Finally, it is important to look at the potential parameters and assess whether the numbers are physically sensible. For instance, it is not uncommon for dispersion terms to become extremely large if allowed to fit unconstrained. While this might have improved the sum of squares for one particular system, it means all hope of transferability has been lost. Similarly, there can often be problems with fitting  $A$  and  $\rho$  of a Buckingham potential concurrently due to the strong correlation coefficient between the parameters.

The focus above has been primarily on empirical derivation of interatomic potentials. However, with the increasing ability to perform periodic *ab initio* calculations on solids an attractive alternative is to derive forcefields that attempt to reproduce the results of such methods. There are several reasons to take this approach. Firstly, by fitting the outcomes of a single Hamiltonian it is possible to guarantee that the training set is fully consistent (i.e. there are no differences in temperature, pressure, sample quality, or variable uncertainties in the observables). Secondly, data can be obtained for materials where no experimental information exists or at geometries that are significantly perturbed from the equilibrium one. Thirdly, the data from quantum mechanical methods is free of statistical mechanical effects, such as thermal vibrations and zero point motion. Hence, if the aim is to perform free energy minimisation then the interatomic potentials will represent a proper starting point for the inclusion of these quantities.

Fitting of quantum mechanical data can be performed in one of two ways, either by proceeding in the same fashion as for empirical derivation, or by use of an energy hypersurface. In the latter case, this is achieved by specifying a series of structures with their corresponding energies, and optionally first derivatives. Typically the structures would include the equilibrium configuration and as many distinct distortions about this point in order to probe as many different interatomic distances between atoms as possible. Perhaps the most difficult decision is how to weight

the configurations. Unless the forcefield is able to reproduce the *ab initio* data very accurately, then it is usually desirable to weight the fit in favour of configurations nearer the equilibrium structure. One approach that has been taken is to use a Boltzmann factor weighting based on the energy difference to the minimum energy configuration, with an appropriate choice of temperature to the task ultimately to be performed [134]. However, there are many other possible choices too. A further issue concerns the fitting of quantum mechanical energies. Unless these values have been converted to a binding or lattice energy with reference to the dissociated state of the species within the system then it is inappropriate to fit the absolute values of the energies. Consequently, the easiest solution is to include an additive energy shift parameter in the fit, such that only relative energies are actually fitted.

Finally, the option exists within GULP to perform fitting using genetic algorithms as well as via least squares techniques. This may be potentially useful in cases where a complex system is being fitted when there is no reasonable starting approximation to the forcefield available or where there may be multiple local minima in the parameter space. However, to date we have yet to encounter a situation where this approach has proved beneficial over the more conventional methodology. This emphasizes that there is no substitute for making physically sensible choices for the functional form of the forcefield and the initial parameters.

### 1.4.23 Calculation of derivatives

In order to be able to optimise structures efficiently and to calculate many properties requires the availability of derivatives. While finite difference methods can be used to determine these, this is both inefficient and inaccurate for forcefields, since numerical errors can cause problems, especially when potentials do not go exactly to zero at the cut-off distance. Consequently all derivatives are determined analytically in GULP. All functional forms for the energy have up to analytic second derivatives available, while two-, three- and four-body interactions include third derivatives. In addition, analytic third derivatives can be calculated for the embedded atom method, but currently not for any other many-body potential functions.

Because the determination of derivatives is central to many quantities, a brief description of the approach to their calculation is given here, while fuller details can be found in both the original Harwell Report [135], and the subsequent publication of many of these details[136]. Ultimately two types of derivative are required - those with respect to atomic degrees of freedom and those with respect to the unit cell. In GULP, all atomic coordinate derivatives are calculated in the Cartesian frame of reference and then transformed to the fractional coordinate derivatives, when appropriate to the periodicity. For the unit cell, strain derivatives are taken as previously described.

Both the Cartesian and strain derivatives can be related to a set of pivotal quantities, which are the first derivatives with respect to the interatomic distances, divided

by the distance:

$$\frac{\partial U}{\partial \alpha} = \left( \frac{1}{r} \frac{\partial U}{\partial r} \right)_{\alpha}$$

$$\frac{\partial U}{\partial \varepsilon} = \left( \frac{1}{r} \frac{\partial U}{\partial r} \right)_{\alpha\beta}$$

where, in the expression for the strain derivative, the components  $\alpha$  and  $\beta$  are the appropriate Cartesian directions for the given strain (e.g.  $\varepsilon_4$  implies  $\alpha = y$  and  $\beta = z$ ). It is implicit that all quantities are subscripted with  $ij$  to indicate that the terms refer to a specific pairwise interaction. Let us introduce the shorthand:

$$U_1 = \left( \frac{1}{r} \frac{\partial U}{\partial r} \right)$$

$$U_2 = \left( \frac{1}{r} \frac{\partial}{\partial r} \left( \frac{1}{r} \frac{\partial U}{\partial r} \right) \right)$$

$$U_3 = \left( \frac{1}{r} \frac{\partial}{\partial r} \left( \frac{1}{r} \frac{\partial}{\partial r} \left( \frac{1}{r} \frac{\partial U}{\partial r} \right) \right) \right)$$

The second derivatives can then be obtained by differentiating the above expressions once more and written as:

$$\frac{\partial^2 U}{\partial \alpha \partial \beta} = U_2 \alpha \beta + U_1 \delta_{\alpha\beta}$$

$$\frac{\partial^2 U}{\partial \alpha \partial \varepsilon} = U_2 \alpha \beta \gamma + U_1 (\beta \delta_{\alpha\gamma} + \gamma \delta_{\alpha\beta})$$

$$\frac{\partial^2 U}{\partial \varepsilon_{\alpha\beta} \partial \varepsilon_{\gamma\zeta}} = U_2 \alpha \beta \gamma \zeta + U_1 (\delta_{\alpha\beta} \delta_{\gamma\zeta}) + \frac{1}{4} U_1 (\delta_{\alpha\gamma} \beta \zeta + \delta_{\alpha\zeta} \beta \gamma + \delta_{\beta\gamma} \alpha \zeta + \delta_{\beta\zeta} \alpha \gamma)$$

Likewise, the third derivatives can be obtained by further differentiation:

$$\frac{\partial^3 U}{\partial \alpha \partial \beta \partial \gamma} = U_3 \alpha \beta \gamma + U_2 (\alpha \delta_{\beta\gamma} + \beta \delta_{\alpha\gamma} + \gamma \delta_{\alpha\beta})$$

$$\frac{\partial^3 U}{\partial \alpha \partial \beta \partial \varepsilon_{\gamma\zeta}} = U_3 \alpha \beta \gamma \zeta + U_2 (\alpha (\gamma \delta_{\beta\zeta} + \zeta \delta_{\beta\gamma}) + \beta (\gamma \delta_{\alpha\zeta} + \zeta \delta_{\alpha\gamma}) + \gamma \zeta \delta_{\alpha\beta}) + U_1 (\delta_{\alpha\gamma} \delta_{\beta\zeta} + \delta_{\alpha\zeta} \delta_{\beta\gamma})$$

Note that for free energy minimisation, which is where the third derivatives are required, only the derivatives with respect to two Cartesian coordinates and one strain, or three Cartesian coordinates are needed.

In both three-body and four-body terms there exist derivatives with respect to either a trigonometric function of an angle, or the angle itself. These derivatives can be converted into the above forms through the use of the cosine rule:

$$\cos(\theta) = \frac{r_{12}^2 + r_{13}^2 - r_{23}^2}{2r_{12}r_{13}}$$

where  $\theta$  is the angle at the pivot atom 1, lying between the vectors  $r_{12}$  and  $r_{13}$ . Derivatives with respect to angles are therefore obtained through the expression:

$$\frac{\partial \theta}{\partial r} = -\frac{1}{\sin(\theta)} \frac{\partial \cos(\theta)}{\partial r}$$

Care must be taken in handling the limit as  $\theta$  tends to either  $0^\circ$  or  $180^\circ$ .

### 1.4.24 Crystal symmetry

An important topic, particularly in the context of optimisation, is crystal symmetry. For periodic crystals, there is the option to specify the solid via the asymmetric unit atoms, the space group number/symbol, and the origin setting. It should be noted that the use of space group symbols is preferable since it distinguishes between different settings of the same space group. Apart from the building of the full unit cell from the asymmetric unit, the symmetry can be utilised to greatly accelerate the structural optimisation through several different means. The first benefit of symmetry is that it lowers the number of independent geometric variables, since many atomic coordinates are related via a roto-translation operation. Furthermore, the existence of special positions implies that some coordinates are not allowed to vary, typically for sites such as  $(\frac{1}{2}, \frac{1}{2}, \frac{1}{2})$ , and that in other cases coordinates are not independent and must be related by constraints. Even larger reductions in scale can be achieved by using unit cell centring to reduce the centred-cell down to the primitive representation, thereby reducing the number of atoms by a factor of between 2 and 4. All of these factors reduce the number of variables, and since the rate of convergence is usually correlated to the number of independent variables, depending on the algorithm, this can lead to fewer optimisation steps being required. Furthermore, the amount of memory to store the Hessian matrix is reduced, as well as there being a large improvement in the cost of inverting this matrix.

The second gain from the use of symmetry is that it is possible to use new algorithms to calculate the energy and its derivatives that involve fewer computations, provided the symmetry is high enough [137]. Considering a two-body potential model, instead of looping over all possible pairs of atoms in order to compute the energy, when symmetry is present it is sufficient to only calculate the interactions between the atoms of the asymmetric unit and all other atoms. For a system of  $N^f$  atoms in the full unit cell and  $N^a$  atoms in the asymmetric unit, then the execution times for the algorithms,  $T^f$  and  $T^a$ , respectively, will be given by:

$$T^f \propto \frac{1}{2} N^f (N^f + 1)$$

$$T^a \propto N^a N^f$$

It can therefore be seen that provided the number of atoms in the asymmetric unit is roughly less than half the number in the full unit cell then the symmetry adapted

algorithm will be faster. The extension of symmetry to other types of potential is also straightforward. For example, for a three-body angular potential it is only necessary to calculate the terms that arise when an asymmetric unit atom lies within a valid triad of species.

While the symmetry-adapted evaluation of the energy is trivial, more care is required for the derivatives since these are vector/tensorial properties. For the first derivatives with respect to atomic positions, it is sufficient to again only evaluate the derivatives with respect to the asymmetric unit atoms and then to scale these terms by the number of symmetry-equivalent atoms in the full cell. Conversely, the first derivatives with respect to cell strain are more complex, since although the interaction of the asymmetric unit with all other atoms spans all possible unique derivatives, the orientation of the terms now matters. In short, the strain derivatives will violate the crystal symmetry if the terms are evaluated for the asymmetric unit interacting with the rest of the crystal alone. However, given that the crystal symmetry is specified and that the sum of the terms is correct, when again scaled by the site multiplicities, it is possible to obtain the correct first strain derivatives by appropriate averaging.

Turning now to the second derivatives, the symmetry-adapted generation of the Hessian matrix is more complex. Considering the process by which the Hessian is generated in the absence of symmetry, there are three steps. Firstly, the Cartesian derivatives that are initially generated have to be transformed into fractional space by multiplying each 3 x 3 block by the unit cell vector matrix and its transpose. This generates the matrix  $D_{ff}$ , where the subscript  $f$  signifies a dimension equal to number of atomic coordinates in the full unit cell. Secondly,  $D_{ff}$  is reduced to the smaller matrix  $D_{aa}$ , where the subscript  $a$  now signifies that the dimension is equal to the number of atomic coordinates in the asymmetric unit. This is achieved using the transformation matrix,  $T_{fa}$ , and its transpose:

$$D_{aa} = T_{af}D_{ff}T_{fa}$$

The transformation matrix is sparse and contains 3 x 3 blocks between each asymmetric unit atom and its symmetry equivalent images, which are just the rotation matrices,  $R$ , that created those images. The third, and final, step is to reduce the matrix  $D_{aa}$  according to any constraints that are present between coordinates. It is possible to combine the second and third steps into one by pre-multiplying the transformation matrix by the constraint matrix.

All the symmetry unique information concerning the second derivatives is contained within the columns between the asymmetric unit and the full cell. Hence, it is more efficient just to calculate the sub-matrix  $D_{fa}$  instead. This can then be transformed to the required matrix according to:

$$D_{aa} = S_{af}D_{fa}$$

This not only reduces the computational effort in calculating the second derivatives,

but also reduces the memory required and lowers the number of matrix multiplications required to form the Hessian. The 3 x 3 blocks of the required transformation matrix are given by:

$$S_{af} = \frac{1}{N_{eqv}^a} \sum_{n=1}^{N_{eqv}^a} R_n^{-1} R_{f'}$$

where  $N_{eqv}^a$  is the number of symmetry equivalent atoms to the asymmetric unit atom  $a$ , and  $f'$  is the atom to which the atom  $f$  maps under the transformation  $R_n^{-1}$ . Again the second derivatives with respect to strain-strain and strain-internal are more complex since they are initially generated such that symmetry is violated. However, resymmetrisation by averaging symmetry related matrix elements solves this problem.

The use of crystal symmetry in reciprocal space is even more straightforward than in real space. Because the Ewald sum can be written to be a sum over one-centred terms in reciprocal space, instead of a pairwise expression, the only change necessary is to restrict the sum to the asymmetric unit with appropriate weighting for site multiplicity. The same strategy is used in the symmetrisation of other one-centre terms in real space, such as the Einstein model. Crystal symmetry is also exploited in the calculation of charges via the electronegativity equalisation method, which is thereby accelerated, especially through the reduction of the size of the matrix to be inverted.

### 1.4.25 Code details

The original version of GULP [137] was written in Fortran 77 since the more recent standards had yet to be released. This implied that memory was statically allocated via a series of parameters. Subsequently, non-standard extensions were introduced to allow the second derivative arrays to be dynamically declared, since they represented the dominant use of memory. For the current version Fortran 90 has now been adopted leading to full use of dynamic memory.

The program has been compiled and tested for most Unix-style operating systems, including Linux and Apple OS X (under which it is developed). The GNU gfortran compiler is supported by default, with the Intel compiler also being an option. Other compilers may work and can be configured by the user. While compilation under MS-DOS is in principle possible, this operating system is not supported since it is the only operating system that cannot be automatically catered for within a single standard Makefile.

The code has also been parallelised for the evaluation of the energy and first derivatives using MPI, based upon a replicated data paradigm. When performing calculations on sufficiently large systems that require the use of parallel computers, then the most appropriate types of calculation are usually either conjugate gradient optimisation or molecular dynamics. Hence, the absence of second derivatives is

less critical. However, a distributed data algorithm for the second derivatives using Scalapack for matrix diagonalisation/inversion would be feasible and may be implemented in the future. Because GULP is currently targetted primarily at crystalline systems, where unit cells are typically small, the distribution of parallel work does not use a spatial decomposition. Instead the Brode-Ahlich algorithm [138] is used for the pairwise loops in real space in order to try to ensure load balancing over the processors. A similar approach is used for the four-body potentials based on the first two atoms of the sequence of four. In the case of three-body potentials, the work is divided by a straight distribution of pivot atoms over the nodes. Parallelisation in reciprocal space is achieved by an equal division of reciprocal lattice vectors over nodes. Given that the number of operations per  $k$ -vector is equal, this should guarantee load balancing as long as the number of reciprocal lattice vectors is large compared with the number of processors (which is almost always the case).

# Chapter 2

## Results

In this section we present a few illustrations of the application of the new functionality within GULP, including validation studies to compare with previous implementations.

### 2.0.1 Mechanical properties

The range of mechanical, and related, properties computed by GULP has been significantly extended for the present version. Since no article on simulations of ionic materials would be complete without a mention of the ubiquitous and evergreen perennial MgO, we choose to take this well-studied system as an example.

Magnesium oxide adopted the cubic rock salt structure and possesses the well-known characteristic of exhibiting a Cauchy violation in the elastic constants (i.e.  $C_{12} \neq C_{44}$ ). No simple two-body forcefield is capable of reproducing this many body effect. Consequently, it is necessary to use a breathing shell model to describe this material accurately. While there have been previous breathing shell models for MgO [139], we choose to fit a new set of potentials here that reproduce the structure, elastic constants, and high and low frequency dielectric constants under ambient conditions. The resulting potential model is described in Table 2.1, while the calculated properties are given in Table 2.2.

The calculated properties for magnesium oxide can be seen to be in excellent agreement with experiment under ambient conditions, with the exception of the Poisson ratio. Of course, this agreement is a consequence of fitting a model with the correct essential physics to a subset of the experimental data. The disagreement in the Poisson ratios is because the values are calculated using different expressions. If the Poisson ratio is evaluated based on the sound velocities according to:

$$\sigma = \frac{\left(\frac{V_p}{V_s}\right)^2 - 2}{2 \left[ \left(\frac{V_p}{V_s}\right)^2 - 1 \right]}$$

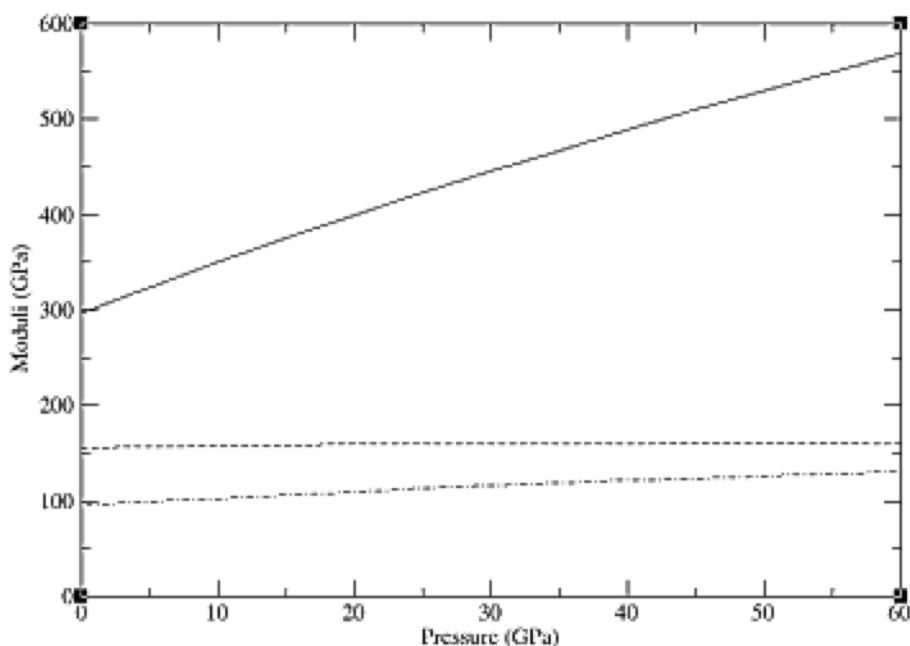
Table 2.1: Breathing shell model for magnesium oxide. Here “shel” denotes a potential that acts on the central position of the shell, while “bshel” denotes an interaction that acts on the radius of the shell which was fixed at 1.2Å. The charge on *Mg* is +2, while the core and shell charges for *O* are +0.8 and −2.8, respectively.

Species 1	Species 2	$A(\text{eV})$	$\rho(\text{Å})$	$C_6(\text{eVÅ}^6)$	$k_{cs}(\text{eVÅ}^{-2})$	$k_{BSM}(\text{eVÅ}^{-2})$
Mg core	O bshel	28.7374	0.3092	0.0	-	-
O shel	O shel	0.0	0.3	54.038	-	-
O core	O shel	-	-	-	46.1524	-
O shel	O bshel	-	-	-	-	351.439

Table 2.2: Calculated and experimental properties for magnesium oxide under ambient conditions. All experimental elastic properties are taken from reference [140]. Note, for the calculated bulk ( $K$ ) and shear ( $G$ ) moduli the Hill value is taken, though the variation between definitions is small.

Properties	Experiment	Calculated
$a(\text{Å})$	4.212	4.2123
$C_{11}(\text{GPa})$	297.0	297.1
$C_{12}(\text{GPa})$	95.2	95.1
$C_{44}(\text{GPa})$	155.7	155.7
$\epsilon^0$	9.86	9.89
$\epsilon^\infty$	2.96	2.94
$K(\text{GPa})$	162.5	162.4
$G(\text{GPa})$	130.4	130.9
$V_s(\text{km/s})$	6.06	6.05
$V_p(\text{km/s})$	9.68	9.70
$\sigma$	0.18	0.24

Figure 2.1: The variation of the elastic constants of magnesium oxide with applied pressure as determined by breathing shell model calculation.  $C_{11}$ ,  $C_{12}$ , and  $C_{44}$  are presented by a solid, dashed and dot-dashed line, respectively.



then our calculated value becomes 0.182 in good agreement with the determination of Zha *et al* [140].

To provide a test of the model, it is possible to calculate the variation of the elastic properties of magnesium oxide as a function of applied pressure. The variation of the elastic constants up to 60 GPa is shown in Figure 2.1.

When compared to the experimental results of Zha *et al*, the calculated trend in the value of  $C_{11}$  is in good agreement in that it consistently increases under pressure and approximately doubles in magnitude by the time that 60 GPa is reached. Unfortunately, the trends for the other elastic constants are not so good, since the curve for  $C_{12}$  flattens with increasing pressure, rather than becoming steeper, and the curve for  $C_{44}$  passes through a maximum which is not observed in the experimental data from the aforementioned group. However, the calculated trends do match the extrapolated behaviour based upon the results of ultrasonic measurements [141].

## 2.0.2 Born effective charges

The Born effective charges represent a useful means of characterising the response of a potential model to perturbations, particularly those that create an electric field.

Table 2.3: Born effective charges (in a.u.) calculated according to the shell model of Sanders *et al* [142] and from first principles techniques [143]. Values are shown for the asymmetric unit atoms with the approximate positions of the Si atom at (0.46,0,0) and the O atom at (0.41,0.27,0.11) in space group 154, with the origin set to (0,0,1/3).

	Si			O		
Shell model	3.122	0.0	0.0	-1.406	0.368	0.252
	0.0	3.530	0.292	0.364	-1.920	-0.517
	0.0	-0.171	3.422	0.176	-0.568	-1.711
LDA	3.016	0.0	0.0	-1.326	0.429	0.222
	0.0	3.633	0.282	0.480	-1.999	-0.718
	0.0	-0.324	3.453	0.298	-0.679	-1.726

Increasingly values are becoming available from *ab initio* techniques for solids through the application of linear response methods. Hence, this quantity can provide a useful comparison between the results of formal-charge shell model calculations and more accurate first principles methods.

One of the first materials for which the Born effective charges were determined using planewave techniques is  $\alpha$ -quartz. In Table 2.3 the values obtained from the shell model of Sanders *et al* [142] are compared with those yielded by a planewave calculation using the Local Density Approximation and norm-conserving pseudopotentials [143].

The comparison of the Born effective charge tensors demonstrates that the oxygen shell model is surprisingly successful at reproducing the quantum mechanical data, especially in comparison to rigid ion models, which would yield a diagonal matrix with all components equivalent. Furthermore, the polarisability of the shell leads to the ions behaving as partially charged species with realistic magnitudes. Consequently, this explains why the seemingly unreasonable use of a formal charge for  $Si^{4+}$  actually works extremely well in practice. Similar observations have been previously made for perovskite materials [144].

### 2.0.3 Frequency-dependent optical properties

Ever since the early days of atomistic simulation within the shell model context it has been routine to calculate the static and high frequency dielectric constant tensors. Indeed this data has often been used during the fitting process as well. However, the values obtained from experiment will always be measured at a particular frequency and this will never exactly correspond to the limiting values determined by the direct means of calculation. As described in the background theory section, it is possible to evaluate the dielectric properties and refractive indices as a function of radiation frequency for the gamma point.

Here we present results for the frequency variation of the dielectric constant tensor of quartz, shown in Figure 2.2, as calculated using the previously mentioned shell model potential of Sanders *et al* [142]. Note that the limiting values are the same as the ones obtained without reference to the phonon frequencies.

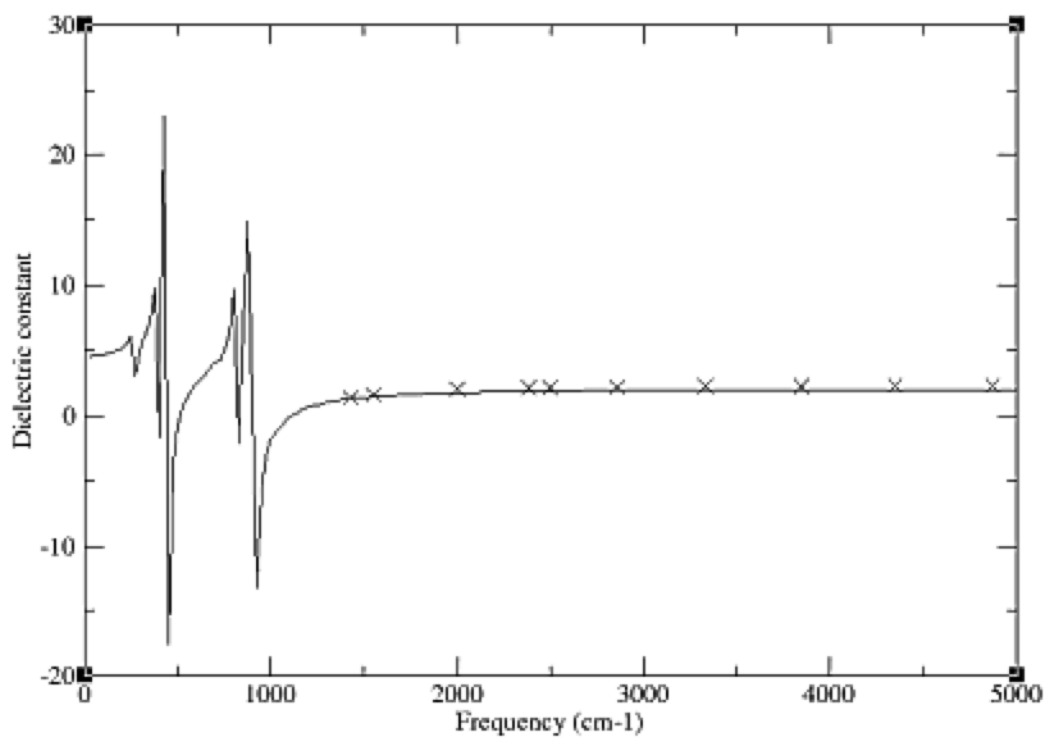
In accord with experiment, the dielectric constant decreases slowly with the frequency of measurement until the highest phonon mode of quartz - the Si-O stretch - is approached. At frequencies below this the curve contains considerable variation caused by the discontinuities when a lattice phonon mode is reached. For simplicity, the curve shown is for the dielectric constant in the *ab* plane only. The corresponding curve for the principal tensor component parallel to the 001 direction is almost identical, except that the limiting values are slightly different and the positions of the discontinuities due to coincidence with phonons are displaced to higher frequency.

While the qualitative agreement with experimental data is good, there is a quantitative discrepancy in the dielectric constant variation. This is a result of the imperfection of the original fit to the dielectric data for quartz, though there are also issues concerning the variation with temperature since the calculations are formally performed at absolute zero, while the experiment data was measured at 293 K. However, the use of empirical fitting implies that the interatomic potentials do partially account for the temperature difference already. At the lowest measured frequency, the calculated values are an almost perfect match due to the faster rate of decrease of the dielectric constant in the experiment data.

## 2.0.4 Surface calculations

Before applying GULP to surfaces problems that were previously not possible, it must first be validated. Firstly, we focus on comparing our results to MARVIN, starting with the simple inorganic salt corundum. In the original MARVIN paper [110], the twelve faces with the lowest interplanar spacings were identified and their surfaces relaxed using several different potential models. The calculations utilising the QM5 model were repeated using both MARVIN with the BFGS minimiser and the same surfaces generated using GDIS and minimised in GULP using its BFGS minimiser. The unrelaxed surface and attachment energies were compared and both sets of calculations agreed to better than  $0.0001\text{Jm}^{-2}$  for the surface energies and within  $0.0001\text{eVmol}^{-1}$  for the attachment energies. This indicates that the 2-D Ewald sum incorporated into GULP is correct. Next the relaxed surface and attachment energies were compared. Except for the (310) face, all the GULP calculations returned the same relaxed surface energy as the corresponding MARVIN run to within  $0.0001\text{Jm}^{-2}$ . The relaxed attachment energies agreed to within  $0.003\text{eVmol}^{-1}$ . Excluding the (310) face, the MARVIN calculations took 138 s on a 1133MHz Intel Pentium III CPU Linux system, whilst the GULP calculations took just 108 s. This difference in timing is primarily due to the faster energy calculation

Figure 2.2: The on-diagonal component of the dielectric constant tensor for  $\alpha$ -quartz in the  $ab$  plane as a function of frequency of measurement. The solid line represents the calculated shell model values, while the crosses represent values estimated from experimental measurements of the refractive index as a function of frequency.



time in GULP since the MARVIN minimiser is based on the GULP algorithm and consequently the number of cycles to minimise a face in GULP and MARVIN only differed by at most one cycle, except for the (21-1) where GULP took 31 cycles versus the 24 for MARVIN. The (310) face is interesting as the relaxed surface energy calculated by GULP is the same as that reported in the original paper [110] and it is the minimised surface energy from the present calculation with MARVIN that is different. Although not stated in the MARVIN paper, the minimisations were done using a combination of minimisers; conjugate gradients until the gradient norm is unity, followed by a BFGS minimisation. If the MARVIN calculations are repeated with this combination, all surface energies between MARVIN and GULP agree to within  $0.0001 Jm^{-2}$ . In conclusion then, we can say that for this simple inorganic system, GULP and MARVIN produce essentially the same results.

As an example of the application of the new GULP surface capabilities, they have been recently utilised to search for surface reconstructions of the (10-14) cleavage plane of calcite [145]. The previous modelling studies have not found any evidence of surface reconstructions, despite the LEED results of Stipp [146]. A very efficient and assumption free way of finding reconstructions is to determine the surface phonon dispersion across the Brillouin zone, where the presence of any imaginary phonons will indicate that a reconstruction wants to occur. This calculation was performed on the cleavage plane of calcite, using a new calcite potential model that we have recently developed. An imaginary mode was found to be present at  $(1/2, 0)$  in reciprocal space, which indicates that the system is unstable within the  $(1 \times 1)$  surface cell and that the reconstruction requires the formation of a  $(2 \times 1)$  supercell. On creation of the surface supercell, the system was perturbed along the eigenvector of the imaginary mode and re-minimised using the rational function optimisation technique to ensure that the final Hessian matrix had the correct character for an energy minimum. Finally, the optimised  $(2 \times 1)$  cell was examined to ensure that there were no imaginary phonon modes anywhere within the Brillouin zone. The calculations were repeated using other calcite models in the literature, which were found not to possess any imaginary modes.

In the reconstructed surface, as shown in Figure 2.3, every second row of surface carbonate anions are found to rotate. The rotation moves the O atom of each carbonate such that it is  $13^\circ$  closer to the vertical. This is accompanied by significant change in the carbonate geometry with an increase of the O-C-O angle of  $3^\circ$ , where the two oxygen atoms are those pointing out of the surface and a compensating decrease in the other two O-C-O angles. Finally, we note that the reconstruction is confined to the top layer of the surface. In order to confirm the correct nature of the surface reconstruction, we have calculated the LEED pattern that would result, which is found to be an excellent match to the experimental pattern measured by Stipp under low pressure conditions.

Figure 2.3: Comparison of the geometry for (a) a doubled unit cell of the (1x1) structure for the (10-14) surface of calcite and (b) the optimised (2x1) reconstruction of the same surface. The reconstruction results in every second vertical row, labelled B, adopting a different configuration to the unreconstructed rows, labelled A.

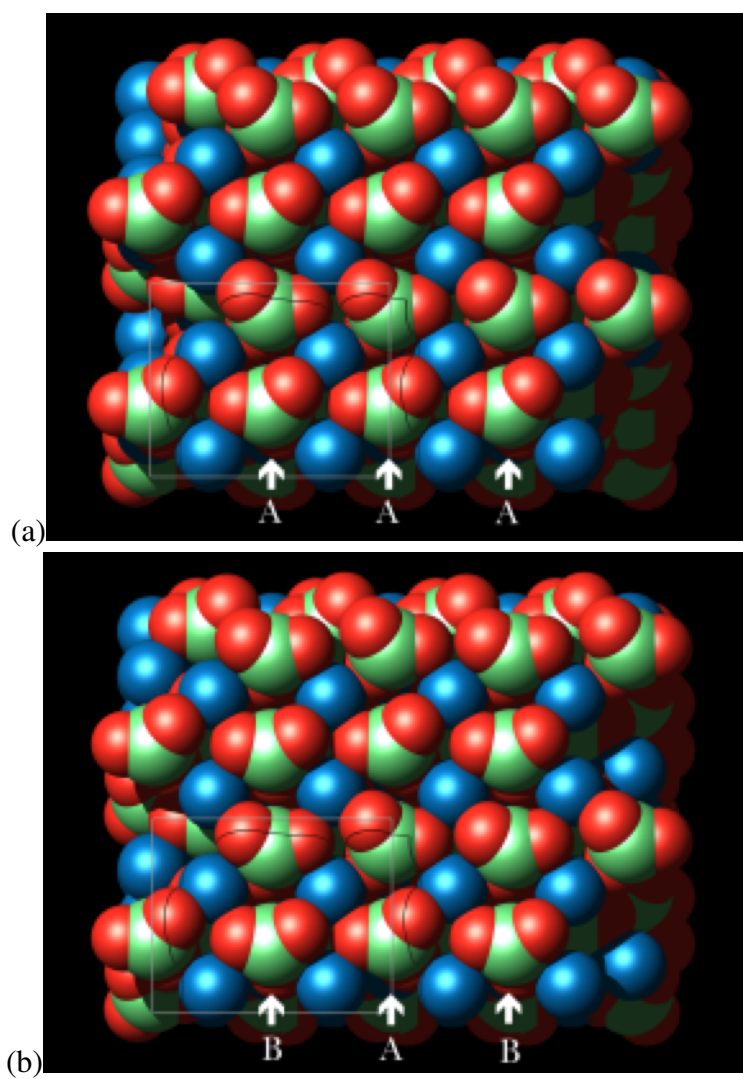


Table 2.4: Calculated properties of diamond based on the model of Brenner *et al* [68]. Note that the calculated values for the bond length and energy are not quoted in the original reference. However, since the experimental values were part of the fitted data, we take these values to be equal to the observed ones.

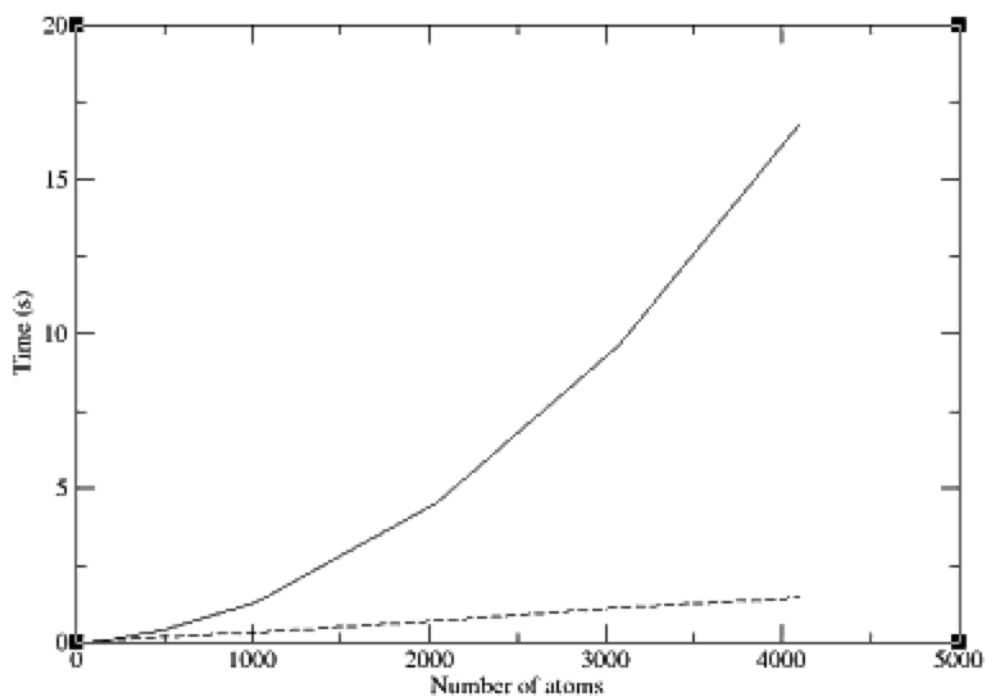
Property	Experiment	Original value	GULP value
Bond length(Å)	1.54	1.54	1.5441
Bond energy (eV)	3.68	3.68	3.684
$C_{11}$ (GPa)	10.8	10.7	10.75
$C_{12}$ (GPa)	1.3	1.0	1.26
$C_{44}$ (GPa)	5.8	6.8	7.21

## 2.0.5 Bond-order potentials

Given that new implementation of the Brenner model has been introduced into GULP we present here some results for diamond, Table 2.4, as previously studied in the original paper [68], in order to validate the code. For the second derivative properties, there is also the difference that the values obtained here are fully analytic whereas the published values are obtained via finite differences. This may explain the small discrepancies in the elastic constants.

As stated in the background section, two algorithms have been implemented for the evaluation of the Brenner potential based on either pairwise atom looping or a spatial decomposition in order to determine the neighbour list. The computational cost of the two approaches for increasing supercells of diamond are illustrated in Figure 2.4. The linear scaling behaviour of the spatial decomposition can clearly be seen, as can the fact that this algorithm is effectively superior in performance for systems containing beyond a 100 atoms. Obviously this trade off point is dependent on the density of the system, though there are few cases for hydrocarbons where the density is greater than that of diamond. For systems much below a 100 atoms the cost of evaluating the Brenner potential is so negligible in comparison to other tasks, such as a matrix inversion for property calculation, that the choice of algorithm is irrelevant.

Figure 2.4: A comparison of the computer times required for a single energy-force evaluation using the Brenner model according to whether the algorithm used involves a pairwise sum (solid line) or a spatial decomposition (dashed line) to evaluate the neighbour list. Timings given are for a Mac PowerBook G4 laptop with a clock speed of 700 MHz.



# Chapter 3

## Further background

In this section some of the theory behind GULP is explained and references are supplied for those who require a more detailed description of the methods involved.

### 3.0.0.1 Cut-offs and molecules

All short-ranged two-, three- and four-bodied potentials have finite cut-offs in real space which must be set by the user in some way. Unless the cut-off chosen is so large that convergence is genuinely achieved then it effectively becomes a parameter of the potential. Hence when publishing new potentials it is good practice to publish the cut-offs. Similarly, if you are trying to reproduce the results of previously published potentials make sure you use the same cut-offs.

The main effect of finite cut-offs is to introduce discontinuities into the energy surface as atoms move across the boundary. Generally speaking, the energy minimisation procedure in GULP is not too sensitive to these because of the use of analytical second derivatives. However, if working with only first derivatives or particularly short cut-offs this can be the reason for a minimisation failing to satisfy the required convergence criteria.

An important difference between GULP and some other programs is that it is perfectly allowable for potentials to overlap, i.e. two or more potentials can act between the same species at the same distance. Hence, there are no resulting restrictions for the cut-offs and complex potential functions can be built by combining several potentials together. Conversely, it is important not to duplicate potentials when not intended.

For some types of potential the cut-offs may correspond to chemical criteria such as bond lengths or they may only need to act between molecules or conversely only within them. In such cases it is best not to use distance cut-offs to achieve the correct effect, but instead to use the molecule handling facilities within GULP. There are three keywords which when specified activate the molecule facility within the program - `molecule`, `molq` and `molmec`. If any of these words are present

Table 3.1: Common functional forms for two-body interatomic potentials incorporated into GULP (where  $r$  represents the distance between two atoms  $i$  and  $j$ ). For full documentation see help.txt.

Potential Name	Formula	Units for input
Buckingham	$A \exp(-r/\rho) - Cr^{-6}$	$A$ in eV, $\rho$ in Å, $C$ in eVÅ <sup>6</sup>
Lennard-Jones <sup>†</sup>	$Ar^{-m} - Br^{-n}$ or $\varepsilon(c_1(\frac{\sigma}{r})^m - c_2(\frac{\sigma}{r})^n)$ $c_1 = (n/(m-n))(m/n)^{(m/(m-n))}$ $c_2 = (m/(m-n))(m/n)^{(n/(m-n))}$	$A$ in eVÅ <sup><math>m</math></sup> , $B$ in eVÅ <sup><math>n</math></sup>  $\varepsilon$ in eV, $\sigma$ in Å
Harmonic*	$\frac{1}{2}k_2(r-r_0)^2 + \frac{1}{6}k_3(r-r_0)^3 + \frac{1}{12}k_4(r-r_0)^4$	$k_2$ in eVÅ <sup>-2</sup> , $r_0$ in Å $k_3$ in eVÅ <sup>-3</sup> , $k_4$ in eVÅ <sup>-4</sup>
Morse	$D\{[1 - \exp(-a(r-r_0))]^2 - 1\}$	$D$ in eV, $a$ in Å <sup>-2</sup> , $r_0$ in Å
Spring (core-shell)	$\frac{1}{2}k_2r^2 + \frac{1}{24}k_4r^4$	$k_2$ in eVÅ <sup>-2</sup> , $k_4$ in eVÅ <sup>-4</sup>
Cosh-spring	$k_2r^2(\cosh(r/d) - 1)$	$k_2$ in eVÅ <sup>-2</sup>
General	$A \exp(-r/\rho)r^{-m} - Cr^{-n}$	$A$ in eVÅ <sup><math>m</math></sup> , $\rho$ in Å, $C$ in eVÅ <sup><math>n</math></sup>
Stillinger-Weber (sw2)	$A \exp(\rho/(r-r_{max}))(Br^{-4} - 1)$	$A$ in eV, $\rho$ in Å, $B$ in Å <sup>4</sup>
<sup>†</sup> combination rules permitted * $k_3, k_4$ are optional		

Table 3.2: Common functional forms for three-body potentials incorporated into GULP (where  $r$  represents the distance between two atoms  $i$  and  $j$ ,  $\theta_{ijk}$  represents the angle between the two interatomic vectors  $i-j$  and  $j-k$ ). For full documentation of all the functional forms available see help.txt.

Potential Name	Formula	Units for input
Stillinger-Weber (sw3)	$K \exp(\rho/(r_{12} - r_{\max}) + \rho/(r_{13} - r_{\max}))(\cos(\theta_{213}) - \cos(\theta_0))^2$	K in eV, $\rho$ in Å
Three-body <sup>†</sup>	$\frac{1}{2}k_2(\theta - \theta_0)^2 + \frac{1}{6}k_3(\theta - \theta_0)^3 + \frac{1}{12}k_4(\theta - \theta_0)^4$	$\theta_0$ in ° $k_2$ in eVrad <sup>-2</sup> $k_3$ in eVrad <sup>-3</sup> $k_4$ in eVrad <sup>-4</sup>
Three-body*	$\frac{1}{2}k_2(\theta_{213} - \theta_0)^2 \exp(-r_{12}/\rho) \exp(-r_{13}/\rho)$	$k_2$ in eVrad <sup>-2</sup> $\theta_0$ in °, $\rho$ in Å
Axilrod-Teller	$K(1 + 3 \cos \theta_{213} \cos \theta_{123} \cos \theta_{132})/(r_{12}r_{13}r_{23})^3$	$K$ in eVÅ <sup>9</sup>
Exponential	$A \exp(-r_{12}/\rho) \exp(-r_{13}/\rho) \exp(-r_{23}/rho)$	$A$ in eV, $r$ in Å
Urey-Bradley	$\frac{1}{2}k(r_{23} - r_0)^2$	$k$ in eVÅ <sup>-2</sup> $r_0$ in Å
Cosine-harmonic	$\frac{1}{2}k_2(\cos \theta - \cos \theta_0)^2$	$k_2$ in eV
Linear3 (lin3)	$k(1 \pm \cos(n\theta))$	$k$ in eV
Hydrogen-bond	$(\frac{A}{r^m} - \frac{B}{r^n}) \cos^p \theta$	$A$ in eVÅ <sup>m</sup> , $B$ in eVÅ <sup>n</sup>
UFF3	$K(C_0 + C_1 \cos \theta + C_2 \cos 2\theta)$	$K$ in eV
Equatorial	$\frac{2K}{n^2}(1 - \cos(n\theta)) + 2K \exp(-\beta(r_{13} - r_0))$	$K$ in eV, $\beta$ in Å <sup>-1</sup>
Bond-angle cross (bacross)	$(k_1(r_{ij} - r_{ij}^0) + k_2(r_{jk} - r_{jk}^0))(\theta - \theta_0)$	$k_1$ & $k_2$ in eV Å <sup>-1</sup> deg <sup>-1</sup>
Bond cos cross	$k_1(r_{ij} - r_{ij}^0)(r_{jk} - r_{jk}^0)(1 + b \cos(n\theta)^2)$	$k_1$ in eV Å <sup>-2</sup>
Bond cross	$(k_1(r_{ij} - r_{ij}^0)(r_{jk} - r_{jk}^0))$	$k_1$ in eVÅ <sup>-2</sup>
<sup>†</sup> harmonic, option three		
* harmonic + exponential, option three expo		

Table 3.3: Common functional forms for four-body potentials incorporated into GULP (where  $\phi_{ijkl}$  is the torsional angle between the planes  $ijk$  and  $jkl$ ). For full documentation see the file help.txt.

Potential Name	Formula	Units for input
Torsion	$k(1 + \cos(n\phi - \phi_0))$	$k$ in eV, $\phi_0$ in $^\circ$
ESFF torsion	$k_1 \sin_1^2 \sin_2^2 \pm k_2 \sin_1^n \sin_2^n \cos(n\phi)$	$k$ in eV
Ryckaert-Bellemans	$\sum k_n (\cos \phi)^n$	$k_n$ in eV
Tortaper/torex	As per torsion multiplied by taper or exponential decay	
Torharm	$\frac{1}{2}k(\phi - \phi_0)^2$	$k$ in $eV rad^{-2}$ , $\phi_0$ in $rad$
UFF4	$\frac{k}{2}(1 - \cos(n\phi_0) \cos(n\phi))$	$k$ in eV
Torangle	$k \cos(\phi)(\theta_{123} - \theta_{123}^0)(\theta_{234} - \theta_{234}^0)$	$k$ in $eV rad^{-2}$
Torcosangle	$k \cos(\phi)(\cos(\theta_{123}) - \cos(\theta_{123}^0))(\cos(\theta_{234}) - \cos(\theta_{234}^0))$	$k$ in eV
Out of plane	$k_2 d^2 + k_4 d^4$	$k_2$ in $eV \text{\AA}^{-2}$ , $k_4$ in $eV \text{\AA}^{-4}$
Inversion	$k(1 - \cos(\phi))$	$k$ in eV
Cross angle (xangleangle)	$k_{213/4}(\theta_{213} - \theta_{213}^0)(\theta_{214} - \theta_{214}^0) +$ $k_{312/4}(\theta_{312} - \theta_{312}^0)(\theta_{314} - \theta_{314}^0) +$ $k_{412/3}(\theta_{412} - \theta_{412}^0)(\theta_{413} - \theta_{413}^0)$	$k_{213/4}$ , $k_{312/4}$ , $k_{412/3}$ in $eV rad^{-2}$
Cross angle cosine (xcosangleangle)	$k_{213/4}(\cos(\theta_{213}) - \cos(\theta_{213}^0))(\cos(\theta_{214}) - \cos(\theta_{214}^0)) +$ $k_{312/4}(\cos(\theta_{312}) - \cos(\theta_{312}^0))(\cos(\theta_{314}) - \cos(\theta_{314}^0)) +$ $k_{412/3}(\cos(\theta_{412}) - \cos(\theta_{412}^0))(\cos(\theta_{413}) - \cos(\theta_{413}^0))$	$k_{213/4}$ , $k_{312/4}$ , $k_{412/3}$ in eV
UFF out of plane	$k(c_0 + c_1 \cos(\phi) + c_2 \cos(2\phi))$	$k$ in eV

then a search will be performed to locate any molecules within the structures input. This is done by searching for bonds based on the sum of the covalent radii plus a percentage tolerance factor. For most common compounds the default covalent radii will be sufficient to locate all the bonds - if this is not the case then it is possible for the user to either increase the tolerance factor or to adjust the covalent radii using the `covalent` option from the `element` group of commands.

An alternative scenario is that atoms become bonded which shouldn't be. For example, metal atoms often can become bonded in ionic compounds because the covalent radii is no longer relevant for a positively charged ion. These bonds can be removed either by manually setting the radii of the element to zero or by using the `nobond` option to exclude the formation of certain bond types. Whether the correct molecules have been located or not can be seen from the molecule print out in the output file. The three molecule-based keywords mentioned above differ in what they imply for the treatment of intramolecular electrostatics:

- `molecule`  $\Rightarrow$  exclude all Coulomb interactions within the molecule
- `molq`  $\Rightarrow$  retain all Coulomb interactions within the molecule
- `molmec`  $\Rightarrow$  exclude all Coulomb interactions between atom which are bonded (1-2) or two bonds away (1-3)

The specification of `molmec` does not automatically imply that all potentials will be treated in a molecular mechanics fashion, only the electrostatic terms. Providing one of the above three terms is present then optional words may be added to a

potential specification line which control aspects of the potential cut-offs. Below is a list of the words that are available and whether it is necessary to still give any cut-offs on the potential parameter line:

Option	Effect	Cut-offs?
intra	only act within a molecule	yes
inter	only act between molecules	yes
bond	only act between bonded atoms	no
x12	do not act between bonded atoms	yes
x13	do not act between 1-2 and 1-3 atoms	yes
x14	do not act between 1-2, 1-3 and 1-4 atoms	yes
o14	only act between 1-4 atoms	yes
g14	act between 1-4 atoms and beyond	yes
single	only act where atoms are singly bonded	no
resonant	only act where atoms are resonantly bonded	no
double	only act where atoms are doubly bonded	no
triple	only act where atoms are triply bonded	no
quadruple	only act where atoms are quadruply bonded	no
amide	only act where atoms are part of an amide group	no
custom	only act where atoms are joined by a custom bond	no
half	only act where atoms are half bonded	no
quarter	only act where atoms are a quarter bonded	no
third	only act where atoms are one third bonded	no

In addition to atoms being bonded, GULP now offers the ability to specify a bond type for each bond. This can be used so a potential only acts between two species when they have a particular bond order. At present the bond order has to be specified via the connect option (see below).

Although with some options it is necessary to still specify a cut-off for generality, the value may not be important any more. For example, if an O-H potential for water is specified as being intramolecular then as long as the maximum distance cut-off is greater than about 1.0 Å then it doesn't matter particularly what it is. Similarly for a potential which is given as being x12 then it doesn't matter if the minimum cut-off distance is zero - the potential won't act between bonded atoms.

By default, GULP dynamically calculates the molecular connectivity during a calculation. The reason for this is that it ensures that the restart file will yield the same answer as the point in the calculation where it left off. However, sometimes difficulties occur because a bond becomes too long and the molecule breaks into two. When this happens GULP will stop with an error message as this often indicates that the potential model is not working well for the system under study. If the user wants to proceed regardless then there is a keyword `fix` which tells the program to fix the connectivity as that at the starting geometry and not to update it. This means that the program will never stop with this error, but it does mean that

a restart may not give the same answer as the initial run if atoms have moved too far. There is now also the option for the user to specify the connectivity explicitly in the input deck using the `connect` option. Note that when using symmetry the `connect` option must be specified based on the full cell atom numbers and for all images at present.

In the case of ionic materials where the user would like to try to remove some of the numerical problems associated with cut-offs then there are some other options. The normal way of doing this is with a cut-and-shifted potential. In this approach the potential is forced to go to zero at the cut-off by adding a constant to the energy. This makes the energy continuous, but the gradient still has a discontinuity. Again this can be resolved by adding a second term which shifts the gradient to be zero at the cut-off. In GULP this takes the form of a linear term in the distance which, provided the cut-off isn't very short, will have minimal effect in the region of the potential minimum. These corrections are activated using the potential options `energy` or `gradient` after the potential type, but are only currently applicable to certain two-body potentials where it is appropriate. It should be noted that some potential functions go to zero by construction at the cut-off, for example the Stillinger-Weber two- and three-body potentials.

### 3.0.0.2 Combination rules

When using Lennard-Jones potentials it is common to use combination rules to determine the interaction parameters between two species. This means that the parameters for the interaction are determined from one-centre only parameters by some form of averaging. The main advantage of this approach is that it reduces the number of parameters to be determined and aids transferability of potentials. Conversely, the resulting potentials may not be as accurate for any one given system. There are two types of combination rule used, depending on whether the potential is being used in the  $\epsilon/\sigma$  or  $A/B$  format (see Table 2 for details). If the potentials are being used in the  $A/B$  form then the average is taken using a geometric mean:

$$A_{ij} = \sqrt{A_i A_j}$$

$$B_{ij} = \sqrt{B_i B_j}$$

However, if the  $\epsilon/\sigma$  form is being employed then a more complex relationship is needed:

$$\epsilon_{ij} = \frac{2(\epsilon_i \epsilon_j)^{\frac{1}{2}} (\sigma_i^3 \sigma_j^3)}{(\sigma_i^6 + \sigma_j^6)}$$

$$\sigma_{ij} = \left( \frac{\sigma_i^6 + \sigma_j^6}{2} \right)^{\frac{1}{6}}$$

Within GULP it is possible to specify the parameters by species, rather than by pairs of species, using the `atomab` or `epsilon` options. If the word `combine` is added to the specification of a Lennard-type potential then the parameters can be omitted from the input and they will be generated using the appropriate combination rules. In turn this makes it possible to fit potentials based on combination rules without having to do this via a series of constraints.

### 3.0.0.3 Mean field theory

One of the biggest problems that can face someone attempting to simulate complex materials is the fact that often they can be partly disordered or involve partial occupancies of sites. One approach to treating such systems is to generate a supercell so that lots of permutations can be examined. However, the number of possibilities is usually too large to examine each one individually to locate the most stable configuration. Furthermore, this process may alter the symmetry of crystal. Fitting potentials to such structures also becomes rather difficult.

An alternative approach to handling partial occupancies is to use mean field theory. The effect of this is that each site experiences a potential which is the mean of all possible configurations on the disordered positions. In doing so we are assuming that all possible configurations are equally as likely, i.e. the less stable configurations are equally as likely as the more stable ones. This may apply to materials where there is little energetic difference between configurations or to ones which were formed under kinetic rather than thermodynamic control and haven't had the chance to achieve a Boltzmann distribution. It must be decided for any given material whether it is therefore appropriate to use this approach.

The practical upshot of the mean field method is that all interactions just become scaled by the site occupancies of both atoms. This has been implemented in GULP such that the user can specify the site occupancy in addition to the coordinates (see the later section on the input for further details) and the program will automatically handle most aspects of the mean field approach. This includes ensuring the total occupancy on a site does not exceed unity and where two different ions share a site with partial occupancy they are constrained to move as a single ion in optimisations.

One important word of warning - it is important that the user thinks through interactions carefully when using the partial occupancy feature to ensure that everything is handled properly. The biggest danger comes in systems where there are two partially occupied sites very close to each other such that in the real system their occupancy would be mutually exclusive. When this happens it is often necessary to specifically exclude potentials between these atoms to obtain the correct behaviour.

### 3.0.0.4 Algorithms for energy and derivative evaluations

GULP actually contains several different algorithms for calculating the energy and its first and second derivatives. By default the program will try to choose the most efficient for any given system, excluding possibilities such as the cell multipole method which would actually lead to slight changes in the answer. Normally the user will need to know nothing about what algorithm is being used, so this section is really for the curious.

Usually real-space interactions are calculated in a lower-half triangular fashion to avoid double counting of interactions which would give rise to loops of the form shown below:

```
do  $i = 2, numat$ 
  do  $j = 1, i-1$ 
    [Calculate interaction between  $i$  and  $j$ ]
  enddo
enddo
```

If there is the possibility of self-terms or interactions between periodic replications of the same atom then the  $i = j$  term would not be excluded, though it may be more efficient to handle this case in a separate loop. For solids where there is significant space group symmetry then a different algorithm may be more efficient:

```
do  $i = 1, nasym$ 
  do  $j = 1, numat$ 
    [Calculate interaction between  $i$  and  $j$ ]
  enddo
enddo
```

where *nasym* is the number of species in the asymmetric unit and *numat* is the number of atoms in the full unit cell. Both the symmetry adapted and standard algorithms are present in GULP with selection being made based on the amount of symmetry in the crystal. The use of symmetry can result in up to an order of magnitude speed-up in favourable cases and therefore is well worth using. More details concerning the use of symmetry, in particular with respect to the calculation of derivatives, can be found elsewhere [11].

The second algorithmic aspect to mention applies to the situation when a constant volume optimisation is being performed and some atoms are held fixed. Typical cases where this occurs are in an optical calculation, in which only shells are relaxed, or where a molecule is docked within a rigid microporous material. In this case the energy of interaction between certain atoms is a constant term and the forces on them are ignored. When this happens these atoms are excluded or frozen

out of the energy calculation after the first point to save computational expense.

### 3.0.1 Phonons

#### 3.0.1.1 Phonon density of states

We may also be interested in the phonon density of states for a solid as the number of frequencies versus frequency value becomes a continuous function when integrated across the Brillouin zone. While full analytical integration across the Brillouin zone is not readily carried out, this integral can be approximated by a numerical integration. We can imagine calculating the phonons at a grid of points across the Brillouin zone and summing the values at each point multiplied by the appropriate weight (which for a simple regular grid is just the inverse of the number of grid points). As the grid spacing goes to zero the result of this summation tends to towards the true result.

For performing these integrations GULP uses a standard scheme developed by Monkhorst and Pack [16] for choosing the grid points. This is based around three so-called shrinking factors,  $n_1$ ,  $n_2$  and  $n_3$  - one for each reciprocal lattice vector. These specify the number of uniformly spaced grid points along each direction. The only remaining choice is the offset of the grid relative to the origin. This is chosen so as to maximise the distance of the grid from any special points, such as the gamma point as this gives more rapid convergence.

In many cases it is not necessary to utilise large numbers of points to achieve reasonable accuracy in the integration of properties, such as phonons, across the Brillouin zone. For high symmetry systems several schemes have been devised to reduce the number of points to a minimum by utilising special points in  $k$  space. However, because GULP is designed to be general the Monkhorst-Pack scheme is used. The user can input special points instead, if known for the system of interest.

Often it is not necessary to integrate across the full Brillouin zone due to the presence of symmetry. By using the Patterson group (the space group of the reciprocal lattice) GULP reduces the integration region to that of the asymmetric wedge which may only be 1/48-th of the size of the full volume [17].

When producing plots of the phonon density of states the critical factor, apart from the resolution of the integration grid, is the 'box' size. The continuous density of states curve has to be approximated by a series of finite regions of frequency or boxes. Each phonon mode at each point in  $k$  space is assigned to the box whose frequency region it falls into. The smaller the box size the better the resolution of the plot. However, more points will be needed to maintain a smooth variation of number density.

### 3.0.1.2 Infra-red phonon intensities

In order to make comparison between theoretically calculated phonon spectra and experiment it is important to know something about the intensity of the vibrational modes. Of course the intensity depends on the technique being used to determine the frequency as different methods have different selection rules. While Raman intensities are not readily calculable from most potential models, due normally to the absence of polarisabilities higher than dipolar ones, approximate values for infra-red spectra can be determined [18]:

$$I_{IR} \propto \left( \sum_{\text{all species}} qd \right)^2$$

where  $q$  is the charge on each species and  $d$  is the Cartesian displacement associated with the normalised eigenvector.

### 3.0.1.3 Pair Distribution Functions

The calculation of Pair Distribution Functions is in accordance with the theory of Chung and Thorpe [107]. It makes use of phonon information calculated within GULP, for an optimised structure, using a Monkhorst-Pack grid (as described in section 3.0.28.1).

Chung and Thorpe [107] state that the probability of finding a pair of atoms  $i$  and  $j$ , with position  $\mathbf{r}_i$  and  $\mathbf{r}_j$  respectively, at position  $\mathbf{r}$  is given by

$$\rho_{ij}(\mathbf{r}) = \langle \delta(\mathbf{r} - (\mathbf{r}_j - \mathbf{r}_i)) \rangle \quad (3.1)$$

where  $\langle \dots \rangle$  is the statistical average implying both configurational and thermal averages. Summing over all such pairs gives the *density function*  $\rho(\mathbf{r})$ , which is averaged by using each atom in turn as the starting point. Working with a crystal lattice, the complexity of such calculations is reduced because only atoms in the first unit cell are used as starting points. Moreover, GULP reduces the crystal symmetry to a primitive cell, minimizing the required number of calculations. (It is, of course, still possible to specify a conventional cell and use these  $k$  points instead.)

Consider a lattice of unit cells each containing  $n$  atoms. Denote the position of atom  $i$  in the original unit cell as  $\mathbf{r}_{i_0}$  and similarly atom  $j$  in the  $\ell$ th unit cell as  $\mathbf{r}_{j_\ell}$ . Define the pair separation vector between two atoms  $i_0$  (in the original unit cell) and  $j_\ell$  (in the  $\ell$ th unit cell) as  $\mathbf{r}_{i_0 j_\ell} = \mathbf{r}_{j_\ell} - \mathbf{r}_{i_0}$ .

The density function (with units of 1/volume) is the weighted sum over all pairs between atom  $i_0$  and atom  $j$  in all unit cells, averaged over the number of atoms in the unit cell,  $n$ . The spherical average is taken, dividing by  $4\pi r^2$ , to remove orientational dependence.

$$\rho(r) = \frac{1}{4\pi r^2 n} \sum_{\ell} \left( \sum_{i_0} \sum_j w_{ij} \rho_{i_0 j_\ell}(\mathbf{r}) \right) \quad (3.2)$$

where the prime indicates  $i_0 \neq j_0$  (i.e.  $\mathbf{r}_{i_0j_\ell} \neq 0$ ). The gaussian peak (with units of 1/length), is given in equation 3.8. The weighting is dependent on the fraction of atoms of type  $i$ ,  $c_i$ , and coherent bound scattering length,  $\bar{b}_i$ , and is expressed as

$$w_{ij} = \frac{\bar{b}_i \bar{b}_j}{\left(\sum_{k=1}^n c_k \bar{b}_k\right)^2} \quad (3.3)$$

As suggested by equation 3.1, if the atoms were completely stationary, the density function would be a series of delta functions located at the interatomic spacings. To account for thermal motion, Chung and Thorpe [147] demonstrated that, within the harmonic approximation, the Debye-Waller theorem can be used to justify the use of a series of weighted Gaussian peaks  $\rho_{ij}(r)$ , centred at  $r_{ij}$  with width  $\sigma_{ij}$ . Taking  $\hat{r}_{ij}$  to be the unit vector between atoms  $i$  and  $j$ , and  $\mathbf{u}_{ij} = \mathbf{u}_j - \mathbf{u}_i$  where  $\mathbf{u}_i$  is the displacement of atom  $i$ , then the width is given by

$$\sigma_{ij} = \left\langle \left[ \mathbf{u}_{ij} \cdot \hat{r}_{ij} \right]^2 \right\rangle^{\frac{1}{2}} \quad (3.4)$$

This can be expressed in terms of phonon modes as

$$\sigma_{i_0j_\ell}^2 = \frac{\hbar}{2N} \sum_{\mathbf{k}, \nu} \frac{2n[\omega(\nu, \mathbf{k})] + 1}{\omega(\nu, \mathbf{k}) |\mathbf{r}_{i_0j_\ell}|^2} \left| \left[ \mathbf{u}_{j_\ell}(\nu, \mathbf{k}) - \mathbf{u}_{i_0}(\nu, \mathbf{k}) \right] \cdot \mathbf{r}_{i_0j_\ell} \right|^2 \quad (3.5)$$

where the displacements  $\mathbf{u}_{i_\ell}$  are as given in equation 3.6. It should be noted that this corrects a typographical error by Reichard et al [148] equation 3, where the numerator is multiplied by a factor of  $\sqrt{m_i}$  rather than divided by it.

$$\mathbf{u}_{i_\ell} = \frac{\mathbf{e}^{\text{sig}_i(\nu, \mathbf{k})} \exp[i\mathbf{k} \cdot \mathbf{r}_{i_\ell}]}{\sqrt{m_i}} \quad (3.6)$$

$N$  is the number of  $\mathbf{k}$ -points,  $\nu$  is the mode index,  $n[\omega(\nu, \mathbf{k})]$  is the Bose occupation number

$$n = \frac{1}{\left(\exp\left(\frac{\hbar\omega}{kT}\right) - 1\right)} \quad (3.7)$$

$\omega(\nu, \mathbf{k})$  is the frequency from the eigenvalues of the dynamical matrix, and  $\mathbf{e}^{\text{sig}_i(\nu, \mathbf{k})}$  is the eigenvector for atom  $i$  (see section 3.0.2). The mass of atom  $i$  is  $m_i$ . When this is implemented within GULP, a Monkhorst-Pack grid [98] of a specified density is used to generate an even distribution of  $\mathbf{k}$ -points.

In summary, the Gaussian peak (with units of 1/length) for each pair is calculated from the width

$$\rho_{i_0j_\ell}(r) = \frac{1}{\sqrt{2\pi\sigma_{i_0j_\ell}^2}} \exp\left[-\frac{|\mathbf{r}_{i_0j_\ell} - r|^2}{2\sigma_{i_0j_\ell}^2}\right] \quad (3.8)$$

These are summed and averaged as in equation 3.2 to give the Chung & Thorpe (1999) density function (with units of 1/volume). The partial density function for atomic pair  $ij$  is the contribution from  $\rho_{i_0j_\ell}(r)$  for that pair: the sum of all partials is the total density function

### 3.0.2 Eigenvectors

Within the literature, there are two commonly used settings for calculating the dynamical matrix depending on whether the atomic position in the unit cell is included in the eigenvector, or taken out as a phase factor. The default setting in GULP is the same as that used by Lovesey [149], where the eigenvector of atom  $j$  at a given  $\mathbf{k}$ -point is phased by the position of the atom in the unit cell ( $\mathbf{r}_{j_0}$ ). Lovesey [149] writes this as  $\sigma$ , but we have used  $\mathbf{e}^{\text{sig}}$  here to avoid confusion with peak widths. This is the eigenvector used by Chung and Thorpe [147] and here. Lovesey [149] also describes an alternative setting, written as  $\mathbf{e}$ , used in several books e.g. Willis & Pryor [150] and Dove [151]. The two settings are related by the phase factor shown (from eq. 4.28 in Lovesey [149])

$$\mathbf{e}^{\text{sig}}_j(\mathbf{v}, \mathbf{k}) = \mathbf{e}_j(\mathbf{v}, \mathbf{k}) \cdot \exp[i\mathbf{k} \cdot \mathbf{r}_{j_0}] \quad (3.9)$$

### 3.0.3 Commonly Used Correlation Functions

A number of different formalisms for PDFs exist in the literature. Keen [152] performed an extensive survey of these and we follow his recommendations. The three main real space correlation functions,  $G(r)$ ,  $D(r)$  and  $T(r)$  are variously used depending on the purpose.  $T(r)$ , which scales as  $r$  at large  $r$ , is often used for peak fitting, and for analyzing structural detail at low  $r$  (e.g. in amorphous systems).  $D(r)$  is similar to  $T(r)$ , but has a term subtracted that scales with  $r$ , making it the correlation function of choice for studying mid to high  $r$  structural detail.  $G(r)$  is also used as it makes the low  $r$  peaks prominent. A comparison of the different forms is given by Dove [153].

Keen [152] writes the density function of Chung and Thorpe [107] as  $\rho^{PDF}(r)$ . It is the same as that used in the PDFFIT program [154] as well as by several current workers in this field, e.g. [155] [156]. This real space correlation function tends to  $\rho_o$  at high  $r$  and is zero below the minimum interpair spacing.

The PDFFIT program also outputs a *radial distribution function* [147], also known as a *pair distribution function* [107], with units of 1/area. It is written as  $G^{PDF}(r)$  by Keen [152], and defined as

$$G^{PDF}(r) = 4\pi r [\rho^{PDF}(r) - \rho_o] \quad (3.10)$$

where  $\rho_o = \frac{n}{V_{\text{unitcell}}}$ , the average number density (units of 1/volume). While  $\rho^{PDF}(r)$  oscillates around the number density,  $G^{PDF}(r)$  oscillates around zero. This can be converted to a Keen [152] *total radial distribution function*,  $G(r)$ , which has units of area. At values of  $r$  less than the minimum interpair spacing, this function tends to  $-(\sum_{i=1}^n c_i b_i)^2$ , and to  $\infty$  at high  $r$ .

$$G(r) = \frac{G^{PDF}(r) (\sum_{i=1}^n c_i b_i)^2}{4\pi r \rho_o} \quad (3.11)$$

$G(r)$  is often expressed in units of Barns ( $1 \times 10^{-28} \text{ m}^2 = 1 \times 10^{-8} \text{ \AA}^2$ ), but in the GULP output we use  $\text{\AA}^2$  to be consistent with the other correlation functions.

The *differential correlation function*,  $D(r)$ , and *total correlation function*,  $T(r)$ , are used as part of the ATLAS suit of programs [157], as used at the ISIS pulsed spallation neutron source, and defined as

$$D(r) = 4\pi r \rho_o G(r) \quad (3.12)$$

$$= G^{PDF}(r) \left( \sum_{i=1}^n c_i b_i \right)^2 \quad (3.13)$$

$$T(r) = D(r) + 4\pi r \rho_o \left( \sum_{i=1}^n c_i b_i \right)^2 \quad (3.14)$$

$$= (G^{PDF}(r) + 4\pi r \rho_o) \left( \sum_{i=1}^n c_i b_i \right)^2 \quad (3.15)$$

$D(r)$  and  $T(r)$  have units of 1/length.

In addition to the total pair distributions functions written to the .pdfs file, a .pdfs file is produced for every pair-type (root\_pairnumber\_atom1\_atom2.pdfs) containing a selection of partial pair distribution functions. First, the weighted  $\rho_{ij}(r)$  function: the sum of all of these is the total pair distribution function of Chung and Thorpe. Secondly, a weighted version of  $g_{ij}(r)$ , which again sums directory to give  $G(r)$ . Finally, an unweighted (true)  $g_{ij}(r)$ , which corresponds to the  $g_{ij}(r)$  of Keen[152]. This output can be suppressed using the `nopart ial` keyword.

### 3.0.3.1 Thermodynamic quantities from phonons

There are a range of quantities that can be readily calculated from the phonon density of states. The accuracy with which they are determined though clearly depends on the  $k$  points or shrinking factors selected for the Brillouin zone integration. For systems with large unit cells a small number of  $k$  points, perhaps even the  $\Gamma$ -point alone, will be sufficient. However, for those systems with small to medium unit cells it is important to examine how converged the properties calculated are with respect to the grid size.

If a phonon calculation is performed then GULP will automatically print out the relevant thermodynamical quantities. This output depends partly on whether a temperature has been specified for the given structure. If the calculation is set for zero Kelvin then only the zero point energy is output:

$$ZPE = \sum_{k\text{-points}} w_k \sum_{\text{all modes}} \frac{1}{2} h\nu$$

where  $w_k$  is the weight associated with the given  $k$  point. In principal, the zero point energy should be added to the lattice energy when determining the relative

stability of two different structures. However, because the derivatives of the zero point energy are non-trivial it is normally neglected in an energy minimisation.

For temperatures above absolute zero we can calculate the vibrational partition function, which in turn can be readily used to calculate three further properties:

Vibrational partition function:

$$Z_{\text{vib}} = \sum_{k\text{-points}} w_k \sum_{\text{all modes}} \left( 1 - \exp\left(-\frac{h\nu}{kT}\right) \right)^{-1}$$

Vibrational entropy:

$$S_{\text{vib}} = R \ln Z_{\text{vib}} + RT \left( \frac{\partial \ln Z_{\text{vib}}}{\partial T} \right)$$

Helmholtz free energy:

$$A = U - TS_{\text{vib}}$$

where

$$U = U_{\text{lattice energy}} + U_{\text{vibrational energy}}$$

Heat capacity at constant volume:

$$C_v = RT \left( 2 \left( \frac{\partial \ln Z_{\text{vib}}}{\partial T} \right) + T \left( \frac{\partial^2 \ln Z_{\text{vib}}}{\partial T^2} \right) \right)$$

### 3.0.4 Free energies

Although the most common methods for studying the properties of materials as a function of temperature are molecular dynamics and Monte Carlo simulations, there is an alternative based on static methods within the quasi-harmonic approximation. This is to directly minimise the free energy of the system at a given temperature, where the free energy is calculated from the lattice energy combined with contributions from the phonons including the entropy and zero point energy.

The advantages of working with free energy minimisation are that MD simulations are quite expensive due to the need to reduce the uncertainty by sampling large amounts of phase space. Molecular dynamics and free energy minimisation are in fact complementary techniques. The latter approach breaks down at high temperatures as anharmonic effects become important - typically it works at temperatures up to half the melting point as a rough guide. Conversely, molecular dynamics is not strictly valid at low temperatures because the zero point motions and quantum nature of the vibrational levels is ignored.

Although in principle it is possible to analytically fully minimise the free energy of a solid, in practice this is extremely difficult as it requires the fourth derivatives of the energy with respect to the Cartesian coordinates. Hence, a number of approximations are normally made - the main one being that the principal effect of

temperature is to expand or contract the unit cell and the effect on internal degrees of freedom is less important.

When changing unit cell parameters we are concerned with the Gibbs free energy as this is appropriate to a constant pressure calculation. This quantity is related to the Helmholtz free energy, whose relationship to the vibrational entropy has already been given previously, by the expression;

$$G = A + PV$$

with

$$P = P_{\text{ext}} - P_{\text{int}}$$

where  $P$  is the pressure. The pressure has two components - any external applied pressure plus the internal phonon pressure coming from the vibrations. The phonon pressure is given by:

$$P_{\text{int}} = -\frac{\partial A}{\partial V}$$

In order to calculate the Gibbs free energy it is therefore necessary to calculate the derivative of the Helmholtz free energy with respect to the unit cell volume. This can be done numerically by finite differences. Central differencing is more expensive than using forward differences. However, it is generally necessary to determine the phonon pressure with sufficient accuracy. In turn each calculation of the Helmholtz free energy requires a constant volume minimisation for the given set of unit cell parameters, followed by a phonon calculation.

Once the Gibbs free energy has been calculated then the next stage of a free energy minimisation is to isotropically expand or contract the unit cell until the external pressure balances the internal pressure. Having done this then the derivatives of the Gibbs free energy can be evaluated numerically by finite differences and the unit cell optimised with respect to this quantity.

Because of the three levels of optimisation plus phonon calculations involved, free energy minimisations are rather expensive and shouldn't be undertaken lightly! Due to the numerical nature of several of the derivatives it may be necessary for the user to adjust the finite differencing interval for a calculation to work optimally. Also the calculations are very sensitive to the quality of the underlying energy surface. Potentials with short cutoffs, leading to discontinuities, and soft modes can cause difficulties for the method, so always check your model well before starting.

Free energy minimisation can be used in conjunction with fitting to allow a series of structures at different temperatures to be fitted with inclusion of the thermal effects, though again this is an expensive procedure. It is important to note that a free energy minimisation at 0 K is not the same as an ordinary static calculation. This is due to the presence of the zero point energy in the former method.

## 3.0.5 Defects

### 3.0.5.1 The Mott-Littleton method

The calculation of defect energies is more difficult and approximate than the calculation of bulk properties. In theory, a defect can cause very long range perturbations, particularly if it is not charge-neutral. Consequently the user must always check the convergence of the approximations made.

The simplification in the modelling of defects is to divide the crystal that surrounds the defect into three spherical regions known as regions 1, 2a and 2b [19-21]. In region 1 all interactions are treated exactly at an atomistic level and the ions are explicitly allowed to relax in response to the defect. Except in the case of very short-ranged defects it is not generally possible to achieve the desired degree of convergence by increasing region 1 before running out of computer resources. Consequently, in region 2a some allowance is made for the relaxation of ions but in a way that is more economical.

In region 2a the ions are assumed to be situated in an harmonic well and they subsequently respond to the force of the defect accordingly [22]. This approximation is only thus valid for small perturbations and also requires that the bulk lattice has been optimised prior to the defect calculation. For region 2a individual ion displacements are still considered, whereas for region 2b only the implicit polarisation of sub-lattices, rather than specific ions, is considered.

If the vector  $x$  represents the positions of ions in region 1, while  $\zeta$  represents the displacements of ions in region 2a, then the total energy of the system may be written as:

$$E = E_1(x) + E_{12}(x, \zeta) + E_2(\zeta)$$

where  $E_1$  and  $E_2$  are the energies of regions 1 and 2 respectively, and  $E_{12}$  is the energy of interaction between them. We now assume that the energy of region 2 is a quadratic function of the displacements:

$$E_2(\zeta) = \frac{1}{2} \zeta^T W \zeta$$

We also know that we wish to obtain the displacements in region 2 for which the energy is a minimum:

$$\frac{\partial E}{\partial \zeta} = 0 = \frac{\partial E_{12}(x, \zeta)}{\partial \zeta} + W \zeta$$

This expression can be used to eliminate  $E_2$  from the total energy, leaving it purely in terms of  $E_1$  and  $E_{12}$ :

$$E = E_1(x) + E_{12}(x, \zeta) - \frac{1}{2} \frac{\partial E_{12}(x, \zeta)}{\partial \zeta} \zeta$$

The displacements in region 2 are formally a function of  $x$  for region 1 which makes the minimisation of the total energy with respect to both the positions of region 1 and the displacements of region 2 potentially complicated. This problem can be avoided by using force balance in region 1 as the criteria for convergence (i.e. all forces on ions in region 1 must be zero), rather than purely minimising the energy. The two approaches are equivalent provided that region 2 is at equilibrium also. This will be achieved provided that the displacements in region 2 are small enough that they are genuinely quadratic.

In terms of the minimisation procedure employed for defect calculations the force balance process leads to a slightly different approach to the bulk optimisation. Initially the same Newton-Raphson procedure with BFGS hessian updating and line searches is employed to avoid convergence to stationary points which are not minima. After at least one cycle of the above and when the gradient norm falls below a certain threshold the minimiser abandons the line search procedure and aims purely to reduce the gradients to zero, regardless of the energy. In practice positive changes in the energy near convergence are only ever small.

The defect energy is now the difference in the total energies for the defective and perfect lattice,  $E_d$  and  $E_p$  respectively, with corrections due to the energy of any interstitial or vacancy species at infinite separation from the lattice,  $E_\infty$ :

$$E_{\text{defect}} = E_d - E_p + E_\infty$$

Two final aspects must be dealt with in order to obtain the final working equations for the defect energy. Firstly, due to the slow convergence of electrostatic terms in real space alone we cannot evaluate the region 1 - region 2 energy directly. Instead we must calculate the energy of region 1 interacting with the perfect lattice to infinity and then explicitly subtract and add back the terms due to ions which are no longer on their perfect lattice sites. Secondly, because the displacements in region 2 depend on the force acting on a given ion, which in turn is a function of other region 2 ions, there is in fact a linear dependency of the energy on  $\zeta$ . By suitable manipulation of the energy terms this may be removed to leave the following expression for the defect energy:

$$\begin{aligned} E_{\text{defect}} = & E_{11}(dd) - E_{11}(dp) + E_{1\infty}(dp) - E_{1\infty}(pp) \\ & + E_{12a}(dd) - E_{12a}(dp) + E_{12a}(pp) - E_{12a}(pd) \\ & - \sum \left( \frac{\partial E_{12a}(dd)}{\partial r} - \frac{\partial E_{12a}(pd)}{\partial r} \right) \end{aligned}$$

where the general symbol  $E_{ij}(kl)$  denotes the energy of interaction summed over all ions in region  $i$  interacting with ions in region  $j$  where  $i$  and  $j$  can be 1, 2a or  $\infty$  (signifying a sum over 1, 2a and 2b out to infinity). The letters  $k$  and  $l$  indicate whether the energy is for the perfect or defective coordinates in regions  $i$  and  $j$  respectively, depending on whether they are  $p$  or  $d$ .

### 3.0.5.2 Displacements in region 2a

Expanding the energy as a Taylor series and truncating at second order gives the Newton-Raphson estimate of the vector from the current ion position to the energy minimum position in terms of the force,  $g$ , acting on the ion:

$$\zeta = -W^{-1}g$$

Hence if we know the local second derivative matrix and the force acting on the ion we can calculate its displacement. There are a number of possible ways of calculating the force acting on the ions in region 2a. The most common approach is to use the electrostatic force due to only the defect species - i.e. the force due to any interstitial species based on their current positions, less the force due to any vacancies at the position of the original vacant site. In this way region 2a responds to the change in the multipole moments of the defect species in region 1, but not the influence of other forces. Hence for this approximation to strictly hold the distance between any defects and the boundary of region 2a should be greater than the short-range cutoff.

### 3.0.5.3 Region 2b energy

Region 2b is assumed to be sufficiently far from the defects that the ions only respond by polarising according to the electrostatic field resulting from the total defect charge placed at the centre of region 1. This can be written for cubic systems as follows:

$$E_{2b} = -\frac{1}{2}Q^2 \sum_{i \neq 1, 2a} \frac{q_i m_i}{R_i^4}$$

Because this expression is just dependent on the distance and a couple of lattice site related parameters the region 2b energy can be evaluated using a method analogous to the Ewald sum and then subtracting off the contribution from ions in regions 1 and 2a. An alternative more general, but still not completely general, expression is the following where the lattice site dependent property is now an anisotropic tensor, rather than a scalar [23]:

$$E_{2b} = -\frac{1}{2}Q^2 \sum_{i \neq 1, 2a} \sum_{\alpha\beta} \frac{q_i M_i^{\alpha\beta} R_i^\alpha R_i^\beta}{R_i^6}$$

This can again be calculated by partial reciprocal space transformation based on the second derivatives of the  $R^{-4}$  lattice sum.

## 3.0.6 Fitting

### 3.0.6.1 Fundamentals of fitting

Before any production runs can be performed with an interatomic potential program it is necessary to obtain the potential parameters. If you are lucky there may be good parameters for your system of interest already published in the literature so you can just type them in and get going straight away. Unfortunately most people are not so lucky! The fitting facility within GULP [24] allows you to derive interatomic potentials in either of two possible ways. Firstly, you can determine the parameters by fitting to data from some higher quality calculation, such as an *ab initio* one, normally by attempting to reproduce an energy hypersurface. Secondly, you could attempt to derive empirical potentials by trying to reproduce experimental data.

Regardless of which method of fitting you are using the key quantity is the 'sum of squares' which measures how good your fit is. Ideally this should be zero at the end of a fit - in practice this will only happen for trivial cases where the potentials can be guaranteed to completely reproduce the data (for example fitting a Morse potential to a bond length, dissociation energy and frequency for a diatomic should always work perfectly). The sum of squares,  $F$ , is defined as follows:

$$F = \sum_{\text{all observables}} w(f_{\text{calc}} - f_{\text{obs}})^2$$

where  $f_{\text{calc}}$  and  $f_{\text{obs}}$  are the calculated and observed quantities and  $w$  is a weighting factor. There is no such thing as a unique fit as there are an infinite number of possible fits depending on the choice of the weighting factors. The choice of weighting factor for each observable depends on several factors such as the relative magnitude of the quantities and the reliability of the data (for instance a crystal structure will generally be more reliable than an elastic constant measurement).

The aim of a fit is to minimise the sum of squares by varying the potential parameters. There are several standard techniques for solving least squares problems. By default GULP uses a Newton-Raphson functional minimisation approach to solving the problem, rather than the more conventional methods. This is because it avoids storing the co-variance matrix. The downside is that near-redundant variables are not eliminated. Currently the minimisation of the sum of squares is performed using numerical first derivatives. The reason for using numerical derivatives is because many of the properties, particularly those derived from second derivatives, are rather difficult to implement analytical derivatives for. Consequently the value of the gradient norm output during fitting should only be taken as a rough guide to convergence. In cases where the numerical gradients prove noisy then the use of the simplex algorithm for fitting can be useful as this requires only the function.

The choice of which potential parameters to fit belongs to the user and is controlled by a series of flags on the potential input line (0  $\Rightarrow$  fix, 1  $\Rightarrow$  vary). There are

also options contained within the variables sub-section for allowing more general parameters to fit, such as charge distributions. Note that when fitting charges at least two charges must be varied to have any effect as the program eliminates one variable due the charge neutrality constraint. There is also the option to vary the charge `split` between a core and shell while maintaining a constant overall charge on the ion. The user may also impose their own constraints on fitting variables through the `constrain fit` option.

It is generally recommended that a small number of parameters are fitted initially and the number gradually increased in subsequent restarts. Often if all parameters are allowed to vary from the start unphysical parameters may result. Dispersion terms of Buckingham or Lennard-Jones potentials are particularly prone to poor behaviour during fitting, as they tend to go to zero or become exceedingly large. It is generally recommended that such terms are set equal to a physically sensible value (based on quantum mechanical estimates or polarisability-based formulae) and held fixed until everything else is refined.

A final check that the program looks for is that the total number of variables being fitted is less than the total number of observables!

### 3.0.6.2 Fitting energy surfaces

To fit an energy surface it is basically necessary to input all the structures and the energies that correspond to them. To do this it is just a matter of putting one structure after another in the input file. It is possible to fit the gradients acting on the atoms as well the energy of each structure, though often just the energies are fitted. If the latter is the case, then the easiest way to turn off the fitting of the gradients is to specify `noflag` as a keyword to prevent the program for looking for gradient flags in the absence of a keyword to specify them.

Perhaps the only unique feature of fitting an energy surface is the need to include an energy shift in some cases. This is a single additive energy term which is the same for all structures and just moves the energy scale up and down. The justification for this is that often it is impossible to calculate the energy that corresponds exactly to the interatomic potential one from a quantum mechanical calculation [25]. Most commonly this arises where the potential model has partial charges in which case there is an unknown term in the lattice energy due to ionisation potentials and electron affinities for fractions of an electron.

To simplify the specification of this shift value in the input, if you give the `shift` option after the first structure then this value will apply to all subsequent structures until a different value is input. Similarly, its magnitude can be altered by using the variables sub-section to specify the shift as a variable and this will apply to all structures. It is generally recommended that the shift is fitted first and allowed to fit through out the procedure.

### 3.0.6.3 Empirical fitting

An alternative to fitting quantum mechanical data to derive an interatomic potential is to actually fit experimental data. In this case the procedure serves two purposes. Firstly, the degree to which all the data can be reproduced may serve as some guide as to the physical correctness of the model used. Secondly, it provides a means of extrapolation of experimental data for one system to a different one where the data may not be known, or alternatively to unknown properties of the same material.

Any of the properties that can be calculated for the bulk solid or gas phase molecule can also be used in reverse to fit a potential to. Obviously the essential ingredient in the fit is the experimental structure, without which you won't get very far! The conventional way to fit the structure is by requiring that the forces on the atoms are zero. This is clearly not a perfect strategy as it could be satisfied by a transition state rather than a minimum, though in practice it is rare, except when symmetry constraints are imposed.

Normally a good fit requires some second derivative information as well as the structure. For very high symmetry systems, such as rock salt, the structural data alone is completely inadequate. If we imagine a potential as being a binomial expansion about the experimental geometry, then unless the first and second derivatives are reasonably well reproduced by our model then the range of applicability will be almost zero. Typical sources of second derivative information are elastic, dielectric and piezoelectric (where applicable) constants. Also vibrational frequencies contain far more information than any of the above. However, the fitting of frequencies is not straightforward. To fit the frequency magnitudes is certainly possible, however, you have no guarantee that the correct mode has been fitted to the correct eigenvalue. Hence, frequency fitting only tends to be useful from empirical data for special cases, such as O-H stretching modes which are well separated from other modes and for diatomics where there is no problem in assignment!

One other case where frequency fitting can be useful is at the lower end of the spectrum. For an isolated molecule or a solid at its  $\Gamma$  point the first three modes should have zero frequency as they are just translations. In some cases there may be imaginary modes due the potentials not correctly reproducing the true symmetry. Hence by fitting the first three modes to be zero it is possible to encourage the potentials to yield the correct symmetry.

### 3.0.6.4 Simultaneous fitting

There is one main difficulty in the conventional scheme for fitting in which the forces on the atoms are minimised by variation of the potential parameters which arises when using a shell model. Normally we don't know what the shell coordinates are at the outset unless the ions are sited at centres of symmetry. In the past people have tried fitting with the shells placed on top of the cores. However, this means that the potentials are tuned to minimise the polarisation in the system

and leads to the shell model having only a small beneficial effect. It also doubles the number of observables connected with gradients, but only introduces a small number of extra variables thus making it harder to get a good fit.

The solution to this problem is allow the shell positions to evolve in some way during the fit. There are two possibilities - either we can minimise the shell positions at every point during the fit or we can added the shell coordinates as fitting parameters. In the case where only structural data is being fitted the two methods are equivalent except in the way that they evolve towards the answer. When other properties are included the second approach is not strictly correct, though the difference is usually small.

After experimenting with several test cases it was found that the second scheme in which the shell coordinates become fitted variables was far more stable in convergence and more efficient. Hence this is the scheme that has been adopted and is referred to as 'simultaneous' fitting due to the concurrent fitting of shell positions. Whenever working with shell models it is recommended that the keyword `simultaneous` is added during conventional fitting - it can improve the sum of squares by several orders of magnitude! Not only does this scheme apply to the coordinates of shells, but also to the radii of breathing shells as well.

### **3.0.6.5 Relax fitting**

It has been observed that sometimes in conventional fitting getting an improved sum of squares doesn't always get you what is considered to be a better quality fit. This is because people often use different criteria to make their judgement to the ones input into the fitting process. In particular they look at the difference between the optimised structural parameters and those from experiment, rather than looking at the forces. The reason why the forces can be lower, but lead to a worse structure is because in a harmonic approximation the displacements in the structure are given by the gradient vector multiplied by the inverse hessian. Hence, if the gradients get smaller but the inverse hessian gets much larger then the situation may get worse.

The solution to this problem is to fit according to the criteria by which the structures are judged - this is what relax fitting does. This means that at every point in the fit the structure is optimised and the displacements of the structural parameters calculated instead of the gradients. In this approach the shell model is naturally handled correctly and so there is no need for simultaneous fitting. The downside is that it is much more expensive in computer time than conventional fitting. Also you can only start a relax fit once you have a reasonable set of potential parameters - i.e. one which will give you a valid minimisation. Hence a conventional fit is often a prerequisite for a relax fit.

There is a further benefit to using relax fitting. In a conventional fit the properties are calculated at the experimental structure normally with non-zero gradients which is not strictly correct. In a relax fit the properties are calculated for the opti-

mised structure where they are valid.

### 3.0.7 Genetic algorithms

Conventional minimisation techniques based upon methods such as Newton-Raphson are excellent ways of locating local minima. However, they are of limited use in finding global minima. For example, if we know the chemical composition of a compound and its unit cell, but don't know the structure then we would want to locate the most stable arrangement for placing the atoms within the unit cell. To search systematically for a reasonable set of atomic coordinates may take a very long time by hand. Genetic algorithms [26] are a method by which we can search for global minima rather than local minima, though there can never be an guarantee of finding a global minimum. In many respects it resembles Monte Carlo methods for minima searching, though is regarded by some as being more efficient.

The concept behind the method, as the name might suggest, is to carry out a 'natural selection' procedure within the program in the same way that nature does this in real life. We start off with an even numbered sample of randomly chosen configurations. This is our trial set which is allowed to evolve according to a number of principles described below. Before we can do this we need to consider how to represent our data for each configuration. To do this we encode each number as a binary string by dividing the range between the maximum and minimum possible values (for example 1 and 0 for fractional coordinates) into a series of intervals where the number of such intervals is an integer power of 2. Given this data representation the system now evolves according to the following steps:

**(a) Reproduction (tournament)** - pairs of configurations are chosen at random and the parameters which measure the relative quality of the two are compared (this is the energy for genetic optimisation or the sum of squares for genetic fitting). The best configuration goes forward to the next iteration, except that there is a small probability, which can be set, for the weaker configuration to win the tournament. This process is repeated as many times as there are configurations so that the total number remains constant.

**(b) Crossover** - a random point is chosen at which to split two binary strings, after which the two segments are swapped over.

**(c) Mutation** - a random binary digit is switched to simulate genetic mutations. This can help to search for alternative local minima.

The default output from a genetic algorithm run is a given number of the final configurations, where the ones with the best fitness criteria are selected. However, unless the run smoothly progresses to the region of a single minimum it may be

more interesting to look at a sample of the best configurations from the entire run. This can be done with GULP using the best option.

Genetic algorithms can only locate minima to within the resolution allowed by the discretisation used in the binary representation. Also they are very slow to converge within the region of a minimum. Hence, the genetic algorithm should be used to coarsely locate the regions associated with minima on the global surface, after which conventional Newton-Raphson methods will most efficiently pin-point the precise minimum in each case.

## 3.1 Getting started

### 3.1.1 Setting environment variables

In previous versions of GULP it was necessary to specify where library files and the documentation could be found by editing the source code. This has now been replaced by the use of two environment variables, `GULP_LIB` and `GULP_DOC`, respectively. Under `tsh` these can be set as follows:

```
setenv GULP_DOC /Users/myname/gulp5.0/Docs
setenv GULP_LIB /Users/myname/gulp5.0/Libraries
```

or by using appropriate commands under other Unix shells.

### 3.1.2 Running GULP

Under UNIX:

To run GULP on a machine with the UNIX operating system simply type:

```
<directory>gulp < inputfile
```

where `<directory>` is the path name for the location of `gulp` on your machine, or if the executable is in your current directory or lies in your path then this may be omitted. In this case the output will come to your terminal. If you wish to save it to an output file then type

```
<directory>gulp < inputfile > outputfile
```

You may like to try using one of the example input files (called `exampleN`, where `N` is a number) to see what happens! Input may also be typed directly into the program line by line if no input file is specified. Having finished typing all the required input just type 'start' to commence the run.

If running in parallel, then it is recommended to use a different syntax to run GULP:

```
mpirun -np 4 gulp inputfile
```

Here `mpirun` is the command that launches a parallel job under MPI, `4` represents the number of cores on which to run (for example - other numbers up to the available number of cores are allowed) and `inputfile` here represents the name of your inputfile BUT without the `.gin` extension at the end. This will be added automatically and the output written to a file with the same root name, but with `.gout` at the end. Using this form of running GULP, as opposed to re-directing I/O with `<` and `>`, is better in parallel since it avoids a possible MPI error message relating to

not being able to read the input fast enough.

### 3.1.3 Getting on-line help

To obtain on-line help on GULP type

```
<directory>gulp <CR>  
help <CR>
```

A list of all the possible help topics can then be accessed by typing `topics` or alternatively just type the particular keyword or option that you require help on. Only sufficient characters to specify a unique topic are required. To finish with help type `stop` if you wish to exit the program or `quit` if you want to return to interactive use.

If the help command fails to work it means that the path for the location of the file `help.txt` (which is an ordinary ASCII text file containing all the help information) has not been set at compile time and that the file is not in the present directory either.

An alternative way of accessing help is to generate an HTML file using the `gulp2html` utility (courtesy of Dr. Jörg-R. Hill) which produces a file `help.html` which can then be inspected with a suitable browser, such as netscape.

### 3.1.4 Example input files

With the program you should have received a number of sample input files which illustrate how GULP works for a number of particular run types. They also serve as a test to ensure that the program works correctly on your machine type. Please note that the interatomic potentials should not be taken as correct for general use - some are made up for the purposes of demonstration only! Below is a brief description of what each example file is doing.

Table 3.4: List of examples provided

example1	optimises the structure of alumina to constant pressure and then calculates the properties at the final point
example2	simultaneous fit of a shell model potential to the structure of $\alpha$ -quartz, followed by an optimisation with the fitted potentials - the general potential is used with energy and gradient shifts for the Si-O instead of the usual Buckingham potential
example3	an electronegativity equalisation calculation is used to derive partial charges for quartz and are then used to calculate the electrostatic potential and electric field gradients at each site - bond lengths are also calculated

example4	simultaneous fit of a shell model potential to La <sub>2</sub> O <sub>3</sub> using an Ewald-style sum to evaluate the C6 terms, followed by an optimisation with the production of a table comparing the initial and final structures at the end
example5	calculation of a phonon dispersion curve for MgO from 0,0,0 to 1/2,1/2,1/2 - note that normally the structure should be optimised first and that although a phonon density of states curve is produced this may not be accurate due to restricted sampling of k space.
example6	calculation of the defect energy for replacing a Mg <sup>2+</sup> ion in MgO by a Li <sup>+</sup> ion to create a negatively charged defect
example7a	location of the transition state for a magnesium cation migrating to a vacant cation site in MgO in a defect calculation
example7b	this shows an alternative way of obtaining the same result as in 7a by starting the magnesium in a special position and using the resulting symmetry constraints to allow a ordinary minimisation to the saddle point
example8	a molecular defect calculation in which a sulphate anion is removed from BaSO <sub>4</sub> - note that the use of the mole keyword to Coulomb subtract within the sulphate anion.
example9	an example of how to use a breathing shell model for MgO - including fitting the model, optimising the structure and calculating the properties
example10	optimisation of urea showing how to handle intermolecular potentials
example11	an example of how to map out the potential energy surface for the migration of a sodium cation parallel to the c axis through a crystal of quartz with an aluminium defect using the translate option
example12	optimisation of two structures within the same input file - also illustrates the use of the name option
example13	shows how to use a library to access potentials for an optimisation of corundum
example14	relaxed fit to structure and properties
example15	simple NVE molecular dynamics
example16	example of constant pressure shell model MD
example17	Sutton-Chen calculation for bulk Ni with cutmany = 1.0 (old default)
example17	Sutton-Chen calculation for bulk Ni with cutmany = 0.5 (new default)
example18	example of shell model MD in NVT ensemble
example19	shell model MD run for a zeolite with finite mass
example20	shell model MD run for a zeolite with adiabatic algorithm
example21	charged defect optimisation in a supercell
example22	energy surface fit for a molecular crystal
example23	evaluation of the cost function for a particular structure
example24	example of structure prediction for polymorphs of TiO <sub>2</sub>
example25	free energy minimisation of quartz within the ZSISA approximation
example26	Using the "ditto" option to run the same structure at 3 pressures in the same file
example27	Interface calculation in which a rigid block of MgO is optimised over the 001 surface of MgO
example28	Tersoff model calculation on bulk silicon followed by a vacancy defect calculation
example29	Streitz-Mintmire model calculation on bulk alumina

example30	REBO model calculation for a diamond surface
example31	Constant pressure optimisation of a corundum slab with a 2-D phonon calculation
example32	1-D calculation on MgO using manual specification of flags and the switch minimiser option
example33	Grand Canonical Monte Carlo for a single species being introduced into a box
example34	Grand Canonical Monte Carlo for a rigid molecule being introduced into a box
example35	Voter-Chen EAM for Ag
example36	Frequency dependent property calculation for quartz
example37	SiH4 molecule using the Smith and Dyson REBO 1 model
example38	Electric field applied to a slab from example31
example39	Glue potential for Au with print out of EAM atomic densities and energy contributions
example40	Simple example of 3coulomb potential for a water molecule for validation
example41	Force calculation for a urea molecule in the presence of a continuum solvent model with qgas keyword
example42	Optimisation of the (001) surface of urea in the presence of a continuum solvent model
example43	Example of PDF calculation for MgO - phonons < wmax
example44	Example of PDF calculation for MgO - full phonon range
example45	Example of PDF calculation for MgO - phonons > wmin only
example46	Example of PDF calculation for (Ca,Sr)TiO3
example47	Example of Eckart keyword for removing rotation/translation from molecular vibrations
example48	Fitting of vibration modes using specific eigenvectors for a water molecule
example49	UFF input file with manual specification of bonds for meta-xylene
example50	Example of Dreiding input
example51	Example of a thermal conductivity calculation for Allen-Feldman diffusons in amorphous silicon
example52	Example of a thermal conductivity calculation that uses estimated B and v_s from properties
example53	Calculation of Raman intensities for the vibrations of alpha-quartz
example54	Example of ReaxFF for an ethene molecule
example55	Example of a MEAM-2NN calculation for FCC Cu metal
example56	Example of an input for the ZBL potential that uses default parameters
example57	Example of a Hessian calculation for Tersoff ZRL. Geometry is chosen so that the coordination term is non-zero
example58	As per example57 except using finite differences to compute a numerical Hessian matrix for validation
example59	Example of the use of the mcswap option for exchanging Si and Ge in a zeolite
example60	Example of the use of multiple mcswap options for exchanging Si/Ge and O/S in a hypothetical zeolite
example61	Example of harmonic estimate for energy of relaxation
example62	Example of a phonon calculation using force constant supercell computed for a supercell of urea

example63	Example of the calculation of mean-squared displacements for the vibrations of a diatomic molecule
example64	Example of the calculation of Grueneisen parameters for MgO with a shell model
example65	Example of using the scan_cell option to shear MgO
example66	Example of split bond EEM calculation with multiple ranges for Li2O using MEAM_2NN_QEq
example67	Example of thermal conductivity calculation for MgO using the Alamode-GULP interface to solve the BTE
example68	Example of the use of finite strain optimisation relative to a reference cell for alumina
example69	Example of MD using multiple temperature ramps to anneal a system
example70	Example of a calculation using point ion dipolar polarisability without coupling of dipoles

## 3.2 Guide to input

### 3.2.1 Format of input files

On the whole it is only necessary to use up to the first four letters of any word, unless this fails to specify a unique word, and the input is not case sensitive as all characters are converted to lower case on being read in.

The first line of the input is the only special line and is referred to as the keyword line. Keywords should all be given on this line. These consist of control words which require no further parameters and generally specify the tasks to be performed by the program. For example a typical keyword line would look like:

```
optimise conp properties phonon
```

or in abbreviated form:

```
opti conp prop phon
```

This combination of words tells GULP to do a constant pressure optimisation and then to calculate the lattice properties and phonons at the optimised geometry. The order of words within the keyword line is not significant.

All subsequent lines can be given in any order unless that line relates to a previous piece of input. Such lines contain ‘options’ which generally also require the specification of further information. This information can normally follow on the same line or on the subsequent line. For example the pressure to be applied to a structure could be input as either

```
pressure 10.0          or          pressure
                               10.0
```

In many cases the units may also be specified if you don't wish to use the default:

```
pressure 1000 kbar
```

Any lines beginning with a '#' and anything that follows a '#' part way through a line is treated as a comment and as such is ignored by the program.

When performing runs with multiple structures any structure dependent options are assumed to apply to the last structure given, or the first structure if no structure has yet been specified. Some options should be specified as sub sections of a particular option. For example, `elastic`, `sdlc`, `hfdlc`, `piezo`, `energy` and `gradients` all are sub sections of the `observables` command and should appear as follows:

```
observables
elastic 2
1 1 54.2
3 3 49.8
hfdlc
1 1 2.9
end
```

Provided there is no ambiguity, GULP will accept these options even if `observables` is omitted, however, it makes the input more readable if the section heading is included.

GULP reads only the first 80 characters on a line in an input file. Should an input line be too long to fit within this limit then the line can be continued on a second or further lines by adding the continuation character '&' to the end of the line.

### 3.2.2 Atom names

Many parts of the input to GULP require the specification of atom names, be it when giving their coordinates or when specifying potential parameters. The convention adopted in GULP is that an atom should be referred to by its element symbol, optionally followed by a number to distinguish different occurrences of the same element. Numbers between 1 and 999 are valid numbers. Hence examples of valid atom specifiers are `Si`, `Si12`, `O3` and `H387`. Something like `Si4+` would not be a valid symbol. The reason for using the element symbol is because several calculations use elemental properties such as the mass or covalent radii in dynamical or molecular runs, respectively.

Sometimes it is desirable to label all the atoms in the structure with numbers

to identify them, but with the same interatomic potential acting on them. To avoid having to input the potential multiple times for each symbol there is a convention within GULP which it is important to know. Any reference to just an atomic symbol applies to all occurrences of that element, whereas any reference to an atom type with a number only applies to that specific species. For example a Buckingham potential specified as follows:

```
buck
Si core 0 core 1283.0 0.299 10.66 0.0 12.0
```

would apply to all Si atoms, regardless of whether they are called Si or Si1 etc. However, the following potential:

```
buck
Si1 core 0 core 1283.0 0.299 10.66 0.0 12.0
```

would only act on Si1. It is important to remember this as people have labelled one atom Si and the Si1 in the past and put potentials for both which resulted in twice the potential acting on Si1 as there should have been. If the potential had been specified as just acting on Si then the correct answer would be obtained as it would act on both atoms once.

In addition to the atom label there is optionally a species type specifier which should be one of the following:

- core - represents the main part of an atom including all its mass
- shel - represents the mass-less component in a shell model
- bcor - a core, but with a spherical breathing radius
- bshe - a shell, but with a spherical breathing radius

If not given, then core is the default type. Note that the bcor and bshe types only need to be used in the structure specification. There after they can be treated as an ordinary core or shell in the potential specification and the program will select whether the potential should act on the radius or the centre of the species.

### 3.2.3 Input of structures

The structure for a three-dimensional solid requires the input of three main sets of information - the unit cell, the fractional coordinates and types of the atoms, and finally the space group symmetry. Taking these in order, the unit cell can be input either as the cell parameters:

```
cell
```

```
4.212 4.212 4.212 90.0 90.0 90.0
```

or as the cell vectors:

```
vectors
4.212 0.000 0.000
0.000 4.212 0.000
0.000 0.000 4.212
```

Normally it is easiest to use the cell parameter form and this is recommended. The main reason why you might chose to use the cell vectors is because you want to calculate the properties in a non-standard reference frame (given that quantities such as the elastic constants depend on the unit cell orientation relative to the Cartesian frame). If the cell parameters are input, then the *a* cell vector is aligned along the *x* axis, the *b* cell vector in the *xy* plane and the *c* cell vector in the general *xyz* direction.

If the keywords *comp* or *conv* are not specified, then the program will expect 6 flags to indicate how the unit cell is to be optimised. Here a flag of 1 implies that a degree of freedom should be allowed to vary and 0 will imply that it should be kept fixed. Because GULP works with the strain tensor, these flags refer to the strain components in the order *xx*, *yy*, *zz*, *yz*, *xz* and *xy*, respectively. Examples of how to input the flags for the case given above when only the on-diagonal strain components are to be varied are given below:

```
cell
4.212 4.212 4.212 90.0 90.0 90.0 1 1 1 0 0 0
```

or as the cell vectors:

```
vectors
4.212 0.000 0.000
0.000 4.212 0.000
0.000 0.000 4.212
1 1 1 0 0 0
```

When GULP transposes a system between the primitive and centred unit cells the orientation of the atoms is preserved so that any properties calculated will be the same regardless of the cell used. It is recommend that the cell parameters be used for input where possible as this ensures that symmetry can be used to accelerate optimisations. Turning now to the internal coordinates of the atoms, these can again be given either in fractional or Cartesian form, though the former is the more natural for a periodic system. Each line of input must contain at least the atom label

followed by the coordinates, in which ever units. For example for the case of MgO:

```
fractional
Mg core 0.0 0.0 0.0
O core 0.5 0.5 0.5
```

Note that if the space group symmetry is to be given then it is only necessary to specify the atoms of the asymmetric unit. Furthermore in any cases where a fractional coordinate is a recurring decimal, such as 1/3, then it is necessary to specify this value to six decimal places to be sure of it being recognised correctly as a special position. If we were to include a shell model for oxygen then the input of coordinates would now look like the following:

```
fractional
Mg core 0.0 0.0 0.0
O core 0.5 0.5 0.5
O shel 0.5 0.5 0.5
```

There is no need to specify the number of atoms to be input or to terminate the section as this is automatically done when the program finds something which is not an element symbol or a special character at the start of a line.

If a shell model has been specified for a given atom in the species section (see later), but the shells are omitted from the input for the structure then GULP will attempt to add them automatically. When this happens, the shell be placed at the same location as the core by default.

In addition to the coordinates, there are a number of optional parameters which can follow the  $z$  coordinate on the line. These are, in order, the charge, the site occupancy (which defaults to 1.0), the ion radius for a breathing shell model (which defaults to 0.0) and 3 flags to identify geometric variables (1  $\Rightarrow$  vary, 0  $\Rightarrow$  fix). Note that the flags will only be read if there is no keyword to specify the geometric variables (e.g. `comp` or `conv`). Hence in full the input for MgO could look as follows:

```
fractional
Mg core 0.0 0.0 0.0 2.00000 1.0 0.0 0 0 0
O core 0.5 0.5 0.5 0.86902 1.0 0.0 0 0 0
O shel 0.5 0.5 0.5 -2.86902 1.0 0.0 0 0 0
```

In the case of MgO all the flags can be set to 0 as there are no geometric variables within the unit cell by symmetry.

If we wanted to run a breathing shell calculation for MgO then the input might look like the following for a constant pressure run:

```
fractional
Mg core 0.0 0.0 0.0 2.00000 1.0 0.0
O core 0.5 0.5 0.5 0.86902 1.0 0.0
O bshe 0.5 0.5 0.5 -2.86902 1.0 1.2
```

or for a mean field calculation of the energy of a 40/60 MgO/CaO material:

```
fractional
Mg core 0.0 0.0 0.0 2.00000 0.4 0.0
Ca core 0.0 0.0 0.0 2.00000 0.6 0.0
O core 0.5 0.5 0.5 0.86902 1.0 0.0
O shel 0.5 0.5 0.5 -2.86902 1.0 0.0
```

The space group symmetry can be specified either through the space group number or through the standard Hermann-Mauguin symbol. Again for MgO, either of the following would be valid:

```
space          or          space
225            F M 3 M
```

In general it is better to use the symbol rather than the number as the structure may be in a non-standard setting. The help file contains a full list of the standard symbols for each space group to illustrate how the symbol should be written in the input, though further non-standard settings will be accepted. The space option is not compulsory in the input of a structure and if it is absent then GULP will assume that the structure is in P 1 (i.e. no symmetry).

Related to the space option is the origin option which allows non-standard origins to be handled. The input for this option can take the form of a single integer (1 or 2) if you want to select one of the standard alternative origin settings. Alternatively if three floating point numbers are input then they are taken to be an origin shift in fractional coordinates, or if three integer numbers are input then they are divided by 24 to obtain the shift.

The structural input for a molecular system is just the Cartesian coordinates. Currently the use of point group symmetry is unavailable for isolated systems so there is no equivalent command to space for molecules. There is unlikely to be much benefit from the addition of point group symmetry as most molecular calculations are much faster than their solid state analogues.

Multiple structures can be included in the same file by placing one after another, including mixtures of solid and molecular compounds. A useful option for keeping track of different structures is the name option. This must precede the structure and allows the user to give a one word name to the compound which will then be used as a label in the output file. Using this the structural input for a file containing both

corundum and quartz might look as follows:

```
name corundum
cell
4.7602 4.7602 12.9933 90.0 90.0 120.0
frac
Al core 0.00000 0.0 0.35216
O core 0.30624 0.0 0.00000
space
167
name quartz
cell
4.91485 4.91485 5.40629 90.0 90.0 120.0
frac
Si core 0.4682 0.0000 0.333333
O core 0.4131 0.2661 0.213100
space
152
```

In the situation where you want to run the same structure at several different conditions then the ditto option can be particularly useful to avoid repeating the structure. For example, to run corundum at a pressure of 1 GPa and 2 GPa you could use the following input for the structures:

```
name corundum
cell
4.7602 4.7602 12.9933 90.0 90.0 120.0
frac
Al core 0.00000 0.0 0.35216
O core 0.30624 0.0 0.00000
space
167
pressure 1 GPa
ditto structure
pressure 2 GPa
```

### 3.2.4 Species / libraries

In the input for the coordinates there was the option to input the species charge for each individual atom in the asymmetric unit or even the full cell. Normally this is unnecessary as all atoms of the same type have the same charge. In this latter

case the charges can be assigned by the species option. So for a zeolite structure, for example, where there may be lots of different Si and O sites we could assign charges as follows:

```
species
Si core 4.00000
O core 0.86902
O shel -2.86902
```

The species command can also serve another purpose which is to assign potential library symbols to each atom type. Quite often we may simulate a whole series of materials with a standard set of potentials. Rather than typing them in every time we can call a library. GULP at present comes with two libraries - one for zeolite and aluminophosphate type systems [3,28,29] and one for metal oxides from the work of Bush et al [30]. All we need to do to call these potentials is to assign the potential types to the types in the library files. In the case of bush.lib, there is no need to do anything as the symbols are just the metal element symbols. For the zeolitic materials there is more than one kind of some atom types and so an assignment is needed. Using this our input would look like:

```
species
Si core Si
O core O_02-
O shel O_02-
library catlow.lib
```

### 3.2.5 Input of potentials

The various types of potentials available in GULP have been tabulated earlier and detailed descriptions of the input format for each one can be found in the on-line help. This section will therefore just contain some general pointers as to how to input potentials.

Let us take the example of a Buckingham potential which acts between magnesium cores and oxygen shells with the parameters  $A=1280.0\text{eV}$ ,  $\rho=0.300\text{\AA}$ ,  $C=4.5\text{eV}\text{\AA}^6$  and acts over the range of 0 to 12  $\text{\AA}$ . The input for this would look as follows for an optimisation run:

```
buck
Mg core O shel 1280.0 0.3 4.5 0.0 12.0
```

If we want to perform a fitting run then it is also necessary to specify the flags

which indicate which parameters are to be variables (1) and which ones are not (0). There is one flag for each potential parameter and the order of the flags matches that of the parameters. Hence a fit in which we want to vary A only would look as follows:

```
buck
Mg core 0 shel 1280.0 0.3 4.5 0.0 12.0 1 0 0
```

It would not matter if we had put the flags on the end of the line in the input for an optimisation run - they would have just been ignored. For most potential types some parameters are optional and can be omitted, normally when they are zero. There is always a hierarchy to the order of omission of values. For example, for most two-body potentials if one number is missing then this is assumed to be the minimum cut-off radius and this value is zero (as it quite commonly is). For a Buckingham potential, if a second number is omitted then this is assumed to be the C term which again is often zero. If you are going to omit values it is important to remove the flags when not needed from the input as this may confuse matters. If in doubt give all values!

The number of input parameters can also vary according to any options specified after the potential type. For example, if we wanted the above potential to only act between atoms which are bonded then the input would be:

```
buck bond
Mg core 0 shel 1280.0 0.3 4.5
```

No potential cut-offs are needed as these are set by the fact that the atoms must be bonded. Similarly for a Lennard-Jones potential when given as `lennard combine` then no potential parameters will appear on the input line as these are determined by combination rules.

More than one potential can be specified for each occurrence of the potential type. Hence the following would be perfectly valid:

```
buck
Mg core 0 shel 1280.0 0.3 4.5 0.0 12.0
Ca core 0 shel 1420.0 0.3 6.3 0.0 10.0
```

If the input for one potential is too long to fit on one line then it may be continued on to the next line by using the continuation character '&' at the end of the line.

For two-body potentials there is no ambiguity about the order of the atoms as both are equivalent. For some three-body potentials and all four-body potentials it is important to be aware of the convention regarding the order of input. For a three-body potential which has a unique pivot atom, typically at which the angle is

measured, then this pivot atom must be given first and then the two terminal atoms in any order. Hence the O-Si-O angle bending term widely used for zeolites is input as:

```
three
Si core 0 shel 0 shel 2.09 109.5 1.9 1.9 3.6
```

In the case of four-body terms there is no unique pivot and so the atoms are input in the order which they are connected. A piece of good advice is that three- and four-body terms are often most readily dealt with using connectivity based cut-offs as part of the molecule set of options.

### 3.2.5.1 Input of PDF settings

Appropriate keywords for normal GULP operation should be used. Importantly, the potential model needs to be properly optimised using `opti`. To run the PDF module, the keyword `PDF` should be added. This automatically enables the `phonon` and `eigenvector` keywords, calculating the necessary phonon information. It also activates the keyword `makeEigenArrays` (which stores all phonon data in internal arrays), and `rephase` which rephases the (complex) eigenvectors so that the component with the largest magnitude is all real for all eigenvectors and also checks the normalisation. This rephasing is a rotation in the complex plane that does not change the results of the PDF calculations performed using the eigenvectors, but helps with visualisation. To ensure that the entire Monkhorst-Pack grid of  $\mathbf{k}$ -points is used (not the symmetry reduced one), `noksymmetry` is also enabled. It is often useful to use the `nokpoints` keyword to prevent the output of all the  $\mathbf{k}$ -points used (a typical PDF calculation may require 8000  $\mathbf{k}$ -points before convergence is achieved). Similarly, suppression of phonon output is useful: the keyword `nophonon` is used.

In addition to calculating the PDF from the full phonon data, it is possible to restrict the frequencies ( $\omega$ ) used. A cut-off of  $\omega_{\min}/\omega_{\max}$  can be set in the options (see below). When the keyword `PDFcut` or `PDFbelow` is used, all frequencies above/below the cut-off frequency are excluded. (There is no need to enter the `PDF` keyword separately as it is assumed). Alternatively, all frequencies above/below the cut-off frequency can be set to the cut-off frequency by the addition of `PDFkeep`.

### 3.2.5.2 Options

The configuration should be set up in the normal way. Importantly, in addition to specifying the structure and potentials, a Monkhorst-Pack grid of  $\mathbf{k}$ -points must be generated using the `shrink` option (as described in section 3.0.28.1). (Convergence of phonon properties with number of  $\mathbf{k}$ -points is essential before results can be

considered accurate. If the width of all pairs of type  $x_i - y_j$ , as given in the .wid file are divergent increase the density of the grid.)

As with other output files, the GULP option output can be used to specify the filename:

```
output pdf <filename>
```

It is important to specify an output file for all configurations, otherwise the root <pdf > or <pdf\_config\_# > will be used. Two filetypes are produced

**.wid file** Lists every atomic pair and the width (use of keyword nowidth supresses this)

**.pdfs file** Outputs Pair Distribution Functions up to rmax with the number of bins specified at input

Within the literature, there are a number of different correlation functions; the module expresses the results in several of these:  $\rho(\mathbf{r})$ ,  $G^{\text{PDF}}(\mathbf{r})$ ,  $G(\mathbf{r})$ ,  $D(\mathbf{r})$ , and  $T(\mathbf{r})$ . More details are available in the 'Further Background' section of this manual. Where phonon selection has been used,  $\omega_{\text{max}}/\omega_{\text{min}}$  is also stated in the output files, using the frequency units specified (see below), together with the temperature and number of **k**-points.

All other input options for PDF calculations are entered in lower case within a pdf input block.

The pdf input block is opened with the word pdf and closed with the word end. i.e.

```
pdf
  <PDF options>
end
```

When working with multiple configurations, it is possible to open the pdf block with "pdf all": it then operates on all configurations, ensuring that comparable PDFs are produced with the same cut-offs, maximum radius and binning. Alternatively, a seperate pdf block can be given for each configuration.

For PDFs, the maximum radius (in Å) should be specified (default = 5 Å), and the number of bins used for the output (default = 100). These can be set, within the pdf input block, using rmax and rbins respectively, or the default values used.

```
pdf
  rmax [real]
  rbins [int]
end
```

When using the frequency cut-off facility, either `wmin` or `wmax` (as appropriate) must be set, again in the `pdf` input block. While the default units for frequency input/output in the PDF module is THz, it can (optionally) be changed as shown using the `units` options: (`cm` or `wav` can be used for wavenumbers)

```
pdf
  rmax [real]
  rbins [int]
  units freq [rad/Thz/cm/wav/meV]
  wmin [real]
or
  wmax [real]
end
```

In neutron scattering, advantage is often taken of the different scattering lengths of different isotopes. The library file only contains element information. However, this can be overwritten using the `element` option input block with `bbar` or `siginc` (mass, ionic radius, etc, can also be changed in this way, see command help for more). The units are Å and Å squared. NB. The Sears table, used to produce the `eledata` Library file, uses Fm and Barns ( $= 1 \times 10^{-28}m$ ).

### 3.2.6 Defects

In this section we shall cover the basic input required to perform a Mott-Littleton calculation for an isolated defect in an otherwise perfect solid, as activated by the presence of the keyword `defect`. The main run type that we will be concerned with for defects is optimisation as we normally wish to obtain the defect energy and structure. We may also wish to locate transition states for the migration of defects - this follows the same approach as an optimisation, but with the keyword `trans` rather than `opti`. There is currently no facility to fit to defect quantities.

The first issue to consider is the bulk calculation that must precede a defect calculation. For a correct calculation the bulk structure must be optimised at least to constant volume otherwise negative defect energies may result from the removal of bulk forces, rather than defect related ones. If you intend to perform several defect calculations and the bulk unit cell is a reasonable size it is sensible to optimise the bulk as a first job and then use the restart file for the defect calculations to avoid wasted effort. There are also other reasons for optimising the bulk separately. Firstly, if you want to perform a transition state run then the `trans` keyword will try to be applied to the bulk as well as the defect with strange results (this can avoid by using the `bulk_noopt` keyword). Secondly, when creating defects it is important to know where the bulk atoms are so that they can be placed correctly.

At the end of the bulk calculation a property evaluation must be performed as the second derivatives and dielectric constants are needed for the response tensors

of region 2. This is automatically invoked and there is no need to add the keyword `property`. Again for some materials the calculation of the properties can be expensive. Hence, if multiple defect calculations are to be performed then this step can be minimised by adding the keyword `save` to the first run (which will write out a temporary file `fort.44` which contains the quantities needed for future runs in a binary form to save space) and the keyword `restore` to subsequent runs (which will cause them to read in the information from `fort.44` rather than re-calculating it).

Having dealt with the preliminaries, we are now ready to consider how to input the details of the defect calculation. Remember, the following commands should appear after the structure to which they refer. Firstly, we need to determine the defect centre around which the regions are based. This is given using the option `centre` (`center` will also work for the benefit of those of you who are American-minded!). The defect centre is normally placed at the same position as the defect, in the case of a single defect site, or at the middle of a series of defects so as to maximise the distance between any defect and the region 1 boundary. Symmetry is not explicitly input by the user for a defect calculation. However, the program will automatically try to search for any simple symmetry elements. These can then be used to accelerate the calculation. In order to do this it requires that the defect centre is chosen so as to maximise the point group symmetry about itself. This is worth keeping in mind when choosing the location of the defect centre. A general feature of the `centre` option, and those which specify the positions of defect species, is that there are a number of alternative methods for specifying the location:

**(a) Atom symbol** : this is the label for a species within the unit cell. It is best to use a unique specifier (by changing the type number of one atom if necessary) - if there is ambiguity the program will normally chose the first occurrence of the symbol.

```
centre Mg2 core
```

This will place the defect centre at the final bulk position of the Mg2 core.

**(b) Atom number** : here the position is given by the number of the atom in the asymmetric unit as input.

```
centre 3
```

This will place the defect centre at the final bulk position of the third atom in the asymmetric unit.

**(c) Fractional coordinates** : here the position is explicitly given in fractional units - the `frac` option in the following command is optional as it is the default:

```
centre frac 0.25 0.25 0.25
```

**(d) Cartesian coordinates:** here the position is explicitly given in Cartesian coordinates, the origin of the unit cell being at 0,0,0:

```
centre cart 1.5 2.4 0.8
```

**(e) Molecule number:** this places the defect centre at the middle of the molecule whose number is given (which corresponds to that in the output):

```
centre mol 2
```

Having located the defect centre the next thing we need to do is to specify the region 1 and region 2a radii. This is done with the `size` command:

```
size 4.0 10.0
```

would result in a region 1 radius of 4.0 Å and a region 2a radius of 10.0 Å. It is important to check how sensitive the defect energy is to these values and to increase them until satisfactory convergence is achieved. One way of doing this while minimising computational expense is by using the restart file. If we wanted to restart a defect calculation run with the above radii, but with region 1 increased to 6.0 Å and region 2a to 12.0 Å then we would just need to edit the restart file to contain the new values, plus the old region 1 size (needed for correct restarting) at the end of the line:

```
size 6.0 12.0 4.0
```

We now have specified the regions - next we need to create some defects. There are three options for this:

```
vacancy      - removes an ion from the structure to infinity
interstitial - inserts an ion into the structure from infinity
impurity     - replaces one ion with a different one
```

The last one, an impurity, is obviously just a short-cut combination of the other two. The actual input for each option for specifying the ion(s) involved follows that for `centre` in that the atom label, atom number, fractional or Cartesian coordinates can be used. The molecule number can also be used with the vacancy option, in which case it removes all the atoms of the molecule from the structure (see example8). Note that when molecules are removed and inserted it is important to correct the defect energy for the molecule at infinity, if this is not zero, as this is not done automatically.

An important part of the interstitial and impurity commands is to specify the

type of species to be inserted. For example, the impurity command to replace O2 with S would be:

```
impurity S O2
```

The key thing to note is that the inserting species is always specified first. To make life easy shells are handled automatically in most cases. So if both O2 and S were specified as shell model atoms then the above command would remove both the O2 core and shell, and also insert the S core and shell (initially at the same position). It becomes important when introducing species with a type different to any of the bulk species that all the necessary properties of the inserting ion are given in the species option otherwise the atom will be assumed to have no charge and no shell.

There is one further option when introducing an interstitial to make life easier. For example, imagine we want to protonate an oxygen (typically in a zeolite framework) to generate a hydroxyl group at O2. This can be readily achieved using the bond option:

```
interstitial H bond O2
```

this will place the H into the structure at the sum of the covalent radii from O2. To determine the direction for the bond the program maximises the angles to any other atoms to which O2 has bonds.

Putting all these keywords together, we shall illustrate how a lithium impurity could be created in magnesium oxide to generate a negatively charged defect. For the purposes of this example we will work with the full unit cell structure as given by the following:

```
opti comp defect
cell
4.212 4.212 4.212 90.0 90.0 90.0
frac
Mg core 0.0 0.0 0.0
Mg core 0.0 0.5 0.5
Mg1 core 0.5 0.0 0.5
Mg core 0.5 0.5 0.0
O core 0.5 0.5 0.5
O core 0.5 0.0 0.0
O core 0.0 0.5 0.0
O core 0.0 0.0 0.5
species
Mg core 2.0
```

```
O core -2.0
Li core 1.0
```

Based on the above basic input (+ interatomic potentials) all the following would be valid ways of creating the defect:

```
(a)
centre Mg1
size 6.0 12.0
vacancy Mg1
interstitial Li 0.5 0.0 0.5
```

```
(b)
centre Mg1
size 6.0 12.0
impurity Li Mg1
```

```
(c)
centre 0.5 0.0 0.5
size 6 12
impurity Li 0.5 0.0 0.5
```

```
(d)
centre 3
size 6 12
impurity Li cart 2.106 0.0 2.106
```

There are more permutations than this, but hopefully it gives you the general idea.

### 3.2.7 Restarting jobs

Because on the whole GULP doesn't require very much CPU time per step (the exceptions normally being second derivative calculations on large systems) it doesn't maintain a binary dumpfile with all the details for a restart from exactly where it left off. Instead there is the option to dump out a restart file which is just a copy of the original input (slightly rearranged!) but with any coordinates or potential parameters updated as the run progresses. The frequency with which this is written out can be controlled by the user. If the following is specified:

```
dump every 4 gulp.res
```

then a restart file will be written after every 4 cycles. If the '4' is omitted then it

defaults to being one - i.e. a dumpfile is written after every cycle. As the cost of writing out this file is normally small compared to the cost of a cycle this is the usual choice. If the every option is omitted then the restart file is written just at the end of the run.

### **3.2.8 Memory management**

From version 3.4 of GULP the code was written in Fortran90 and therefore pretty much all memory is dynamically allocated. Hence there should rarely be any need to alter the code to increase a parameter. The only main parameter in the code is the number of elements, which is set to 107 by default. In the event that you wish to study elements further down the periodic table than this, you need to edit this value, add the appropriate element data and recompile.

Even though the code is fully dynamic, you can still exhaust the memory of your computer under certain circumstances. Remember that any runs that require the analytic second derivatives, such as phonons or Newton-Raphson optimisation, will cause a memory requirement of roughly  $\frac{5}{2}(3N+6)^2$  double precision words. Hence if you run out of memory or the machine starts swapping you should first of all try to reduce the memory demands by using an optimisation algorithm that doesn't require full second derivatives, such as unit-Hessian based BFGS, limited memory BFGS or conjugate gradients.

### 3.2.9 Summary of keywords

The following is a concise summary of all the valid keywords available in GULP - for more detail consult the on-line help.

Table 3.5: Valid keywords in GULP

alamode	compute thermal conductivity by calling the interface to Alamode
allbonds	use all bonds for split bond electronegativity equalisation rather than the minimal set
allow_gt_1	allow site occupancies to exceed one
angle	calculate valid three body angles
anneal	perform simulated annealing
atomic_stress	output atomic stress components
average	output average bond lengths
bond	calculate valid bond lengths based on covalent radii
breathe	only calculate gradients for breathing shell radii
broaden_dos	apply Lorentzian broadening to density of states data
bulk_noopt	fix bulk structure prior to a defect calculation
c6	calculate C6 terms using lattice sum method
cartesian	output Cartesian coordinates for initial structure
ceigen	output eigen properties of the elastic constant tensor
cellonly	only calculate gradients for and optimise cell parameters
cmm	calculate cluster electrostatics using cell multipole method
compare	produce a table comparing the initial and final geometries
conjugate	use conjugate gradients
conp	perform constant pressure calculation - cell to vary
conv	perform constant volume calculation - hold cell fixed
coreinfo	output atomic information (for cores not shells) used in phonon calculations
cosmo	use the COSMO continuum solvation model
cosmic	use the COSMIC continuum solvation model
cost	perform cost function calculation
dcharge	output the first derivatives of the atomic charges
decimal_only	only use decimal numbers and not fractions in output
defect	perform a defect calculation after bulk calculation
dfp	use Davidon-Fletcher-Powell update rather than BFGS
dipole	add the dipole correction energy for the unit cell
distance	calculate interatomic distances
dynamical_matrix	output the dynamical matrix from a phonon calculation
eem	calculate charges using electronegativity equalisation
eembond	calculate charges using electronegativity equalisation with split bond charges
efg	calculate the electric field gradients

e harmonic	estimate the harmonic relaxation energy from a single point calculation of the Hessian and forces
eigenvectors	write out eigenvectors for phonons/frequencies
fit	perform a fitting run
fix_molecule	fix connectivity for molecules at start and do not update
frame	rotate molecules to the standard frame of reference
free_energy	perform a free energy instead of internal energy calc
frequency	calculate defect frequencies
fsprop	compute properties based on finite strain derivatives
full	write out structure as full rather than primitive cell
gasteiger	compute charges using the Gasteiger method
gear	use the Gear fifth order algorithm for molecular dynamics
genetic	perform a genetic algorithm run
ghostcell	use smaller ghost cell within supercell for phonons
global	after global optimisation, dump out restart file before opt
gradients	perform a single point calculation of energy and gradients
groupvelocity	calculate the Grueneisen parameters
grueneisen	calculate the group velocities at each k point
hessian	output hessian matrix
hexagonal	write out structure as hexagonal rather than rhombohedral
hideshells	suppress output of shells
include_imaginary	include imaginary frequencies in phonon DOS/dispersion output
intensity	calculate IR intensities for phonon/vibrational modes
isotropic	allow cell parameters to vary isotropically
kcal	output energies in kcal/mol rather than eV
kjmol	output energies in kJ/mol rather than eV
libff	specifies that fitting flags should be read from a library file if this is a fitting run
linmin	output details of line minimisation
lower_sym	try to lower the symmetry using imaginary modes
madelung	include the Madelung correction for a charged simple cubic system
makeeigenarrays	store all eigenvectors and frequencies after calculation
md	perform a molecular dynamics run
minimum_image	use the minimum image convention during MD
molecule	locate molecules and coulomb subtract within them
molmec	locate molecules and coulomb subtract 1-2 and 1-3
molq	locate molecules for intramolecular potentials only
montecarlo	perform a Monte Carlo simulation
msd	compute phonon mean-squared displacements
no4duplicates	do not duplicate torsions with wildcard potentials
noaddshells	do not automatically add missing shells
noanisotropic	use isotropic formula for region 2b energy

nobreathe	freeze breathing shell radii during optimisation
nod2sym	do not use symmetry for second derivatives
nodpsym	do not use symmetry for defect potential calculation
noelectrostatics	turns off Ewald sum even when charges are present
noenergy	do not calculate the energy - useful for debugging datasets
noexclude	do not use atom freezing algorithm during optimisation
nodensity	do not output density of state plot after phonon calculation
nodsymmetry	do not use symmetry during a defect calculation
nofirst_point	skip first point in a translate run
noflags	no variable flags are present and all variables to be excluded
nofrequency	do not print out frequencies at each k point
nokpoints	do not print out k point list
noksymmetry	do not use Patterson symmetry in Brillouin zone
nolist_md	do not use list method for 3- and 4-body terms in MD
nomcediff	controls algorithm for Monte Carlo energy evaluation
nomolecularinternalkin	remove initial intramolecular kinetic energy in MD
nononanal	exclude non-analytic correction at gamma point
nopartial	suppress output of partial PDFs
noquicksearch	turns off timesaving algorithm changes in distance searches
noreal	exclude all real space two-body interactions
norecip	exclude all reciprocal space two-body interactions
norepulsive	do not truncate repulsive terms based on Ewald accuracy
norxQ	turn off charge calculation in ReaxFF
nosasinitevery	do not initialise solvent accessible surface at each step
nosderv	do not use symmetry for gradient calculations
noshellzero	apply shift to shell coordinates that are zero during a simultaneous fit
nosymmetry	turn off symmetry once unit cell has been generated
nowidth	suppress output of peak widths for PDF calculations
nowrap	synonym for nomodcoord
nozeropt	exclude zero point energy from free energy calculation
numdiag	estimate on-diagonal hessian elements numerically
numerical	forces use of numerical second derivatives for properties
num3	forces use of numerical third derivatives for force constant calculation
ocell	optimise using the cell parameters rather than the strains
operators	print out listing of symmetry operators used
optlower	optimise after lowering symmetry
optimise	minimise the energy with respect to geometrical variables
outcon	output constraints in restart file
pacha	compute variable charges using the PACHA formalism of Marc Henry
PDF	calculate the peak widths for each atomic pair and the Pair Distributions
PDFcut	as per PDF but cut-off all phonon contributions greater than $\omega_{\max}$
PDFbelow	as per PDF but cut-off all phonon contributions below $\omega_{\min}$

PDFkeep	as with PDFcut and PDFbelow but set all $\omega > \omega_{\max}$ to $\omega_{\max}$ (or $\omega < \omega_{\min}$ to $\omega_{\min}$ )
pfinite	specifies finite displacements for generating phonons by numerical differentiation
phonon	calculate the lattice phonon modes and cluster frequencies
positive	force hessian to remain positive on the diagonal
pot	calculate the electrostatic potential at the atomic sites
potgrid	calculate the electrostatic potential over a grid
predict	perform structure prediction calculation
pregionforce	output the force on regions
prt_eam	output energy components for EAM
prt_four	output energy components for four-body potentials
prt_six	output energy components for six-body potentials
prt_three	output energy components for three-body potentials
prt_two	output energy components for two-body potentials
property	calculate the bulk lattice properties
pureq	use pure Coulomb potential in COSMO/COSMIC molecular case
qbond	calculate charges using bond increments
qeq	calculate charges using the QEq scheme of Rappe and Goddard
qiter	solve for charges using iterative algorithms rather than matrix diagonalisation
qok	run with a non-charge neutral unit cell
qsas	causes charges and details of solvent accessible surface to be output
raman	causes calculation and output of Raman susceptibility tensors
regi_before	output region 1 coordinates before defect calculation
relax	use relax fitting
rephase	change the eigenvector phases so largest magnitude component is all real for all eigenvectors and renormalize to unity
restore	read in defect calculation restart info and skip property calcn
rfo	use the rational function optimisation method
save	write out defect calculation restart information
sfinite	specifies finite displacements for generating properties by numerical differentiation
shell	only calculate gradients for and optimise shell positions
shopt	explicitly optimise shell positions during numerical third derivatives
site_energy	output energy per atomic site
simultaneous	simultaneously optimise shells while fitting
simplex	use simplex algorithm for fitting
single	perform a single point calculation of the energy
sopt	output shell iterations during molecular dynamics
spme	use smooth particle mesh Ewald if available
strain	use strains applied to a reference unit cell in calculations
static_first	perform a static optimisation before a free energy one

stress_out	output stresses at the final geometry
spatial	use domain decomposition algorithm where possible
thermalconductivity	calculate the Allen-Feldman thermal conductivity for diffusons in an amorphous solid
torsion	calculate valid four body torsion angles
transition_state	optimise using RFO to first order transition state
unit	use a unit matrix as the initial hessian for optimisation
zero_potential	set average potential across lattice sites to zero
zsis	use the ZSISA approximation in a free energy minimisation

### 3.2.9.1 Groups of keywords by use

#### (a) Control of calculation type

alamode, angle, bond, cosmo, cosmic, cost, defect, distance, eem, eembond, efg, eharmonic, fit, free\_energy, gasteiger, genetic, gradients, groupvelocity, grueneisen, md, montecarlo, noautobond, noenergy, optimise, pacha, pot, predict, preserve\_Q, property, phonon, qeq, qbond, raman, single, sm, static\_first, thermalconductivity, torsion, transition\_state

#### (b) Geometric variable specification

breathe, bulk\_noopt, cellonly, comp, conv, isotropic, orthorhombic, nobreathe, noflags, shell, unfix

#### (c) Algorithm

allbonds, c6, dipole, fbfgs, fix\_molecule, fsprop, full, ghostcell, hill, kfull, marvinSE, madelung, minimum\_image, molecule, molmec, molq, newda, noanisotropic\_2b, nod2sym, nodsymmetry, noelectrostatics, noexclude, nofcentral, nofirst\_point, noksymmetry, nolist\_md, nomcediff, nonanal, noquicksearch, noreal, norecip, norepulsive, nosasinitevery, nosderv, nozeropt, numerical, num3, ocell, qiter, qok, spatial, sopt, storevectors, shopt, spme, nomolecularinternalke, voigt, zsis

#### (d) Optimisation method

conjugate, dfp, lbfgs, numdiag, positive, rfo, unit

#### (e) Output control

atomic\_stress, average, broaden\_dos, cartesian, compare, conserved, dcharge, decimal\_only, dynamical\_matrix, eigenvectors, global, hessian, hexagonal, include\_imaginary, intensity, kcal, kjmol, linmin, meanke, msd, nodensity\_out, nodpsym, nofirst\_point, nofrequency, nokpoints, operators, outcon, prt\_eam, prt\_two, prt\_three, prt\_four, prt\_six, prt\_regi\_before, qsas, restore, save, site\_energy, stress\_out, terse,

ceigen

**(f) Structure control**

full, hexagonal, lower\_symmetry, nosymmetry, frame

**(f) PDF control**

PDF, PDFcut, PDFbelow, PDFkeep, coreinfo, nowidth, nopartial

**(g) Miscellaneous**

libff, nomodcoord, nowrap, oldunits, zero\_potential

**3.2.9.2 Summary of options**

The following is a concise summary of all the valid options available in GULP - for more detail consult the on-line help.

Table 3.6: Valid options in GULP

14_scale	specifies the 1-4 scaling factor for molecular mechanics
accuracy	specifies the accuracy of the Ewald summation
ala_cutoff	distance cutoff for force constants in Alamode
ala_disp	specifies finite difference displacements for Alamode
ala_processors	specifies the number of cores for Alamode to run on
ala_shrink	specifies the shrinking factors for sampling the Brillouin zone for Alamode
atomab	specifies the one-centre A and B terms for combination rules
axilrod-teller	specifies an Axilrod-Teller three-body potential
bacoscross	specifies a bond-angle cosine cross term three-body potential
bacross	specifies a bond-angle cross term three-body potential
bagcross	specifies a bond-bond-angle general cross term three-body potential
balcross	specifies a bond-bond-angle linear cross term three-body potential
bbar	used within element input block to overwrite default scattering length
best	output best N configurations from genetic algorithm run
bcross	specifies a bond-bond cross term three-body potential
blocksize	specifies the blocksize for parallel data decomposition
boattractive	specifies parameters for bond order attractive energy
bocharge	specifies parameters for bond order charges
bocoordination	specifies parameters for bond order coordination number
bocnswitch	specifies parameters for bond order coordination number switching function
bocntolerance	specifies parameters for bond order coordination number tolerances
bondtype	specifies the default bond type for a species pair
borepulsive	specifies parameters for bond order repulsive energy
boselfenergy	specifies parameters for bond order charge self-energy

botwobody	specifies parameters for bond order two-body energy
both	all subsequent potentials are both inter- and intra-molecular
box	specify box size/number for dispersion and DOS plots
brenner	specifies that the Brenner REBO energy be calculated
broaden_dos	alters the default DOS broadening factor
bsm	specifies radial parameters for a breathing shell model
bspline	specifies the order of the B-splines for the SPME algorithm
buck4	specifies a four range Buckingham potential
buckingham	specifies a Buckingham potential
bulk_modulus	gives the experimental bulk modulus for fitting (cubic only)
cartesian	input crystal structure using Cartesian coordinates
cell	input unit cell as a, b, c, alpha, beta, gamma
centre	specifies location of defect centre
charge	vary specified atomic charges during fitting
chemshell_mode	sets the output model for ChemShell
cmm	selects cell multipole method for Coulomb terms and order
configurations	controls the number of configurations in genetic algorithm
constrain	input constraints between variables (fitting and optimisation)
contents	specifies the unit cell contents for structure prediction
cosmoframe	manually specifies frame of reference for a molecular COSMO/COSMIC run
cosmoshape	selects between octahedral or dodecahedral triangulation in COSMO/COSMIC
cost	set the parameters for the cost function
coulomb_subtract	specifies a coulomb subtraction potential
covalent	specifies the covalent radii for an element
covexp	specifies the covalent-exponential potential
crossover	specifies the crossover probability in the genetic algorithm
cstrain	specifies a set of strains to be applied to the input reference cell
cutd	cutoff for distance calculation
cutmany	set cutoff scale factor for many body cross terms during optimisation
cutp	overall interatomic potential cutoff
cuts	core-shell cutoff distance
cv	specifies the constant volume heat capacity for fitting
cwolf	controls the Wolf summation used in the COSMO/COSMIC methods
damped_dispersion	C6 and C8 potentials with short range damping
deflist	input defect species list for restart
delay_field	delay start of time-dependent field in MD
delay_force	delay start of time-dependent force in MD
delf	maximum energy change before hessian is recalculated
delta	specifies the differencing interval for numerical gradients
discrete	specifies the discretisation interval for the genetic algorithm
dispersion	produces phonon dispersion curves

ditto	copy information from previous configuration to current one
dump	write out a dumpfile for restarts
j2	species a constant energy for a valid 2-body potential
j3	species a constant energy for a valid 3-body potential
eam_density	specifies the form and parameters for the Embedded Atom density
eam_functional	specifies the functional form of the Embedded Atom Method
edip_accuracy	specifies truncation of exponential terms in EDIP
edip_coordination	specifies coordination number parameters in EDIP
edip_threebody	specifies angular parameters in EDIP
edip_twobody	specifies pairwise parameters in EDIP
edip_zmax	specifies coordination number truncation parameter in EDIP
elastic	specifies elastic constant values for fitting
electroneg	input new parameters for electronegativity equalisation
element	opens the element parameter options section
end_field	stop time for time-dependent field in MD
end_force	stop time for time-dependent force in MD
energy	specifies the lattice energy for fitting
ensemble	selects either the NVE or NVT ensemble for MD
entropy	specifies the entropy for fitting
epsilon/sigma	specifies the one-centre $\epsilon/\sigma$ for combination rules
equilibration	length of equilibration period in a molecular dynamics run
erferfc	specifies the parameters of an erf x erfc potential
erfpot	specifies the parameters of an erf potential
ewaldrealradius	specifies target real space cut-off for Ewald sum
exponential	specifies an exponential three-body potential
factor	temperature reduction factor for simulated annealing
fangle	specifies a bond angle as a fitting observable
fbond	specifies a bond length as a fitting observable
fc_supercell	specifies the size of the supercell to be used for force constants in real space
field	apply an electric field in a non-periodic direction
finite	use finite differences to evaluate numerical derivatives
forceconstant	specifies a force constant model
fractional	input crystal structure using fractional coordinates
frqtol	specifies the tolerance for imaginary frequencies in symmetry lowering
ftol	specifies the function tolerance for optimisations
gamma_angular	controls the spherical averaging for non-analytic corrections
gamma_direction	specifies the direction of approach to gamma for non-analytic corrections
gastdamping	sets the damping factor and algorithm for the Gasteiger method
gastiter	sets the maximum number of iterations for the Gasteiger method
gastparam	specifies species dependent parameters for the Gasteiger method
gasttol	sets the charge tolerance for the Gasteiger method
gcmcexistingmolecules	allows existing GCMC molecules to be specified

gcmcmolecule	specifies molecules for GCMC
gcmcspecies	specifies species for GCMC
gdcrit	controls change from energy to force balance in defect calculation
general	specifies a general interatomic potential
genetic	general option for genetic algorithm sub-options
gexp	specifies exponential weights for genetic algorithms
ghost_supercell	specifies the size of the underlying supercell for the benefit of phonon calculations
gradients	specifies gradients that are to be used in fitting
grid	specifies the grid for genetic algorithms
gtol	specifies the gradient tolerance for optimisations
harmonic	specifies an harmonic potential
hfdlc	specifies high frequency dielectric constants for fitting
hfrefractive	specifies the high frequency refractive index for fitting
ignore	tells the program to ignore input until "erongi" is found
impurity	replace one ion by another for a defect calculation
include	include an external file into a GULP input
index_k	specifies the maximum range of vectors in reciprocal space
intconserved	specifies the integral of the conserved quantity - restart option
integrator	specifies MD integrator algorithm to use
intermolecular	all subsequent potentials are intermolecular only
interstitial	insert an interstitial for a defect calculation
intramolecular	all subsequent potentials are intramolecular only
ionic	specifies the ionic radii for an element
iterations	specifies that the number of cycles of shell optimisation in MD
keyword	allows the input of keywords on any line
kim_model	specifies the name of the OpenKIM model
kpoints	specify explicit k points for phonon calculation
lennard	specifies a Lennard-Jones potential
library	specifies a file containing a library of interatomic potentials
lin3	specifies parameters for the ESFF linear three-body potential
line	maximum number of points in a line minimisation
lorentzian_tolerance	sets the drop tolerance for the Lorentzian broadening
lowest_mode	sets the lowest and highest modes to be included in the free energy
manybody	specifies that a manybody potential should act between two atoms
marvin	input commands to be passed through to a Marvin run
mass	specifies the atomic mass for a species
maths	allows control of maths libraries where several different varieties are linked
matrix_format	specifies whether serial algorithms should use lower-half triangular or 2-D matrices
maxcyc	specifies the maximum number of cycles
maximum	upper bound for genetic algorithm parameters

maxone	limits size of second derivative arrays for dynamic memory
mcchemicalpotential	controls the chemical potential during Grand Canonical Monte Carlo
mccreate	controls the creation probability during Monte Carlo
mcdestroy	controls the destruction probability during Monte Carlo
mclowest	specifies the lowest energy found during Monte Carlo - restart option
mcmmaxdisplacement	controls the maximum displacement during Monte Carlo
mcmmaxrotation	controls the maximum rotation during Monte Carlo
mcmmaxstrain	controls the maximum strain to be trialled during Monte Carlo
mcmeans	specifies running means for Monte Carlo
mcmove	controls the translation probability during Monte Carlo
mcoutfreq	controls the output frequency during Monte Carlo
mcrotate	specifies rotation probability for Monte Carlo
mcsample	controls the sampling frequency during Monte Carlo
mcstep	specifies step number for Monte Carlo restart
mcstrain	specifies strain probability for Monte Carlo
mcswap	controls the atom swap probability during Monte Carlo
mctrial	specifies the number of trial events during Monte Carlo
mcvolume	specifies the volume used in a Grand Canonical Monte Carlo
mdarchive	specifies the name for an MD archive file
mdmaxtemp	specifies the maximum temperature allowed for an MD run
mdmaxvolume	specifies the maximum volume allowed for an MD run
meam_density	specifies the form and parameters for the Modified Embedded Atom Method density
meam_functional	specifies the functional form of the Modified Embedded Atom Method
meam_rhotype	specifies the functional form of the density for MEAM
meam_screening	specifies the Cmin Cmax parameters for the MEAM screening function
mei-davenport	specifies the parameters of the Mei-Davenport potential
minimum	lower bound for genetic algorithm parameters
mm3angle	specifies an angle bending potential in MM3 format
mm3buck	specifies a Buckingham potential in MM3 format
mm3stretch	specifies a bond stretch potential in MM3 format
mode	specifies a vibrational mode for fitting based on the maximum projection on an eigenvector
mode2a	allows the user to chose how region 2a is treated
morse	specifies a Morse potential
move_2a_to_1	after a defect calc region 2a ions are moved to region 1
murrell-mottram	species parameters for the Murrell-Mottram 3-body potential
mutation	specifies the mutation probability in the genetic algorithm
name	give a one-word name to a structure
nor	specifies the NMR parameters for a species in a PACHA calculation
nobond	excludes bond formation between species in molecule run
observables	opens the observables option section

odirection	controls in/out directions for frequency dependent properties
oldvarorder	controls whether new or old variable order is used in serial optimisation runs
omega	controls calculation of frequency dependent properties
omega_damping	damping factor in frequency dependent properties
omega_af	minimum frequency for Allen-Feldman thermal conductivity
outofplane	out of plane distance four-body potential
origin	gives the origin setting number or explicit origin
output	creates dumpfiles for input to other programs
parallel	controls parallel algorithm being used
pdf	start of input block used for PDF options
piezo	specifies the piezoelectric constants for fitting
plane_lj	specifies a Lennard-Jones potential between an atom and a plane
plumed_input	specifies the name of the PLUMED input file
plumed_log	specifies the name of the PLUMED log file
pointsperatom	controls number of points on solvent accessible surface
poisson_ratio	specifies a Poisson ratio for fitting
polynomial	specifies a polynomial potential
potential	inputs electrostatic potential at a point for fitting
potgrid	specifies a grid of points at which to calculate the potential
pressure	specifies the applied external pressure
production	controls the length of the production time for MD run
project_dos	generate projected densities of states
qeqliter	specifies maximum number of iterations for QEq charges
qeqradius	sets the radius at which two-centre integrals switch to $1/r$
qeqtol	tolerance for convergence of QEq charges for H
qerfc	specifies that an erfc screened Coulomb terms should be used
qgrid	specifies the reciprocal space grid dimensions for SPME
qincrement	specifies the bond charge increment for the Gasteiger method
qiterations	specifies the convergence parameters for an iterative charge solve
qmmm	controls the QM/MM embedding scheme used in the energy calculation
qoverr2	specifies the parameters of a charge over distance squared potential
qsolver	controls choice of charge solver for variable charges
qtaper	tapers Coulomb term at short range to a constant value
radial_force	specifies a force acting between all atoms and a point in space
random	specifies the number of random number calls made - used in restarting
rangeforsmooth	controls the smoothing of the solvent accessible surface
rbins	sets number of bins to be used in PDF output (pdf block)
rcspatial	controls the region size for domain decomposition
rdirection	specifies the in and out directions of waves for Raman intensities
reaction	specifies a reaction energy as a fitting observable
reaxfftol	specifies tolerances for ReaxFF
reaxff_chi	specifies element specific electronegativity for ReaxFF

reaxff_mu	specifies element specific hardness for ReaxFF
reaxff_gamma	specifies element specific Coulomb screening parameter for ReaxFF
reaxff0_bond	specifies non-element specific bond parameters for ReaxFF
reaxff0_over	specifies non-element specific over-coordination parameters for ReaxFF
reaxff0_valence	specifies non-element specific valence parameters for ReaxFF
reaxff0_penalty	specifies non-element specific penalty parameters for ReaxFF
reaxff0_torsion	specifies non-element specific torsion parameters for ReaxFF
reaxff0_vdw	specifies non-element specific VDW parameters for ReaxFF
reaxff0_lonepair	specifies non-element specific lonepair parameters for ReaxFF
reaxff1_radii	specifies element specific radii for ReaxFF
reaxff1_valence	specifies element specific valence information for ReaxFF
reaxff1_over	specifies element specific over-coordination parameters for ReaxFF
reaxff1_under	specifies element specific under-coordination parameters for ReaxFF
reaxff1_lonepair	specifies element specific lonepair parameters for ReaxFF
reaxff1_angle	specifies element specific three-body angle parameters for ReaxFF
reaxff1_morse	specifies element specific two-body Morse parameters for ReaxFF
reaxff2_bo	specifies pair-wise bond order parameters for ReaxFF
reaxff2_bond	specifies pair-wise bond energy parameters for ReaxFF
reaxff2_over	specifies pair-wise over-coordination parameters for ReaxFF
reaxff2_morse	specifies pair-wise Morse parameters for ReaxFF
reaxff2_pen	specifies pair-wise penalty parameters for ReaxFF
reaxff3_angle	specifies angular valence energy parameters for ReaxFF
reaxff3_pen	specifies angular penalty energy parameters for ReaxFF
reaxff3_conjugation	specifies angular conjugation parameters for ReaxFF
reaxff3_hbond	specifies hydrogen-bonding parameters for ReaxFF
reaxff4_torsion	specifies torsional energy parameters for ReaxFF
region_1	explicit specification of region ions for defect calculation
reldf	maps defect region 1 atoms to perfect ones for restarting
reperfc	specifies the parameters of a repulsive erfc potential
rfotoleig	specifies the tolerance for negative eigenvalues of the Hessian in RFO
rfotolgrad	specifies the tolerance for projected gradients to control active modes in RFO
rmax	sets maximum radius for a PDF calculation (pdf block)
rspeed	controls the balance between real and reciprocal space
rtol	specifies the bond length tolerance for molecule generation
rydberg	specifies the parameters for a Rydberg potential
ryckaert	specifies a Ryckaert-Bellemans four-body potential
sample	controls sampling frequency during an MD run
sasexclude	excludes atoms from being part of the solvent accessible surface
sasparticles	controls handling of shell charge in COSMO/COSMIC run
scale	specifies scaling factor for vectors and Cartesian coordinates
scan_cell	run a sequence of calculations in which the cell parameters are varied
scmaxsearch	sets maximum search range for many body potentials in FEM

sdlc	specifies static dielectric constants for fitting
seed	specifies seed for random number generator
segmentsperatom	controls the number of segments on the solvent accessible surface
shear_modulus	specifies the shear modulus for fitting (cubic case only)
shellmass	specifies the proportion of atoms mass for the shell in MD
shift	adds an offset to the energy for fitting energy hypersurfaces
shrink	specify shrinking factors for Brillouin zone integration
siginc	used within element input block to overwrite default incoherent cross section
size	specifies the sizes of regions 1 and 2a for a defect calculation
solventepsilon	specifies the dielectric constant in a COSMO/COSMIC run
solventradius	sets the solvent radius in a COSMO/COSMIC run
solventrmax	sets the cut-off between use of segments vs points in COSMO/COSMIC
spacegroup	gives either the space group number or symbol
species	specifies the charges for all atomic species
spin	specifies the spin for a species
spline	specifies spline potential and splining data
split	vary specified core-shell charge split during fitting
spring	specifies core-shell spring constant
srefractive	specifies the static refractive index for fitting
srglue	inputs parameters for the short-range part of the glue model
start	tells the program to ignore the remaining input and to begin
stepmx	controls the maximum step during a minimisation
stop	tells the program to stop executing immediately
stress	specifies stress values as observables for fitting
strain_derivative	specifies strain derivative values as observables for fitting
supercell	creates a supercell
sw2	specifies a Stillinger-Weber two-body potential
sw3	specifies a Stillinger-Weber three-body potential
switch_min	changes the minimiser according to a given criteria
switch_stepmx	changes the maximum step size according to a given criteria
symbol	changes element symbol from those in eledata
symmetry_number	specifies the symmetry number for the rotational partition function
tau_barostat	controls the relaxation time for the stochastic barostat
tau_thermostat	controls the relaxation time for the stochastic thermostat
td_field	applies a time-dependent electric field during MD
temperature	specifies temperature for thermodynamic properties and MD
terse	suppresses output during run
tether	specifies atoms to be fixed during MD instead of flags
three	specifies a three-body potential
threshold	specifies tolerances on third order force constants
time	places a limit on the run time for the job
timestep	controls the timestep in a molecular dynamics run

title	inputs title lines for a job
torsion	specifies a four-body potential
tournament	defines the tournament probability for the genetic algorithm
tpxo	specifies two point crossover in genetic algorithms
translate	scans a potential energy surface by translating atoms
tscale	controls the temperature scaling in a molecular dynamics run
ttol	specifies minimum temperature for simulated annealing
uff_bond	allows the user to change the bond orders used in UFF for each bond type
uff1	specifies the species-wise parameters for UFF combination rules
uff3	specifies a three-body potential of UFF form
uff4	specifies a four-body potential of UFF form
uffoop	specifies an out of plane potential of UFF form
unfreeze	sets optimisation flags to 1 within a spherical region
unique	sets cost function difference for structures to be unique
units	sets the units for quantities (currently only for frequencies in PDF)
update	sets the maximum number of hessian updates
urey-bradley	specifies a Urey-Bradley three-body potential
vacancy	creates a vacancy for a defect calculation
variables	opens the variables option section
vectors	input lattice vectors to define unit cell
volume	specifies the cell volume as a fitting observable for a 3-D system
weight	changes the weights of observables in fitting
wmax	sets maximum phonon frequency for PDF calculation (pdf block)
wmin	sets minimum phonon frequency for PDF calculation (pdf block)
write	controls the frequency of writing for the MD dumpfile
xangleangle	specifies a angle-angle cross potential
xtol	controls the parameter tolerance in optimisation
youngs_modulus	specifies a Youngs modulus for fitting
zbl	specifies a Ziegler-Biersack-Littmark potential

## 3.3 Guide to output

### 3.3.1 Main output

Hopefully, if you understand what has gone into the input for the calculation the output will be largely self-explanatory! Hence this section will give only a few brief pointers as to the nature of the output. Many pieces of the output are specific to particular options. The following is a guide to the order which things will appear in the output file, which in turn mirrors the order in which runtypes are executed:

Banner	gives the version number of the program
Keywords	the program echoes the keywords it has found in the input with the exception of some debugging keywords which only affect the more verbose pieces of output
Title	if input by the user

Structural output

for each configuration (structure) in turn the program will echo the structural information that was input and any derived quantities in the following order:

- Formula for compound (excluding shells)
- Number of species in the asymmetric unit
- Total number of species in the primitive cell
- Dimensionality of system
- Charge if not zero
- Solvation model parameters (if applicable)
- For 3-D systems only
  - Symmetry information
  - Cell vectors for primitive cell
  - Cell parameters for primitive and full cell
  - Cell volume
- For non 3-D systems only
  - Dipole moment in non-periodic directions
- Electric field (if applicable)
- Shrinking factors for reciprocal space
- Temperature
- Pressure or pressure tensor
- Coordinates (fractional for 3-D / Cartesian for 0-D), including the site occupancy and charge. Where applicable, coordinates which are free to vary are indicated by an asterisk following them
- Molecule listing (if requested)
- Geometry analysis output (if requested)

Species output  
Electrostatic accuracy  
parameter

contains all species/element specific data

Time limit for run	
Interatomic potentials	
Fitting output	fitting involves all structures and precedes all other calculation types so that they can use the optimised parameters
Translate output	as translate performs the runtime for each point along the specified path it precedes the run type output
Runtime output	the output appears for each configuration in the following order subject to the runtime having been requested by the user: <ul style="list-style-type: none"> <li>• Electronegativity equalisation</li> <li>• Optimisation / energy / gradient calculation - for non-primitive unit cells values are given for the primitive cell unless specified otherwise</li> <li>• Property calculation</li> <li>• Phonon calculations</li> <li>• Electrostatic potential and derivatives</li> <li>• Molecular dynamics</li> <li>• Defect calculation</li> </ul>
Timing information	
File output information	

### 3.3.2 Files for graphical display

Both phonon dispersion and phonon density of states calculations produce information which is suitable for graphic display. Although there is a crude picture generated in the GULP output it is rather limited by the text nature of the output file. The command `output phonon` can be used to dump the data generated by GULP to two files with the extensions `‘.dens’` and `‘.disp’` which can then be exported into a graph plotting program (after suitable modification) to produce proper plots.

### 3.3.3 Input files for other programs

The `output` option allows the user to generate input files for a number of other programs, both for displaying crystal structures and for other types of run. The file types available are summarised below:

Marvin	(.mvn)	for a surface calculation
THBREL	(.thb)	for a calculation using the program THBREL
xtl	(.xtl)	for input to the Insight graphical interface from Accerlys Inc. Only applicable to solids.
xr	(.xr)	for input to the G-Vis interface from Oxford Materials (modified CSSR file format)
arc	(.arc/.car)	for input to the Materials Studio graphical interface from Accelrys Inc. Available for bulk, cluster and defect calculations (each type produces a separate file with the type appended to the name). This file can be generated to contain multiple structures for visualisation as a movie.
cssr	(.cssr)	for input into the Cerius <sup>2</sup> interface from Accelrys Inc and other programs. Available for bulk calculations
xyz	(.xyz)	for input into a range of other molecule codes, such as Molden.
fdf	(.fdf)	contains the structural information in a form suitable for SIESTA
cif	(.cif)	writes out a simple cif file for input into many other crystallographic codes
drv	(.drv)	writes a file with the derivatives - useful for linking to QM/MM codes
frc	(.frc)	writes a file with the force constants - useful for linking to QM/MM codes
str	(.str)	writes out a file in the CRYSTAL98 format for reading by DLV
history	(.his)	writes out a file in DLPOLY history file format

Note that when generating input files for other programs there is no guarantee of compatibility due to differences in features or because of changes in format.

### 3.3.4 Temporary files

Some use is made by GULP of binary scratch files for certain run types. Most are transient files which are removed before the end of a run. The normal reason for their existence is to economise on memory by allowing large arrays to be overlaid. The following is a list of the Fortran channels that may be used and what they are used for (a 'D' in brackets indicates that the file should be automatically deleted before successful completion of a job):

31/32	restart files for a molecular dynamics run
44	restart file for a defect calculation to avoid bulk property calcn
51	storage of frequencies for passing between routines (D)
59	projection of phonons needed for project_dos option (D)

In addition to the files that GULP uses internally, there are a number of files that can be created for communication with or by Alamode when computing thermal conductivity:

alm.log	output from alm code of Alamode
anharm.log	output from anharm code of Alamode
name_alm.in	input to alm code of Alamode created by GULP
name_anharm.in	input to anharm code of Alamode created by GULP
name.pattern_HARMONIC	displacement patterns for generation of harmonic force constants
name.pattern_ANHARM3	displacement patterns for generation of 3rd order force constants
name_cubic.fcs	force constants from Alamode
name_cubic.xml	force constants from Alamode in XML format
name_disp_cubic.dat	displacements for anharmonic force constant calculation
name_force_cubic.dat	forces from displacements for anharmonic force constant calculation
name_rta.kl	final thermal conductivity results from Alamode
name_rta.result	output from Alamode during thermal conductivity calculation

In the above, "name" refers to the file root name used for the job that comes from the name option in GULP

## 3.4 Guide to installation

### 3.4.1 Environment variables

In previous versions of GULP it was necessary to edit the file local.F (now local.F90) to set the location of the library files and help text. This is no longer necessary since the location is now specified by environment variables:

GULP\_LIB - specifies the directory path for the libraries  
GULP\_DOC - specifies the directory path for the documentation for GULP

If you are working in tcsh/csh then you can set these by putting the following lines in your .cshrc:

```
setenv GULP_LIB /Users/julian/progs/gulp5.0/Libraries
setenv GULP_DOC /Users/julian/progs/gulp5.0/Docs
```

If you would to use the interface to Alamode for thermal conductivity then you need to set the path to the top level directory of this code:

```
setenv ALAMODE_DIR /Users/julian/progs/alamode-1.0.2/
```

### 3.4.2 Compiling GULP

From version 5 onwards there is a new method for installing GULP. A script is now included called `mkgulp` in the `Src` directory that sets the options for compilation based on flags. To compile a serial executable with `gfortran` and no extra features you just need to type:

```
./mkgulp
```

By adding various flags to the command other options can be activated:

Table 3.8: Valid options for `mkgulp`

<code>-m</code>	compile a parallel executable using MPI
<code>-d</code>	compile with debugging turned on
<code>-f</code>	compile and link to FFTW3 libraries for Smooth Particle Mesh Ewald
<code>-p</code>	compile and link to Plumed for metadynamics
<code>-k</code>	compile and link to OpenKIM
<code>-c ARG</code>	specifies the compiler to be used (default is <code>ARG=gfortran</code> )
<code>-t ARG</code>	specifies the task to be performed (default is <code>ARG=gulp</code> )
<code>-h</code>	output help text for <code>mkgulp</code>

Allowed compilers that can be specified are currently `gfortran` and `intel`. The task argument can be one of the following:

Table 3.9: Valid tasks for `mkgulp`

<code>gulp</code>	compile a GULP executable
<code>clean</code>	remove object files and modules for this version
<code>fox-clean</code>	remove compilation files for FoX
<code>lib</code>	build a GULP as a library
<code>tar</code>	build a tar file

For some of the `mkgulp` options it is necessary to have additional libraries installed:

- `-m` => needs MPI, Scalapack, Blacs, Pblas
- `-f` => needs FFTW3 (<http://www.fftw.org>)
- `-k` => needs OpenKIM version 2 (<http://openkim.org>)
- `-p` => needs Plumed version 2 (<http://www.plumed.org>)

Depending on where these libraries are installed then you may need to edit `mkgulp` to set the correct path to these libraries. Search for the `USER` tag to find lines that

might need to be edited in mkgulp. On a Mac, it is assumed by default that Scalapack is installed via Macports. For FFTW3 and Plumed it is assumed by default that the libraries are in a directory that is automatically checked during loading such as usrlocallib. FFTW3 has been tested for version 3.3.4, while Plumed is tested for 2.2.1.

When GULP is compiled with mkgulp, a separate subdirectory is created for each version depending on the options specified (e.g. you can have a directory for the serial and parallel version at the same time). If you want to clean the directories up, therefore this has to be performed for each version that you have compiled separately.

### **3.4.3 Trapping of Control C**

An optional feature during GULP compilation is to enable trapping of Control C so that the program exits either from optimisation or fitting cycles. This allows the user to cleanly exit an iterative process that is going nowhere. A second execution of Control C will then stop the program as normal. To enable this feature you need to add the -DCTRLC flag to UDEFS in mkgulp.

### **3.4.4 Output in XML format**

A further optional feature during GULP compilation is to enable output in XML format using the FoX plug-in from Andrew Walker (<http://fortranwiki.org/fortran/show/FoX>). To enable this feature you need to remove the -DNOFOX flag from UDEFS in mkgulp.

# Bibliography

- [1] E. Madelung. Das elektrische feld in systemen von regelmaessig angeordneten punktladungen. *Phys. Z.*, 19:524–532, 1918.
- [2] M. Born and J.E. Mayer. Zur gittertheorie der ionenkristalle. *Z. Physik*, 75:1–18, 1932.
- [3] A.F. Kapustinskii. Lattice energy of ionic crystals. *Quart. Rev. Chem. Soc.*, 10:283–294, 1956.
- [4] M.J. Norgett. A user's guide to hades. Technical Report AERE-R7015, AERE Harwell Laboratory, 1972.
- [5] J.H. Harding. A guide to midas. Technical Report AERE-R13127, AERE Harwell Laboratory, 1988.
- [6] J.H. Harding. A guide to the harwell pluto program. Technical Report AERE-R10546, AERE Harwell Laboratory, 1982.
- [7] M. Leslie. Cascade. Technical Report DLSCITM36T, Daresbury Laboratory, 1984.
- [8] S.C. Parker and G.D. Price. Computer modelling of phase transitions in minerals. *Adv. Solid State Chem.*, 1:295–327, 1989.
- [9] D.J. Willock, S.L. Price, M. Leslie, and C.R.A. Catlow. The relaxation of molecular crystal structures using a distributed multipole electrostatic model. *J. Comp. Chem.*, 16:628–647, 1995.
- [10] W.R. Busing. Wmin, a computer program to model molecules and crystals in terms of potential energy functions. Technical Report ORNL-5747, Oak Ridge National Laboratory, 1981.
- [11] D.E. Williams. Molecular packing analysis. *Acta Cryst. A*, 28:629–635, 1972.
- [12] G. Eckold, M. Stein-Arsic, and H.J. Weber. Unisoft - a program package for lattice dynamical calculations. *J. Appl. Cryst.*, 20:134–139, 1987.

- [13] W.F. van Gunsteren and H.J.C. Berendsen. Groningen molecular simulation (gromos) library manual. Technical report, Biomos, Groningen, 1987.
- [14] D.A. Pearlman, D.A. Case, J.W. Caldwell, W.S. Ross, T.E. Cheatham III, S. DeBolt, D. Ferguson, G. Seibel, and P. Kollman. Amber, a package of computer programs for applying molecular mechanics, normal mode analysis, molecular dynamics and free energy calculations to simulate the structural and energetic properties of molecules. *Comput. Phys. Commun.*, 91:1–41, 1995.
- [15] B.R. Brooks, R.E. Bruccoleri, B.D. Olfson, D.J. States, S. Swaminathan, and M. Karplus. Charmm: A program for macromolecular energy, minimization, and dynamics calculations. *J. Comp. Chem.*, 4:187–217, 1983.
- [16] W. Smith and T.R. Forester. Dl\_poly\_2.0: A general purpose parallel molecular dynamics simulation package. *J. Mol. Graphics*, 14:136–141, 1996.
- [17] W. Smith, C.W. Yong, and P.M. Rodger. Dl\_poly: application to molecular simulation. *Mol. Simul.*, 28:385–471, 2002.
- [18] G. Watson, E.T. Kelsey, N.H. de Leeuw, D.J. Harris, and S.C. Parker. Atomistic simulation of dislocations, surfaces and interfaces in mgo. *J. Chem. Soc., Faraday Trans.*, 92:433–438, 1996.
- [19] M.B. Taylor, G.D. Barrera, N.L. Allan, T.H.K. Barron, and W.C. Mackrodt. Shell: A code for lattice dynamics and structure optimisation of ionic crystals. *Comp. Phys. Commun.*, 109:135–143, 1998.
- [20] H.M. Evjen. On the stability of certain heteropolar crystals. *Phys. Rev.*, 39:675–687, 1932.
- [21] P.P. Ewald. Die berechnung optischer und elektrostatischer gitterpotentiale. *Ann. Phys.*, 64:253–287, 1921.
- [22] M.P. Tosi. Cohesion of ionic solids in the born model. *Solid State Phys.*, 16:1–120, 1964.
- [23] R.A. Jackson and C.R.A. Catlow. Computer simulation studies of zeolite structure. *Mol. Simul.*, 1:207–224, 1988.
- [24] U. Essmann, L. Perera, M.L. Berkowitz, T. Darden, H. Lee, and L.G. Pedersen. A smooth particle mesh ewald method. *J. Chem. Phys.*, 103:8577–8595, 1995.
- [25] L. Greengard and V. Rokhlin. A fast algorithm for p@article simulations. *J. Comput. Phys.*, 73:325–348, 1987.

- [26] H.G. Petersen, D. Soelvason, J.W. Perram, and Smith E.R. A very fast multipole method. *J. Chem. Phys.*, 101:8870–8876, 1994.
- [27] S.W. de Leeuw, J.W. Perram, and E.R. Smith. Simulation of electrostatic systems in periodic boundary conditions. i. lattice sums and dielectric constants. *Proc. R. Soc. London, Ser. A*, 373:27–56, 1980.
- [28] M. Leslie and M.J. Gillan. The energy and elastic dipole tensor of defects in ionic-crystals calculated by the supercell method. *J. Phys. C, Solid State Phys.*, 18:973–982, 1985.
- [29] U. Essmann, L. Perera, M.L. Berkowitz, T. Darden, H. Lee, and L.G. Pedersen. A smooth particle mesh ewald method. *J. Chem. Phys.*, 103:8577–8593, 1995.
- [30] D.E. Parry. The electrostatic potential in the surface region of an ionic crystal. *Surf. Sci.*, 49:433–440, 1975.
- [31] D.E. Parry. Errata: The electrostatic potential in the surface region of an ionic crystal. *Surf. Sci.*, 54:195–195, 1976.
- [32] E. Wasserman, J.R. Rustad, and A.R. Felmy. Molecular modeling of the surface charging of hematite i. the calculation of proton affinities and acidities on a surface. *Surf. Sci.*, 424:19–27, 1999.
- [33] J.H. Harding. A guide to midas. Technical Report AERE R-13127, AERE Harwell Laboratory, 1988.
- [34] A. Arnold and C. Holm. A novel method for calculating electrostatic interactions in 2d periodic slab geometries. *Chem. Phys. Lett.*, 354:324–330, 2002.
- [35] V.R. Saunders, C. Freyia-Fava, R. Dovesi, and C. Roetti. On the electrostatic potential in linear periodic polymers. *Comp. Phys. Commun.*, 84:156–172, 1994.
- [36] D. Wolf, P. Keblinski, S.R. Philpot, and J. Eggebrecht. Exact method for the simulation of coulombic systems by spherically truncated, pairwise  $r^{-1}$  summation. *J. Chem. Phys.*, 110:8254–8282, 1999.
- [37] R.S. Mulliken. Electronic population analysis on lcao-mo molecular wave functions. i. *J. Chem. Phys.*, 23:1833–1840, 1955.
- [38] S. Baroni, S. de Gironcoli, A. Dal Corso, and P. Giannozzi. Phonons and related crystal properties from density-functional perturbation theory. *Rev. Mod. Phys.*, 73:515–562, 2001.

- [39] R.T. Sanderson. An interpretation of bond lengths and a classification of bonds. *Science*, 114:670–672, 1951.
- [40] K.A. van Genechten, W.J. Mortier, and P. Geerlings. Intrinsic framework electronegativity: A novel concept in solid state chemistry. *J. Chem. Phys.*, 86:5063–5071, 1987.
- [41] A.K. Rappe and W.A. Goddard III. Charge equilibration for molecular dynamics simulations. *J. Phys. Chem.*, 95:3358–3363, 1991.
- [42] S.L. Njo, J.F. Fan, and B. van de Graaf. Extending and simplifying the electronegativity equalization method. *J. Mol. Catal. A*, 134:79–88, 1998.
- [43] C.E. Wilmer, K. Chul Kim, and R.Q. Snurr. An extended charge equilibration method. *J. Phys. Chem. Lett.*, 3:2506–2511, 2012.
- [44] M. Henry. Nonempirical quantification of molecular interactions in supramolecular assemblies. *Chem. Phys. Chem.*, 3:561–569, 2002.
- [45] H. Senouci, B. Millet, C. Volkringer, C. Huguenard, F. Taulelle, and M. Henry. Full spectroscopic characterization of an hydrolytically stable and colored ti(iv)-precursor in solution. *Comptes Rendus Chimie*, 13:69–96, 2010.
- [46] R.A. Nistor, J.G. Polihronov, M.H. Mueser, and N.J. Mosey. A generalization of the charge equilibration method for nonmetallic materials. *J. Chem. Phys.*, 125:094108, 2006.
- [47] D.E. Williams. Accelerated convergence treatment of  $r^{-n}$  lattice sums. *Cryst. Rev.*, 2:3–25, 1989.
- [48] K.T. Tang and J.P. Toennies. An improved simple-model for the van der waals potential based on universal damping functions for the dispersion coefficients. *J. Chem. Phys.*, 80:3726–3741, 1984.
- [49] J. Applequist. A multipole interaction theory of electric polarization of atomic and molecular assemblies. *J. Chem. Phys.*, 83:809–826, 1985.
- [50] T. Beyer, G.M. Day, and S.L. Price. The prediction, morphology, and mechanical properties of the polymorphs of paracetamol. *J. Am. Chem. Soc.*, 123:5086–5094, 2001.
- [51] P.A. Madden and M. Wilson. 'covalent' effects in 'ionic' systems. *Chem. Soc. Rev.*, pages 339–350, 1996.
- [52] J.H. Harding and N.C. Pyper. The meaning of the oxygen 2nd-electron affinity and oxide potential models. *Phil. Mag. Lett.*, 71:113–121, 1995.

- [53] B.G. Dick and A.W. Overhauser. Theory of the dielectric constants of alkali halide crystals. *Phys. Rev.*, 112:90–103, 1958.
- [54] R. Car and M. Parrinello. Unified approach for molecular-dynamics and density-functional theory. *Phys. Rev. Lett.*, 55:2471–2474, 1985.
- [55] P.J.D. Lindan and M.J. Gillan. Shell-model molecular-dynamics simulation of superionic conduction in  $CaF_2$ . *J. Phys. Condens. Matter*, 5:1019–1030, 1993.
- [56] U. Schroeder. A new model for lattice dynamics (breathing shell model). *Solid State Commun.*, 4:347–349, 1966.
- [57] P.M. Axilrod and E. Teller. Interaction of the van der waals type between three atoms. *J. Chem. Phys.*, 11:299–300, 1943.
- [58] A. Banerjea and J.R. Smith. Origins of the universal binding-energy relation. *Phys. Rev. B*, 37:6632–6645, 1988.
- [59] A.P. Sutton and J. Chen. Long-range Finnis-Sinclair potentials. *Phil. Mag. Lett.*, 61:139–146, 1990.
- [60] M.W. Finnis and J.E. Sinclair. A simple empirical n-body potential for transition metals. *Phil. Mag. A*, 50:45–55, 1984.
- [61] J. Cai and Y.Y. Ye. Simple analytical embedded-atom-potential model including a long-range force for fcc metals and their alloys. *Phys. Rev. B*, 54:8398–8410, 1996.
- [62] M.I. Baskes. Modified embedded-atom potentials for cubic materials and impurities. *Phys. Rev. B*, 46:2727–2742, 1992.
- [63] G.C. Abell. Empirical chemical pseudopotential theory of molecular and metallic bonding. *Phys. Rev. B*, 31:6184–6196, 1985.
- [64] J. Tersoff. New empirical-model for the structural-properties of silicon. *Phys. Rev. Lett.*, 56:632–635, 1986.
- [65] J. Tersoff. New empirical-approach for the structure and energy of covalent systems. *Phys. Rev. B*, 37:6991–7000, 1988.
- [66] D.G. Pettifor, I.I. Oleinik, D. Nguyen-Manh, and V. Vitek. Bond-order potentials: bridging the electronic to atomistic modelling hierarchies. *Comp. Mater. Sci.*, 23:33–37, 2002.
- [67] D.W. Brenner. Empirical potential for hydrocarbons for use in simulating the chemical vapor deposition of diamond films. *Phys. Rev. B*, 42:9458–9471, 1990.

- [68] D.W. Brenner, O.A. Shenderova, J.A. Harrison, S.J. Stuart, B. Ni, and S.B. Sinnott. A second-generation reactive empirical bond order (rebo) potential energy expression for hydrocarbons. *J. Phys.: Condens. Matter*, 14:783–802, 2002.
- [69] J. Che, T. Cagin, and W.A. Goddard III. Generalized extended empirical bond-order dependent force fields including nonbond interactions. *Theor. Chem. Acc.*, 102:346–354, 1999.
- [70] A.C.T. van Duin, S. Dasgupta, F. Lorant, and W.A. Goddard III. Reaxff: A reactive force field for hydrocarbons. *J. Phys. Chem. A.*, 105:9396–9409, 2001.
- [71] M.Z. Bazant, E. Kaxiras, and J.F. Justo. *Phys. Rev. B*, 56:8542–8552, 1997.
- [72] J.F. Justo, M.Z. Bazant, E. Kaxiras, V.V. Bulatov, and S. Yip. Interatomic potential for silicon defects and disordered phases. *Phys. Rev. B*, 58:2539–2550, 1998.
- [73] N.A. Marks. Generalizing the environment-dependent interaction potential for carbon. *Phys. Rev. B*, 63:035401, 2000.
- [74] A. Einstein. Die plancksche theorie der strahlung und die theorie der spezifischen waerme. *Ann. Phys.*, 22:180–190, 1907.
- [75] D. Frenkel and A.J.C. Ladd. New monte carlo method to compute the free energy of arbitrary solids. application to the fcc and hcp phases of hard spheres. *J. Chem. Phys.*, 81:3188–3193, 1981.
- [76] G. Paglia, A.L. Rohl, C.E. Buckley, and J.D. Gale. A computational investigation of the structure of  $\kappa$ -alumina using interatomic potentials. *J. Mater. Chem.*, 11:3310–3316, 2001.
- [77] G.W. Watson and D.J. Willock. The enumeration of structures for  $\gamma$ -alumina based on a defective spinel structure. *Chem. Commun.*, pages 1076–1077, 2001.
- [78] N.L. Allan, G.D. Barrera, M.Y. Lavrentiev, I.T. Todorov, and J.A. Purton. Ab initio calculation of phase diagrams of ceramics and minerals. *J. Mater. Chem.*, 11:63–68, 2001.
- [79] P.J.M. van Laarhoven and E.H.L. Aarts. *Simulated annealing: Theory and applications*. Reidel, 1987.
- [80] J.H. Holland. *Adaption in natural and artificial systems*. The University of Michigan Press, 1975.

- [81] T.S. Bush, C.R.A. Catlow, and P.D. Battle. Evolutionary programming techniques for predicting inorganic crystal-structures. *J. Mater. Chem.*, 5:1269–1272, 1995.
- [82] W.H. Press, S.A. Teukolsky, W.T. Vetterling, and B.P. Flannery. *Numerical recipes in Fortran: The art of scientific computing*. Cambridge University Press, 1986.
- [83] R. Fletcher and M.J.D. Powell. A rapidly convergent descent method for minimization. *Comput. J.*, 6:163–168, 1964.
- [84] D.F. Shanno. Conditioning of quasi-newton methods for function minimization. *Math. Comput.*, 24:647–656, 1970.
- [85] G. Mills, H. Jonsson, and G.K. Schenter. Reversible work transition-state theory - application to dissociative adsorption of hydrogen. *Surf. Sci.*, 324:305–337, 1995.
- [86] A. Banerjee, N. Adams, J. Simons, and R. Shepard. Search for stationary points on surfaces. *J. Phys. Chem.*, 89:52–57, 1985.
- [87] A.F. Voter, F. Montalenti, and T.C. Germann. Extending the time scale in atomistic simulation of materials. *Ann. Rev. Materials Research*, 32:321–346, 2002.
- [88] S.M. Woodley, P.D. Battle, J.D. Gale, and C.R.A. Catlow. The prediction of inorganic crystal structures using a genetic algorithm and energy minimisation. *Phys. Chem. Chem. Phys.*, 1:2535–2542, 1999.
- [89] D. Frenkel and B. Smit. *Understanding molecular simulation: from algorithms to applications*. Academic Press, 2001.
- [90] J.F. Nye. *Physical properties of crystals*. Oxford University Press, 1957.
- [91] J.W. Akitt. *NMR and chemistry*. Chapman and Hall, 1983.
- [92] R.F.W. Bader, T.T. Nguyendang, and Y. Tal. A topological theory of molecular-structure. *Rep. Prog. Phys.*, 44:893–948, 1981.
- [93] C. Eckart. Some studies concerning rotating axes and polyatomic molecules. *Phys. Rev.*, 47:552–558, 1935.
- [94] W. Cochran and R.A. Cowley. Dielectric constants and lattice vibrations. *J. Phys. Chem. Solids*, 23:447–450, 1962.
- [95] J.M. Seddon and J.D. Gale. *Thermodynamics and statistical mechanics*. Royal Society of Chemistry, 2002.

- [96] A. Baldereschi. Mean-value point in the brillouin zone. *Phys. Rev. B*, 7:5212–5215, 1973.
- [97] D.J. Chadi and M.L. Cohen. Special points in the brillouin zone. *Phys. Rev. B*, 8:5747–5753, 1973.
- [98] H.J. Monkhorst and J.D. Pack. Special points for brillouin-zone integrations. *Phys. Rev. B*, 13:5188–5192, 1976.
- [99] R. Ramirez and M.C. Boehm. The use of symmetry in reciprocal space integrations - asymmetric units and weighting factors for numerical-integration procedures in any crystal symmetry. *Int. J. Quantum Chem.*, 34:571–594, 1988.
- [100] P.B. Allen and J.L. Feldman. *Phys. Rev. B*, 48:12581–12588, 1993.
- [101] T. Tadano, Y. Gohda, and S. Tsuneyuki. Anharmonic force constants extracted from first-principles molecular dynamics: applications to heat transfer simulations. *J. Phys.: Condens. Matter*, 26:225402, 2014.
- [102] F. Zernike and J.A. Prins. Die beugung von roentgenstrahlen in fluessigkeiten als effekt der molekuelanordnung. *Z. Physik A Hadrons and Nuclei*, 41:184–194, 1927.
- [103] B.E. Warren. Calculation of powder-pattern intensity distributions. *J. Appl. Crystallogr.*, 11:695–698, 1978.
- [104] R. Kaplow, B. L. Averbach, and S. L. Strong. Pair correlations in solid lead near the melting temperature. *J. Phys. Chem. Solids*, 25(11):1195–1204, 1964.
- [105] T. Egami, J.D. Jorgensen, B.H. Toby, and M.A. Subramanian. Observation of a local structural-change at  $T_c$  for  $Tl_2Ba_2CuO_8$  by pulsed neutron-diffraction. *Phys. Rev. Lett.*, 64:2414–2417, 1990.
- [106] W. G. Williams, R. M. Ibberson, P. Day, and J. E. Enderby. GEM - General Materials Diffractometer at ISIS. *Physica B*, 241:234–236, 1997.
- [107] J.S. Chung and M.F. Thorpe. Local atomic structure of semiconductor alloys using pair distribution functions. ii. *Phys. Rev. B*, 59:4807–4812, 1999.
- [108] E.R. Cope and M.T. Dove. Pair distribution functions calculated from inter-atomic potential models using the general utility lattice program. *J. Appl. Crystallogr.*, 40:589–594, 2007.
- [109] J.D. Gale and A.L. Rohl. The General Utility Lattice Program (GULP). *Mol. Simul.*, 29:291–341, 2003.

- [110] D.H. Gay and A.L. Rohl. Marvin: A new computer code for studying surfaces and interfaces and its application to calculating the crystal morphologies of corundum and zircon. *J. Chem. Soc., Faraday Trans.*, 91:926–936, 1995.
- [111] P.W. Tasker. The stability of ionic crystal surfaces. *J. Phys. C*, 12:4977–4984, 1979.
- [112] J.D.H. Donnay and D. Harker. A new law of crystal morphology extending the law of bravais. *Am. Miner.*, 22:446–467, 1937.
- [113] G. Wulff. Zur frage der geschwindigkeit des wachsthums und der auflösung der krystallflächen. *Z. Kryst.*, 34:449–530, 1901.
- [114] J.W. Gibbs. *Collected works*. New York, Longman, 1928.
- [115] P. Hartman and P. Bennema. The attachment energy as a habit controlling factor 1. theoretical considerations. *J. Crystal Growth*, 49:145–156, 1980.
- [116] J.D. Gale and A.L. Rohl. An efficient technique for the prediction of solvent-dependent morphology: the cosmic method. *Mol. Simul.*, 33:1237–1246, 2007.
- [117] A. Klamt and G. Schueuermann. *J. Chem. Soc., Perkin Trans. 2*, pages 799–805, 1993.
- [118] M.P. Allen and D.J. Tildesley. *Computer simulation of liquids*. Oxford University Press, 1987.
- [119] R. LeSar, R. Najafabati, and D.J. Srolovitz. Thermodynamics of solid and liquid embedded-atom-method metals - a variational study. *J. Chem. Phys.*, 94:5090–5097, 1991.
- [120] A.P. Sutton. Direct free-energy minimization methods - application to grain-boundaries. *Phil. Trans. R. Soc. London A*, 341:233–245, 1992.
- [121] E.W. Montroll. Frequency spectrum of crystalline solids. *J. Chem. Phys.*, 10:218–229, 1942.
- [122] L.N. Kantorovich. Thermoelastic properties of perfect crystals with non-primitive lattices. 1. general-theory. *Phys. Rev. B*, 51:3520–3534, 1995.
- [123] M.B. Taylor, G.D. Barrera, N.L. Allan, and T.H.K. Barron. Free-energy derivatives and structure optimization with quasiharmonic lattice dynamics. *Phys. Rev. B*, 56:14380–14390, 1997.

- [124] J.D. Gale. Analytical free energy minimization of silica polymorphs. *J. Phys. Chem. B*, 102:5423–5431, 1998.
- [125] N.L. Allan, T.H.K. Barron, and J.A.O. Bruno. The zero static internal stress approximation in lattice dynamics, and the calculation of isotope effects on molar volumes. *J. Chem. Phys.*, 105:8300–8303, 1996.
- [126] N.F. Mott and M.J. Littleton. Conduction in polar crystals. i. electrolytic conduction in solid salts. *Trans. Faraday Soc.*, 34:485–499, 1938.
- [127] C.R.A. Catlow, R. James, W.C. Mackrodt, and R.F. Stewart. Defect energetics in  $\alpha - \text{Al}_2\text{O}_3$  and rutile  $\text{TiO}_2$ . *Phys. Rev. B*, 25:1006–1026, 1982.
- [128] N.L. Allinger, X.F. Zhou, and J. Bergsma. Molecular mechanics parameters. *J. Mol. Struct. (Theochem)*, 118:69–83, 1994.
- [129] A.K. Rappe, C.J. Casewit, K.S. Colwell, W.A. Goddard III, and W.M. Skiff. Uff, a full periodic table force field for molecular mechanics and molecular dynamics simulations. *J. Am. Chem. Soc.*, 114:10024–10035, 1992.
- [130] S. Barlow, A.L. Rohl, S.G. Shi, C.M. Freeman, and D. O’Hare. Molecular mechanics study of oligomeric models for poly(ferrocenylsilanes) using the extensible systematic forcefield (esff). *J. Am. Chem. Soc.*, 118:7578–7592, 1996.
- [131] J.D. Gale, C.R.A. Catlow, and W.C. Mackrodt. Periodic ab initio determination of interatomic potentials for alumina. *Modelling Simul. Mater. Sci. Eng.*, 1:73–81, 1992.
- [132] R.G. Gordon and Y.S. Kim. Theory for the forces between closed-shell atoms and molecules. *J. Chem. Phys.*, 56:3122–3133, 1972.
- [133] J.D. Gale. Empirical potential derivation for ionic materials. *Phil. Mag. B*, 73:3–19, 1996.
- [134] T.J. Grey, J.D. Gale, and D. Nicholson. Parameterization of a potential function for the  $\text{Ca}^{2+} - \text{ne}$  and  $\text{Ca}^{2+} - \text{n}_2$  interactions using high-level ab initio data. *Mol. Phys.*, 98:1565–1573, 2000.
- [135] C.R.A. Catlow and M.J. Norgett. Lattice structure and stability of ionic materials. Technical Report AERE-M2936, AERE Harwell Laboratory, 1976.
- [136] C.R.A. Catlow and W.C. Mackrodt. Theory of simulation methods for lattice and defect energy calculations in crystals. *Lecture Notes in Physics*, 166:3–20, 1982.

- [137] J.D. Gale. Gulp: A computer program for the symmetry-adapted simulation of solids. *J. Chem. Soc., Faraday Trans.*, 1:629–637, 1997.
- [138] S. Brode and R. Ahlrichs. An optimized md program for the vector computer cyber-205. *Comp. Phys. Commun.*, 42:51–57, 1986.
- [139] C.R.A. Catlow, I.D. Faux, and M.J. Norgett. Shell and breathing shell model calculations for defect formation energies and volumes in magnesium oxide. *J. Phys. C: Solid State Phys.*, 9:419–429, 1976.
- [140] C.-S. Zha, H.-K. Mao, and R.J. Hemley. Elasticity of mgo and a primary pressure scale to 55 gpa. *Proc. Natl. Acad. Sci.*, 97:13494–13499, 2000.
- [141] I. Jackson and H. Niesler. *In High pressure research in geophysics*. Center for Academic Publishing, Tokyo, 1982.
- [142] M.J. Sanders, M. Leslie, and C.R.A. Catlow. Interatomic potentials for  $\text{SiO}_2$ . *J. Chem. Soc. Chem. Commun.*, pages 1271–1273, 1984.
- [143] X. Gonze, D.C. Allan, and M.P. Teter. Dielectric tensor, effective charges, and phonons in  $\alpha$ -quartz by variational density-functional perturbation theory. *Phys. Rev. Lett.*, 68:3603–3606, 1992.
- [144] Ph. Ghosez, J.-P. Michenaud, and X. Gonze. Dynamical atomic charges: The case of  $\text{ABO}_3$  compounds. *Phys. Rev. B*, 58:6224–6240, 1998.
- [145] A.L. Rohl, K. Wright, and J.D. Gale. Evidence from surface phonons for the (2x1) reconstruction of the (10-14) surface of calcite from computer simulation. *Am. Miner.*, page in press, 2003.
- [146] S.L.S. Stipp. Toward a conceptual model of the calcite surface: Hydration, hydrolysis, and surface potential. *Geochimica Cosmochimica Acta*, 63:3121–3131, 1999.
- [147] J.S. Chung and M.F. Thorpe. Local atomic structure of semiconductor alloys using pair distribution functions. *Phys. Rev. B*, 55:1545–1553, 1997.
- [148] W. Reichardt and L. Pintschovius. Influence of phonons on the pair distribution function deduced from neutron powder diffraction. *Phys. Rev. B*, 63:174302, 2001.
- [149] S.W. Lovesey. *Theory of Neutron Scattering from Condensed Matter. Volume 1: Nuclear Scattering*. Oxford University Press, 1984.
- [150] B.T.M. Willis and A.W. Pryor. *Thermal Vibrations in Crystallography*. Cambridge University Press, Cambridge, 1975.

- [151] M.T. Dove. *Introduction to Lattice Dynamics*. Cambridge University Press, Cambridge, 1993.
- [152] D.A. Keen. A comparison of various commonly used correlation functions for describing total scattering. *J. Appl. Crystallogr.*, 34:172–177, 2001.
- [153] M.G. Tucker, M.T. Dove, and D.A. Keen. Neutron total scattering method: simultaneous determination of long-range and short-range order in disordered materials. *Eur. J. Mineral.*, 14:331–348, 2002.
- [154] T. Proffen and S.J.L. Billinge. PDFFIT, a program for full profile structural refinement of the atomic pair distribution function. *J. Appl. Crystallogr.*, 32:572–575, 1999.
- [155] S.J.L. Billinge and T. Egami. Short-range atomic-structure of  $\text{Nd}_{(2-x)}\text{Ce}_x\text{CuO}_{(4-y)}$  determined by real-space refinement of neutron-powder-diffraction data. *Phys. Rev. B*, 47:14386–14406, 1993.
- [156] S.J.L. Billinge, T. Egami, T. Proffen, and D. Louca. Structural analysis of complex materials using the atomic pair distribution function - a practical guide. *Z. Krist.*, 218:132–143, 2003.
- [157] W.S. Howells, A.K. Soper, and A.C. Hannon. *ATLAS - Analysis of Time-of-Flight Diffraction Data from Liquid and Amorphous Samples, 1989*. 1989.